SYSTEMS BIOLOGY STUDY OF KIFC1, CENTROSOME AMPLIFICATION AND CELL CYCLE RELATIONSHIPS

Lancaster University

Linas Zilinskas

MSc by Research in Biomedical Science

Supervised by Dr. Andrew Fielding and Professor Paul O'Shea

Division of Biomedical and Life Sciences

Faculty of Health and Medicine

Lancaster University

May, 2024

Declaration

I, Linas Zilinskas confirm that the contents of this study are my own and any other is referenced. I confirm that this work is only used for this degree and is not being presented for any other institution for a degree.

Abstract

Many cancer cells exhibit the state known as centrosome amplification, where they have more than two centrosomes as they undergo mitosis. In order to cope with centrosome amplification, cells require mechanisms to cluster their amplified centrosomes. KIFC1 is a kinesin that performs the clustering of multiple centrosomes and this function allows survival of cells with centrosome amplification. KIFC1 is best known for its ability to cluster centrosomes, with minor evidence suggestive of some functions in the cell cycle. Meanwhile, the centrosome is well known for its ability to separate chromosomes, receiving much less attention for housing many cell cycle proteins and associated events.

Here, the aim was to examine the relationships between the cell cycle, centrosome amplification and KIFC1 function, in particular how centrosome amplification affects the cell cycle lengths and parameters occurring on centrosomes and how KIFC1 affects the lengths of the phases of the cell cycle.

The link between KIFC1 and cell cycle lengths and between centrosomes and cell cycle lengths has been investigated and it was found that KIFC1 depletion increases the lengths of G1 phase and the period of the cell cycle from S to Anaphase for both cells with normal and amplified centrosome number. KIFC1 depletion also results into a lower proportional increase of the number of cells in a population over time by 33.5 times. Amplified centrosomes have shown no effect on the length of the cell cycle. To further investigate the effect of centrosomes on the cell cycle, a systemic method has been utilized to identify proteins specific for the cell cycle that could be affected by centrosome amplification, potentially modyfing their cell cycle functions; PLK1, and AURKA, in particular the phosphorylated versions of both. It was found that centrosome amplification affects the amounts and activity of these proteins at centrosomes and disturbs certain relationships between the centrosomal parameters and parameters of these proteins.

Contents

Chapter 1: Introduction

1.1 Centrosome amplification

This study is centered around the concept of centrosome amplification in cancer disease, Sabat-Pospiech et al., (2019). It is perceived as the presence of abnormal numbers of centrosomes in cells, which is more than one during G1 of interphase and more than two during G2 and mitosis. A centrosome or a microtubule organizing center (MTOC), which refers to its ability to create spindle poles during mitosis and pull DNA via microtubules and also for forming basal bodies forming cilium through the elongation of microtubules (Vertii et al., 2016). Lesser known functions are cell cycle control, stress response mediation (both environmental and genomic), and immune functions (Vertii et al., 2016). The effects of centrosome amplification on the ability to form spindle poles are the most obvious and are most studied since they lead to drastic consequences for the genomic integrity of the cell. Most studies on centrosome amplification have focused on examining how it affects the division of the nucleus in mitosis, with some information also available about its effects on invasiveness (Arnandis et al., 2018) and the ability for cancer cells to cope with centrosome deactivating mutations (Harrison et al., 2018). However, no research has been done on how the amplification of centrosomes affects one of its less well studied functions – cell cycle regulation (which is not mutually exclusive with stress response pathways as shown later in this study). In this study the link between centrosomes and the cell cycle has been examined.

Centrosome duplication is tightly coupled to the cell cycle, to ensure a correct number of centrosomes (Slevin et al., 2012). If otherwise, then multiple mitotic spindle poles arise pulling DNA into multiple directions, most of the time causing an aneuploidy-based death (Ganem et al., 2009). Cancer is often associated with cellular abnormalities, and in the case of centrosome amplification, it appears as both a consequence and a cause. KIFC1 clustering multiple centrosomes is a consequence. However it can be a cause because multiple centrosomes allow the cell to drive cancerous pathogenicity through aneuploidy. This leads to loss of tumor suppressors (Ganem et al., 2009), much more rarely gain of oncogenes (Duijif et al., 2013), increased invasiveness (Arnandis et al., 2018). Sometimes it can compensate for centrosome deactivating mutations (Harrison et al., 2018), and possibly through altering cell cycle pathways (see chapter 5). Duijif et al., (2013) have found that 68% of solid tumors contain aneuploidy, which is much more often a loss of chromosomes than a gain. The lost regions may include genes such as PTEN,

CDKN2A, RB1, and BRCA1, which are tumor suppressors (Albertson et al., 2003). The increased invasiveness in centrosome amplified cells stems from the formation of actin-based invasive structures which can degrade basement membranes. The latter is caused by the secretion of Interelukin-8, Mesothelin, GDF-15, and several other signaling factors, which are secreted by centrosome-amplified cells. The ligands are received by several receptors including HER2. Such secretion is caused by an early stress response induction by the centrosome-amplified cells (Arnandis et al., 2018).

KIFC1, also known as HSET, allows survival of cells with multiple centrosomes by clustering them, thus avoiding aneuploidy-based death (Sabat-Pospiech et al., 2019). As a result, it has been identified as a biomarker for specific types of cancer, with a potential to become a drug target (Patel et al., 2018). It has also been shown that KIFC1 contains activities that can accelerate the cell cycle, more specifically G2 and M phases (Pannu et al., 2015) and the S-phase of the cell cycle (Wei et al., 2019). Both studies were based on flow cytometry experiments measuring cell population proportions in KIFC1 inhibited and test samples. As a result, the link between KIFC1 and the cell cycle is still vague and more studies need to be done on this subject, and this study will partly focus on examining the effects of KIFC1 on the cell cycle. On the other hand, the link between KIFC1 and centrosomes is well-studied (Kleylein-Sohn et al., 2012; Lucanus et al., 2018; Sansregret et al., 2011; Xiao et al., 2016). Hence, this study is focused on establishing the link between KIFC1 and the cell cycle and between centrosomes and the cell cycle.

Figure 1.1:

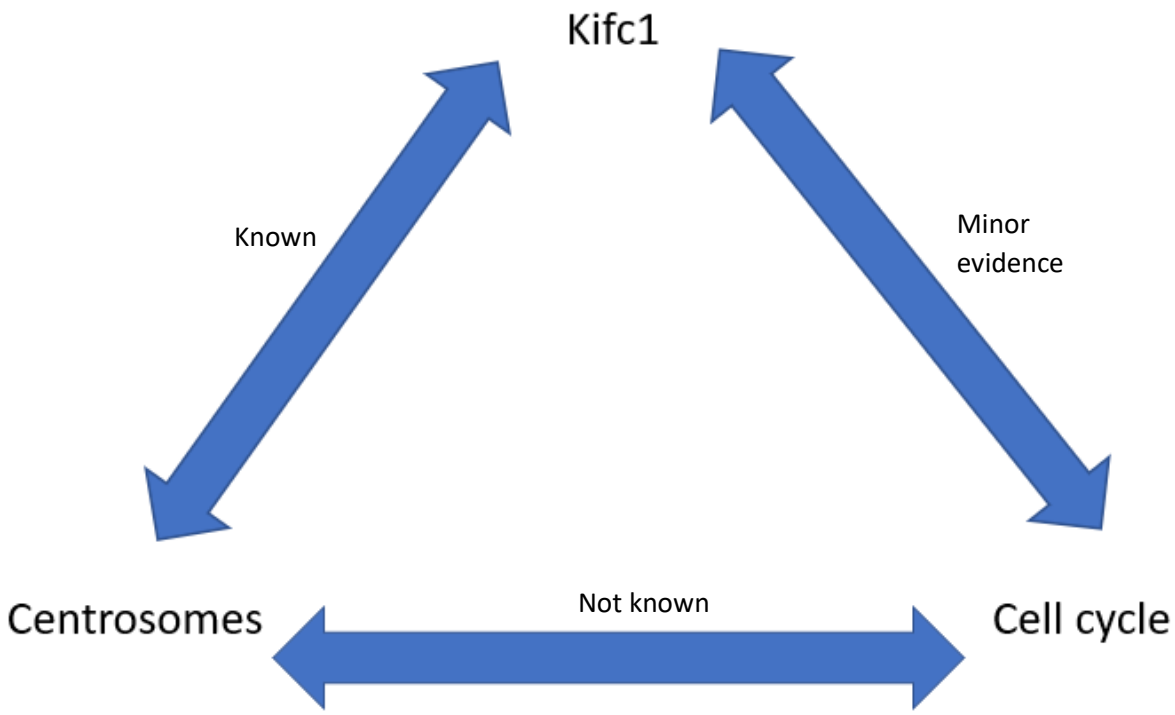

Figure 1.1: **The scheme representing the areas of focus of this study**. The link between KIFC1 and centrosomes is well established, but in this study the link between KIFC1 and cell cycle and the link between centrosomes and the cell cycle will be examined.

The main characteristic of a cancerous cell is the uncontrolled division, which ultimately is controlled by the cell cycle. A single mutation in a protein regulating the cell cycle will render the cell more proliferative. If the latter is not dealt with, then mutations accumulate exponentially as a result of uncontrolled division which further drives carcinogenesis (Collins et al., 1997). Much of the cell cycle machinery is located on centrosomes (Dodson et al., 2012; Astuti and Gabrielli 2011; Bouche et al., 2008; Lammer et al., 1998), also DNA damage checkpoint control (Grallert et al., 2013; O'connell et al., 1997; Saini et al., 2015; van Gugt et al., 2004), which is closely tied to cell cycle control as depicted later in this study. Centrosomes, as well as their microtubule nucleating activity, also act as a scaffold for cell cycle machinery (Lin et al., 2022). As a result, here it is hypothesized that amplified centrosomes will change the rates of the cell cycle phases. Thus, so far it appears that for a cell to have multiple centrosomes it must have undergone an unknown

type of deregulation first, which must have included KIFC1 overproduction. Eventually, centrosomes have amplified themselves leading to a cell having multiple centrosomes, but since KIFC1 has been already upregulated, the cell has avoided aneuploidy. As a result, the cell cycle may have been accelerated both due to KIFC1 and multiple centrosomes being present.

Figure 2:

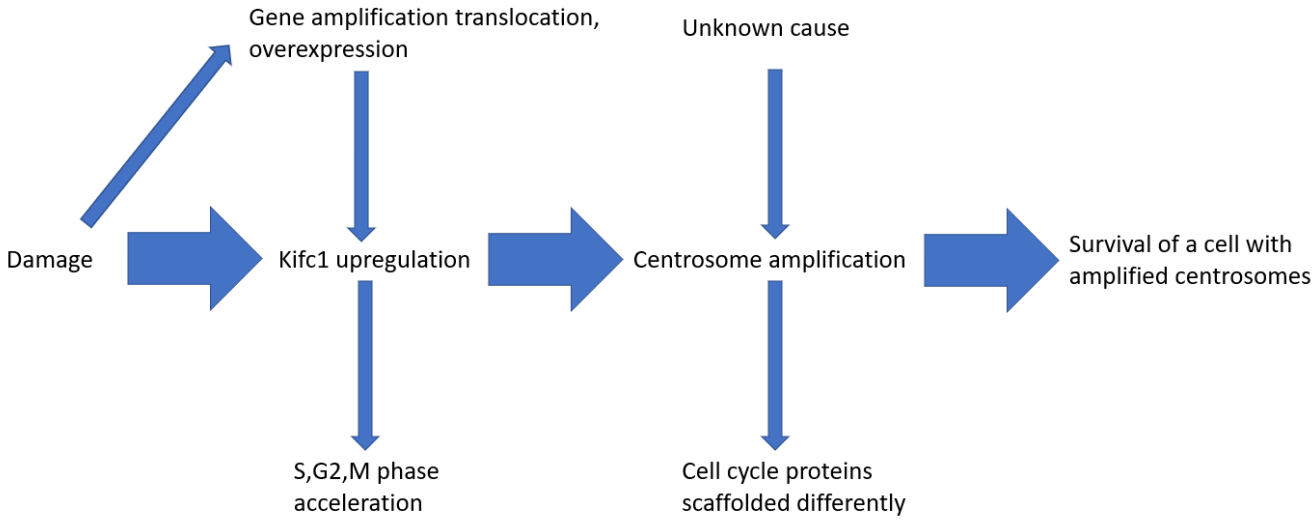

Figure 1.2: **The development of centrosome amplification**. Centrosome amplification on its own will either result into aneuploidy or cell death (Sabat-Pospiech et al., 2019). However, if KIFC1 is present the latter is prevented. Not in every case of KIFC1 upregulation the mechanism is known, hence a direct connection between KIFC1 and damage is portrayed. KIFC1 can be upragulated by ANCCA or Cux1 pathways (Sansregret et al., 2011).

1.2: KIFC1:

KIFC1 itself is a member of the kinesin 14 family. It has homologous proteins in other species such as *D. melanogaster* Ncd, *X. laevis* XCTK2, *S. cerevisae* Kar3, *M. musculus* KIFC1, *A. thaliana* ATK5, *S. pombe* Pkl1. It has a C-terminal domain which is also called the head domain. The head domain has an ATP-binding site and a microtubule-binding site. The N-terminal tail contains the nuclear localization sequence and also contains a microtubule-binding site. The head domain connects to the neck which then connects to the central coiled-coil stalk which is connected to the N-terminal

domain. The protein dimerizes via the coiled-coil stalk (Xiao and Yang, 2016 ; She and Yang, 2017).

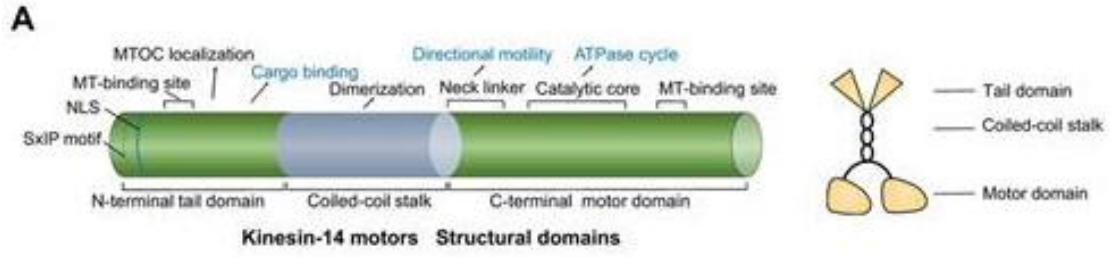

Figure 1.3: **The structure of KIFC1 visualised**. The tail domain microtubule binding site is not mobile and it functions to prevent the protein from leaving the microtubules while the head domain moves along the mirotubules (She and Yang, 2017).

While KIFC1 is on the microtubules, it moves towards the minus ends which are capped with gamma-tubulin at the centrosome. KIFC1 can also locate centrosomes through binding Cep215 centrosomal receptor and is held at centrosomes by being bound to CEP215. Cep215 double knockout cells show lower quantities of KIFC1 on centrosomes and results in centrosome displacement (Lawrence et al., 2004; She and Yang, 2017).

KIFC1's normal functions are organelle and vesicle trafficking (Nath et al., 2007); oocyte development (Hall et al., 2007); spermatogenesis (Yang and Sperry, 2003), and double-stranded DNA transporting and trafficking (Farina et al., 2013). Xiao and Yang (2016) have shown that KIFC1 is dispensable in human adults and thus is a promising drug targets. KIFC1 clusters centrosomes by binding two microtubule streams near chromosomes on each end of itself and then moves towards the minus-ends forcing the centrosomes to get close (Sabat-Pospiech et al., 2019).

1.3 KIFC1 and the link with the cell cycle:

Pannu et al., (2015) describe that KIFC1 is usually elevated in cancer cells due to either gene amplification or translocation. Subsequently, elevated KIFC1 resulted in higher Cdk1 activity and some other advantages for the cancer cells other than the clustering of centrosomes. For example, cell cycle events have been found to have accelerated slightly before the peak of Cyclin B levels. Another effect of KIFC1 was that Mad1 and Mad2 spindle checkpoint protein ratio has been changed, likely through the KIFC1's ability to bind importins (Pannu et al., 2015). Lastly, they have found that KIFC1 overexpression co-occurs with several cell cycle proteins such as Hif1a, Mad1, Survivin, Cyclin B, and Aurora B.

Looking further into the elevated expression of KIFC1, the Cut homeobox 1 (Cux1) transcription factor is thought to be a cause of KIFC1 overexpression (Sansregret and Nepveu, 2008). Goulet et al., (2004) explain how a specific isoform of of Cux1 is produced in cancer cells without an autoinhibitory domain. The cause of this isoform is due to a short isoform of a Cathepsin L protein of a Ras oncogene causing a downstream AUG translation of cathepsin L (Goulet et al., 2007). The short isoform of Cux1 shows stronger DNA binding resulting in the higher expression levels of various kinesins including KIFC1. Cdc25A can increase the transcriptional activity of Cux1 by dephosphorylating it increasing its binding to DNA (Sansregret et al., 2011).

The survival of centrosome amplified cells has been shown to become dependent on the presence of KIFC1 (Patel et al., 2018), meanwhile KIFC1 levels have been already shown to become elevated in certain lines of cancer cells. Patel et al., (2018) have found that 13 genes are co-upregulated with KIFC1 and are involved in cell cycle regulation, DNA damage response pathway, and mitosis. This shows that together with KIFC1 there may be faults in the indicated systems. Furthermore, they have shown that one of the transcription factors involved in KIFC1 expression (E2F8) also expresses cell cycle and mitosis genes (*MYBL2, FOXM1, TTK, NUF2, MASTL*). As a result, it is also possible that cell cycle machinery may be coincidentally affected by KIFC1.

So far it has been shown that the G2 and M phases (Pannu et al., 2015) and the S-phase of the cell cycle (Wei and Yang., 2019) are affected by KIFC1, while Patel et al., (2018) have shown that *KIFC1* overexpression co-occurs with several cell cycle genes. The latter may explain why KIFC1 abnormalities may be linked to the cell cycle. However, whether KIFC1 overexpression is required for cancer cell survival is unknown. It is also unknown if centrosomes have been amplified due to faults in cell cycle machinery due to them being closely tied to the cell cycle (Lin et al., 2022). Either way, an increased number of these cell-cycle machinery-bearing entities will likely affect the cell-cycle events in addition to KIFC1 potentially accelerating cell cycle phases. In this study, using fluorescent cell cycle phase markers, the effects of the inhibition and degradation of KIFC1 on the lengths of the cell cycle phases G1 (represented by CDT1) and S to Anaphase (represented by Geminin) were tested.

1.4 KIFC1 as a drug target:

As stated previously, KIFC1 is a promising drug target due to its functions being dispensable in an adult human. AZ82 (Wu et al., 2013), CW069 (Sekino et al., 2019), and Monastrol (Ali et al., 2024) are the known KIFC1 inhibitors.

However, AZ82 is of special interest, since a KIFC1-PROTAC (PROTAC stands for proteolysis targeting Chimera) degrader used in this study (developed in the Fielding lab, Lancaster University) is a derivative of the AZ82 inhibitor. The principle of how PROTAC degraders work is described by Bekes et al., (2022). PROTAC consists of two ligands joined together. One ligand binds the protein of interest and the other binds E3 ubiquitin ligase. This causes ubiquitylation of the protein and its degradation by the proteasome. In the case of KIFC1 PROTAC, AZ82 is joined to a ligand that binds the E3 ubiquitin ligase Cereblon. AZ82 is a small-molecule, phenylalanine-derived inhibitor and binds to the KIFC1-microtubule complex. It binds to the active site of the KIFC1 ATPase domain and subsequently prevents the ability of KIFC1 to move along microtubules from the chromosomes towards the minus-end/centrosomes, and as a result, centrosomes will remain unclustered, forming multipolar spindles and resulting in apoptosis or aneuploidy-based death (Wu et al., 2013).

1.5 Centrosome assembly:

KIFC1 does not cause centrosome amplification, but enhances the likelihood of cell survival with centrosome amplification. It is not known what causes centrosome amplification in specific cases, but any step within the duplication pathway can become defective causing it. PLK4 is often referred to as the central molecule around which the growth of new centrosomes revolves, including those that are amplified (Cotee et al., 2017; Lin et al., 2022; Sabat-Pospiech et al., 2019). PLK4 is the first visually distinguishable protein to perform the first microscopically observable shape changes upon the assembly of a daughter centriole (Cotee et al., 2017; Lin et al., 2022; Sabat-Pospiech et al., 2019). As a result, Brownlee et al., (2011) have found that Plk4 stabilization through prevention of autophosphorylation of a phosphodegron induces centrosome amplification. Park et al., (2019) have found that Polo-like kinase 4 contains a polo-box 2 which is critical to generate the PLK4 dot on the mother centrosome wall. Park et al., (2019) explain that the first morphologically noticeable change in the formation of a new centriole is the movement of

PLK4 from around the mother centriole wall into one specific part of the wall. This is also known as loss of asymmetry, PLK4 ring-to-dot formation, and PLK4 condensation. The latter is triggered by the autophosphorylation of PLK4 in the Cryptic polo-box (CPB). Polo box 3 of PLK4 then binds Stil/ANA2 allowing PLK4 to phosphorylate them starting the formation of the cartwheel of the centrosome. Park et al., (2019) have looked into the structure of the cryptic polo box (Polo boxes 1 and 2) in PLK4 to discover 8 potential phosphoclusters, of which the 3rd was found to be the one phosphorylated most likely by PLK4 itself initiating cartwheel formation. The figure below portrays the structure of PLK4.

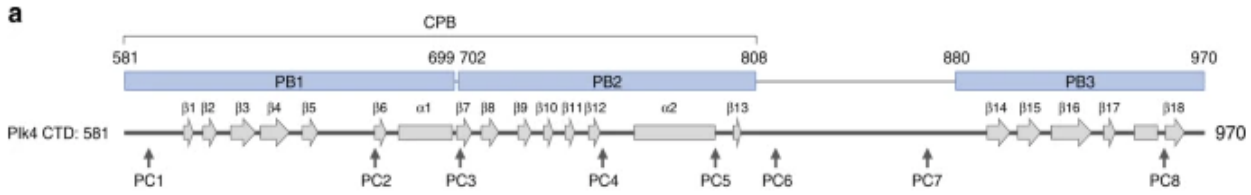

Figure 1.4: **The human structure of PLK4 and the eigth phosphoclusters of PLK4** (Park et al., 2019). Phosphoclusters are CTD residues of PLK4, which by mass spectrometry were identified to be phosphorylated sites. PC3 has been identified to be the phosphorylation required for catalytic activity as SDS-PAGE results have shown that it has migrated the same distance as the K41M catalytically inactive mutant. This suggests that PC3 is involved in controlling the autophosphorylation state of Plk4 in cohort with K41 through conformational changes. PC3 itslef is also phosphorylated by K41 (Park et al., 2019).

The assembly of a daughter centriole begins with the formation of a PLK4 spot on the wall of the mother centriole which is recruited by Asl (Dzhindzhiev et al., 2010). CEP152/Asl, CEP192/SPD-2 CEP57, and CEP63 reorganize PLK4 from around the centriole to a single spot (Jana, 2021). PP2A stabilizes PLK4 during M phase, restricting its activity (Brownlee et al., 2011). The formation of the cartwheel structure initiates when Plk4 plaque is is formed on one spot of the centriole wall. Cartwheel begins to be built when PLK4 recruits ANA2/STIL, phosphorylating the latter causing SAS-6 recruitment. PLK4 also initiates centrosome assembly by FBXW5 inactivation (SCF component which degrades SAS-6) (Puklowski et al., 2011). 9 SAS-6 homodimers oligomerize into higher-order ring structures forming the central HUB of 18 juxtaposed N-terminal domains and 9 extending spokes, each composed of a pair of coiled coils. Spokes connect to the pinhead which itself connects to the A-microtubule. Furthermore, SAS-6, STIL/ANA2, and CEP135 form the central hub of the cartwheel and stalks, which connect to pinhead proteins. Inside the central hub of the cartwheel are the cartwheel inner densities (CID), which are also 9-fold symmetric (Fu et al., 2015).

Cartwheel inner densities, the Central hub, and the spokes stack together to make the full structure. PLK4 then phosphorylates STIL/ANA2 which stabilizes all of the proteins. On the peripheral regions of the cartwheel, SAS-4 and CTD of SAS-6 recruit A-tubules thus starting the growth of centriole triplets from gamma tubulin ring complexes. CP110-CEP97 restricts elongation at the distal end (Jana, 2021). The figure below portrays the inside of a centrosome.

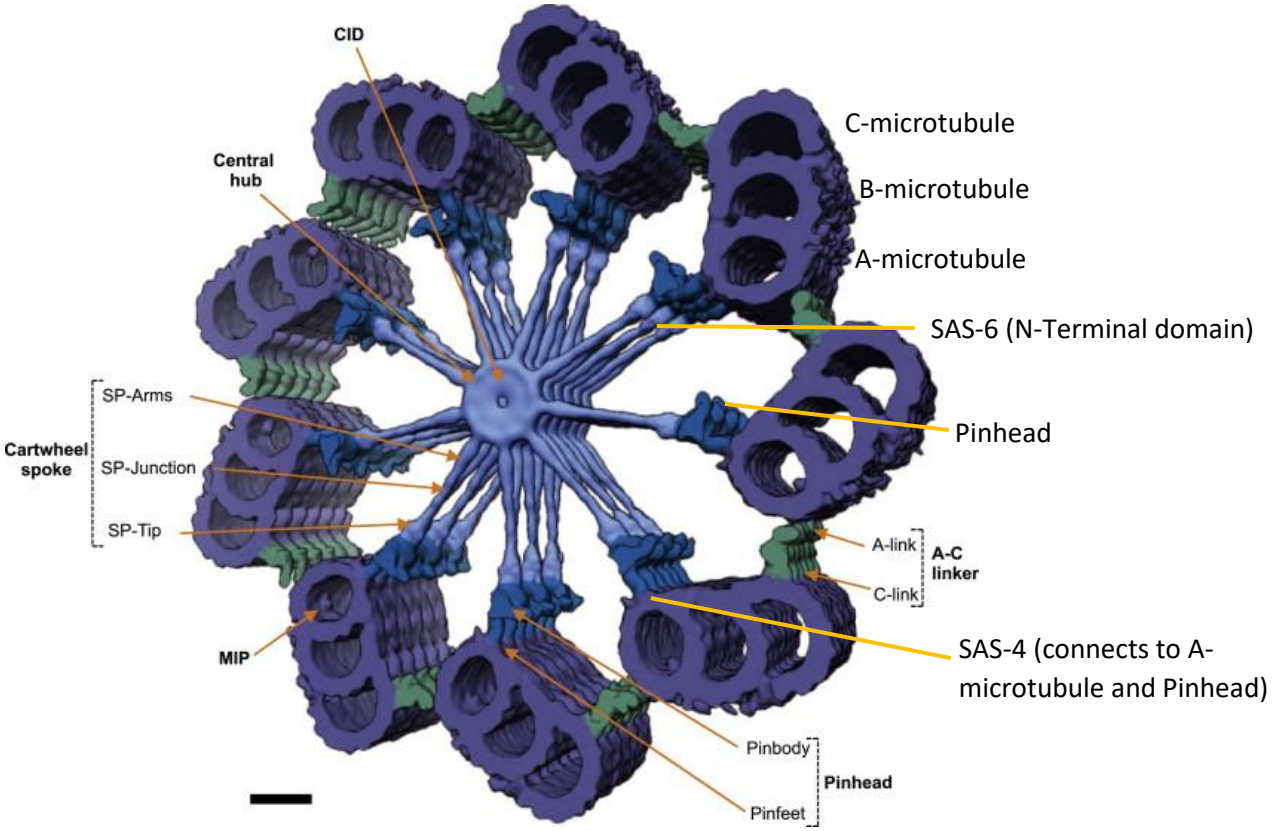

Figure 1.5: **The 3D structure of centrosome and its cartwheel.** In the middle of the cartwheel are the SAS-6, STIL, CEP135 proteins. Sas-6 homodimerise to form structure with space in the middle containing cartwheel inner densities (CIDs). Towards NTD, SAS-6 extends forming spokes. Spokes connect to pinhead and pinhead connects to microtubules. The A-microtubule consists of 13 protofilament streams, while the subsequent microtubules overlap with each other containing only 10 protofilament streams, while the other 3 are compensated through the overlap. The C microtubule connects to another triplet;s A-microtubule through the A-C linker . Image from Guichard et al., (2013).

1.6 Centrosome structure:

Centrosomes structure even though is complex, it is yet well conserved and organised. The ability to scaffold cell cycle proteins may lie in the precise nature of the microtubules being able to gather the pericentriolar material around, part of which might just be cell cycle machinery (Fu et al., 2015; Lin et al., 2022; Jana, 2021). A mature centrosome contains two orthogonally arranged centrioles, which are surrounded by pericentriolar material. Centriole has a diameter of 25nm and a length of up to 500nm. It exhibits proximal to distal polarity. In humans, centriole is made up of 9 triplet microtubules, where each triplet is made of one complete microtubule consisting of 13 protofilament streams and two microtubules with 10 protofilament streams each because B and C tubules share 3PF streams with A and B tubules respectively, as shown in the figure below (Bettencourt-Dias and Glover, 2007):

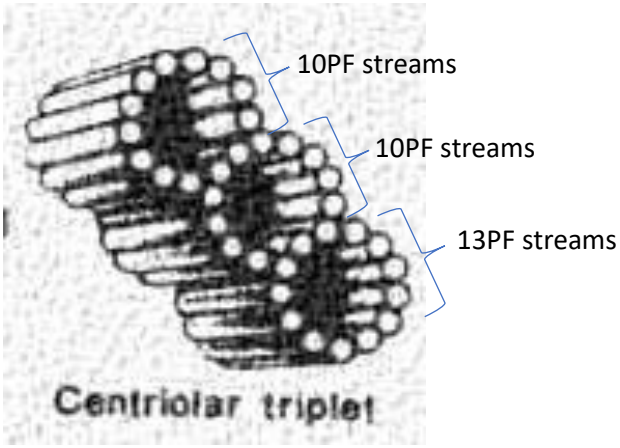

Figure 1.6 : **Centriolar triplet**. 9 such units arranged into a circle make up a centriole. The microtubule with 13 protofilament stream is called the A-tubule, the one adjacent to it is the B-tubule, and the upper most one is the C-tubule (Bettencourt - Dias and Glover, 2007). Image from Childs Gwen (2014).

Each protofilament stream consists of an array of alpha and beta tubulins. A and C microtubules of adjacent triplets are connected by a protein called the A-C linker. Adjacent triplets are twisted by 110 degrees, but this angle is inconsistent along centriole length (Jana, 2021).

Centrioles begin to grow a daughter centriole at a 90-degree angle to their walls at the G1/S transition. At this point of the cell cycle, there is one centrosome, and two centrioles (connected by a flexible linker), and each centriole begins to grow a daughter centriole (Bettencourt-Dias and

Glover, 2007). The figure below portrays the latter:

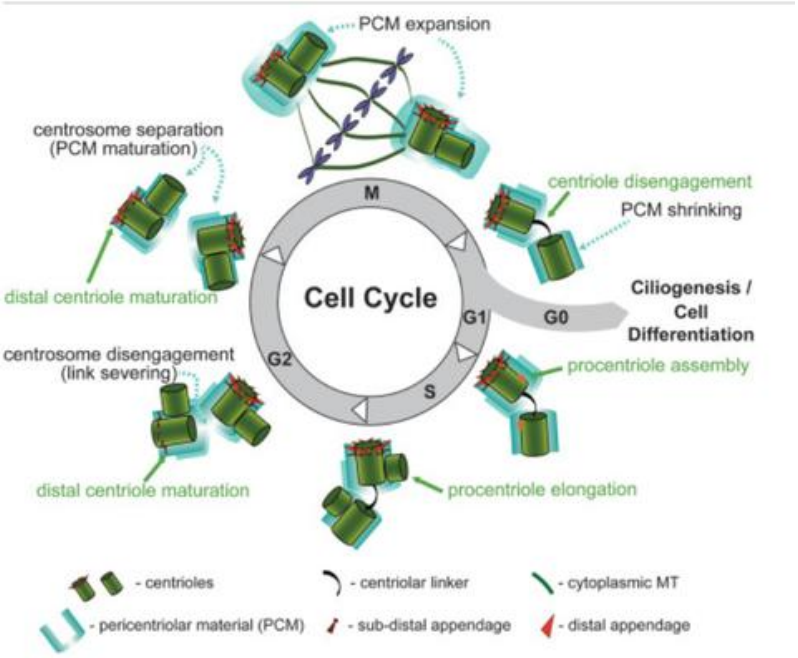

Figure 1.7: **The centrosome duplication cycle**. At G1/S transition an orthogonally arranged procentriole is assembled at the proximal end of pre-exisitng centriole. During S and G2, each procentriole remains engaged with its parent centriole and elongates up to 400nm. At the end of G2, the centriole linker between two parental centrioles is severed allowing the two centrosomes, each with a pair of orthogonally arranged centrioles to separate and govern mitotic spindle formation. During mitosis, each newly formed centriole disengages from parent centriole, but remains linked by the flexible linker (Jana, 2021). After centrosome duplication during S phase, the centrosome is still considered as one centrosome, regardless of the fact it has two centrioles. After the disengagement in G2/M transition, two separate centrosomes are seen (Dobbellaere et al., 2008). Image from Jana (2021).

The newly developing daughter centriole is already embedded in the pericentriolar material matrix as it starts growing since the mother centriole is embedded in it before hand (Jana, 2021; Woodruf et al., 2014). The growth of the pericentriolar material happens during interphase and mitosis. During the interphase, pericentrin and Asterless (Asl) accumulate in the pericentriolar material, while during mitosis Cep192, CDK5RAP2 and γ-tubulin accumulate (Fu et al., 2015). Only four proteins are required for the mitotic maturation of pericentriolar material: PLK1, AURKA, Cep192, and CDK5RAP2 (Dobbelaere et al., 2008), altough this study was done on a fly model. Aurora Kinase A and Polo-like kinase 1 (Asteriti et al., 2015) are required for the mitotic maturation of the pericentriolar material. During interphase, pericentrin accumulates and forms the bulk of the scaffold (Lee and Rhee, 2011; Jiang et al., 2021).

PCM is divided into two zones (1 and 2): Zone 1 contains PCNT, CEP57, CEP63, CPAP/SAS4 CEP295/ANA1, CEP44, etc.. and is close to the centriole wall. Zone 1 then functions to recruit components to Zone 2 which serves to nucleate microtubules (Woodruf et al., 2014). Zone 1 and Zone 2 proteins are not necceserilly mutually exclusive, since during the duplication of the centrosome and its splitting, some matrix is always passed to the new centrosome (Fu et al. 2015; Ganem et al., 2009; Cotee et al., 2017).

During interphase, the proteins of PCM are distributed in organized structures of a certain size spanning away from the centriole (100nM). Some of these proteins include CDK5RAP2, pericentrin, and CEP152. Their structure is lost during metaphase. Pericentrin is thought to be the determinant of the size of the inner layer or Zone 1 (Gopalakrishnan et al., 2011). The exact canonical sequence of protein assembly and the list of proteins in the inner layer of PCM is not known. Expansion of the PCM during mitosis happens through microtubule-associated proteins and microtubule nucleating proteins. The most notable two are Polo-like kinase 1 (PLK1) and Aurora Kinase A (AURKA) (Dobbelaere et al., 2008). PLK1 substrates are pericentrin, Cnn, SPD-5. Aurora Kinase-A is responsible for further PCM maturation (Sumiyoshi et al., 2015). Due to Pericentrin representing the growth of the centrosomes (Fu et al., 2015), forming the bulk of the centrosomal scaffold (Lee and Rhee, 2011; Jiang et al., 2021;), being a determinant of the size of PCM (Gopalakrishnan et al., 2011), it was used here to represent centrosomal parameters (size and maturity in chapter 5). The parameters were compared with cell cycle parameters described later and are hypothesized to show correlations due to centrosomes housing cell cycle proteins (Lin et al., 2022) and being controlled by them (Dobbelaere et al., 2008). Pericentrin is a direct substrate of PLK1 (Dobbelaere et al., 2008), creating a direct link between cell cycle machinery and centrosome size/maturity strongly suggesting that centrosome amplification might correlate with PLK1 changes irrespective of which one of the two is a cause and consequence of each other.

1.7 The link between centrosomes and the cell cycle:

Once the centrosome is functional and contains the pericentriolar material, the centrosome is a scaffold for the events of the cell cycle on the PCM (Lin et al., 2022) The pathway of the G2/M transition is centralized around centrosome with the different pathways converging to proteins located on the centrosome (Cazales et al., 2005; Vigneron et al., 2018; Lin et al., 2022). These events lead to the activation of Cdc25 phosphatases and inactivation of Wee1 and Myt1 kinases to activate the mitotic Cyclin B-CDK1. In simple terms, initially, Cyclin B binds with CDK to form Cyclin B-CDK1 complex. Then, CDK activating kinase (CAK) phosphorylates CDK2 T-loop at a conserved threonine (160) for initial activation (Kaldis et al., 1998). Finally, Cdc25C phosphatase and Wee1/myt1 kinase activities are activated and inhibited respectively to ensure full activation of the Cyclin-B CDK complex (Potapova et al., 2011).

It is not known what is the cause of centrosome amplification, but it is known that their duplication is closely tied to the cell cycle (Fu et al., 2015). At the same time, the centrosome has been proposed as a cell cycle regulator (Lin et al., 2022; Gönczy et al., 2015). For example, Aurora A kinase and PLK1 function in the growth and maturation of the pericentriolar material (Jana, 2021), while centrosome is a scaffold for other cell cycle proteins. Moreover, Lin et al., (2022) describe how multiple proteins are recruited on the centrosome including CDK1, before the entry into the G2 phase, and there, active Cyclin B1-CDK1 complex is first seen. Boutros et al., (2007) show that Cdc25B, an activator of mitotic CDK1, is phosphorylated by kinases responding to environmental cues, such as Chk1 and pEG3 on centrosomes, inhibiting the Cdc25B phosphatase and thus preventing mitotic entry. Aurora A kinase phosphorylates Cdc25B on S353 on centrosomes activating it (Lindqvist et al., 2009). Aurora-A itself is associated with centrosomes and is crucial for mitotic entry (Dodson and Bayliss, 2012). The activation of Aurora A kinase by multiple proteins occurs on centrosomes, which almost act like a scaffold: CEP192, Ajuba, Bora, Nucleophosmin, ILK, TACC3, and Arpc1b, while FBXW7 localizes on centrosomes in late G2 to degrade Aurora A kinase (Lucie et al., 2017). Cdc25C, another phosphatase required for mitotic Cdk1 activation, downstream of Cdc25B is located and activated on centrosomes. Multiple phosphorylations of Cdc25C occur on centrosomes, including T67 (Franckhauser et al., 2010). Interestingly, Brca1, a protein involved in DNA damage repair, when inactive is held on centrosomes through the interaction with gamma-tubulin (Hsu, 2007). Chk1 must be localized on centrosomes for it to function properly: cells deficient in centrosomal proteins PCNT, MCPH1, and CDK5RAP2 result in Chk1 not being recruited on centrosomes and thus being dysfunctional (Lin et al., 2022). Cdc25A is another phosphatase important in the pathway of cyclin B-CDK1 activation and is phosphorylated by Chk1 on S123 on centrosomes targeting it for degradation and avoiding mitotic entry in the presence of DNA damage (Zhao et al., 2002). Mutants of S123 of Cdc25A promote centrosome amplification (Zhao et al., 2002). Cdc14 is kept on centrosomes during interphase, when active it downregulates Cdc25A (Vazquez-Novelle et al., 2010). PLK1, a major regulator of mitotic entry is likewise held on centrosomes and is found colocalized with cell cycle proteins such as Cdc25 phosphatases (Watanabe et al., 2005). PLK1 being on the PCM recruits other PCM proteins required for microtubule nucleation (Colicino and Hehnly, 2018). There are many other cell cycle events occurring on centrosomes, there will be more information about the cell cycle events and chronology later in this study.

On the other hand, the centrosome is also controlled by the cell cycle, as Cyclin E-Cdk2 controls the assembly of the daughter centriole at the start of the S phase (Fu et al., 2015). Nucleophosmin, being a component of PCM is phosphorylated by CDK2. Cyclin A promotes Orc1 recruitment to centrosomes where it prevents cyclin E-dependent reduplication of centrioles. p53 and SAPKKKs have also been implicated in linking cell cycle machinery to centrosomes, but the link is not fully established (Fu et al., 2015). The exact structure of the centrosome is complicated and how it is being built in cohort with the cell cycle is unknown. PLK4 is the initial building block of a new centriole, but it is not entirely known how the cell cycle regulates the initial assembly of the centrosome from around the mother centriole walls to a single spot (Park et al., 2019; Ganem et al., 2009). However, the events of the cell cycle are well studied and are presented below for the purpose of linking the centrosomes to the cell cycle: centrosome duplication is controlled by the cell cycle through PLK4 condensation, but here it will be studied whether amplified centrosomes affect the cell cycle, knowing that they act as cell cycle regulators (Lin et al., 2022).

1.8 The cell cycle:

G2/M transition is of special interest, since it appears to be tightly controlled by centrosome-localized events (Lin et al., 2022). It is important to understand the events of the G2/M transition for the purpose of choosing a respective set of antibodies to examine the effects of centrosome amplification on the kinetics of the cell cycle. These antibodies must be cell cycle regulatory proteins and either be linked with centrosomes, located on centrosomes, or regulated by the centrosomes. Providing a pathway for the G2/M transition will provide understanding of the systemic context of the chosen proteins.

The decision to enter mitosis culminates with the activation of the Cyclin B-CDK1 complex through a positive feedback loop where Wee1 and Myt1 CDK1 inhibiting kinases are inactivated and Cdc25C phosphatase is activated by the cyclin B-CDK1 complex (Desai et al., 1995). The complexity of the latter events increases exponentially when attempting to understand the upstream events. For example, the regulation cyclin B and CDK1 expression and complex formation, then subsequently, the regulation of the formation of CDK-activating kinase CAK which phosphorylates CDK1 on T161 (Coulonval et al., 2011) allowing the Cyclin B-CDK1 complex formation.

The regulation of CDK1 activity by CAK and Wee1 kinases, as well as the activity of the CDC25C phosphatase in more detail is overviewed in the results section.

Cyclin B is synthesized during the S and G2 phases of the cell cycle and it eventually reaches a certain threshold level where it can bind CDK1 in a regulated manner (Barbiero et al., 2022). Cyclin B potential transcription factors are MyoD (Ishibashi et al., 2005), and E12-E47n (Beck et al., 2009) NF-Y (Park et al., 2007), SP1 (Chuang et al., 2012) due to E-box sequences (CACGTG) and USF (Cogswell et al., 1995). These transcription factors were speculated to become activated in previous cyclin-dependent pathways (Landry et al., 2014). Cyclin B is expressed in a cell cycle-dependent manner through the use of alternative transcription start sites (Mouawad et al., 2020). Lastly, FoxM1 was shown to be able to transcribe cyclin B in a timely manner (Laoukili et al., 2005), which is potentially activated by PLK1 as explained previously. CDK1 on the other hand is kept at constant levels throughout the cell cycle through coordination of its synthesis and degradation. As the cell grows, CDK1 concentration must be maintained, thus it is being synthesized (Gavet and Pines, 2010). CAK is composed of Cyclin H, Mat1, and CDK7. Once assembled they form the active CAK1 which operates in a positive feedback loop with the cyclin B-CDK1 complex in the nucleus (Sava et al., 2020). Coulonval et al., (2011) explain the coupling of the two inhibitory phosphorylations of CDK1 (T14 and Y15) with the activatory T161 phosphorylation and have concluded that these phosphorylations are precisely timed due to them affecting the ability of cyclin to bind CDK1. For example, T161 phosphorylation must be timed exactly when cyclin B binds the CDK, etc… The removal of the two inhibitory phosphates on CDK1 residing on T14 and Y15 is accurately timed with the latter. Cdc25A,B and C phosphatases are dependent on Chk1 activity drop (Gardino and Yaffe, 2011), which must be coordinated with PLK1 activity to remove 14-3-3 proteins (Jaiswal et al., 2024); to control cyclin B movement into the nucleus (Jackman et al., 2003). Lastly, Wee1 activity must be inhibited in cohorts with the latter (Potapova et al., 2011), which also appears to be dependent partly on Chk1 (Gardino and Yaffe, 2011). There are many other proteins involved in the pathway of cyclin B-CDK1 activation, but due to their complexity of it, systemic tools are more practical than journal articles.

The exact role of each protein in G2/M transition is not fully known – proteins are not mutually exclusive for a specific pathway e.g. Cdc25C activiation or PCM expansion. Instead stress pathway, perpetual cell cycle machinery and DNA damage pathway appear to be largely interlinked. As a result, this study provides a sysgtemic overview of each protein to be able to judge its role in the 3

pathways and determine its suitability for immunofluorescent antibody testing. A ‘suitable’ protein in this study is one that participates in all 3 pathways in addition to centrosomal dynamics. In the current study, using online tools, the proteins of interest were identified. Potential candidates are Aurora Kinase-A, CDC25 phosphatases and 14-3-3. In cases where a phenomenon is attempted to be examined through the understanding of its component parts, it is called reductionism. However, in the case here, the role of each protein in the cell cycle has been examined through its interactions with other proteins, which is a holistic approach, often used in systems biology (Mazzocchi, 2012). The identified proteins were subjected to further analysis to test how their parameters and dynamics are affected by the amplification of centrosomes using fluorescent antibodies.

Chapter 2: Methods

2.1 Pathway construction of the G2/M transition:

G2/M transition needs to be visualized in detail because later in this study, the kinetics of key G2/M transition proteins have been tested. The proteins to be determined must be both participants of the cell cycle kinetics and centrosome kinetics or growth. To determine the regulatory proteins and their position in the cell cycle, systematic tools have been utilized and are explained below.

The platform Visant (Granger et al., 2016) provides directly interacting proteins for the protein of interest. Reactome (Gillespie et al., 2022) database shows the protein interactions in the context of pathways. Pathcards (Belinky et al., 2015) show the list of pathways and processes in which the protein is involved. Lastly, the STRING database (Szklarczyk et al., 2021) shows specific interactions of queried protein or a gene and the type of interaction.

The process of construction of a pathway goes as follows:

1. The initial proteins are subjected to VisANT from the information presented in the literature described in the introduction.
2. Visant (Granger et al., 2016) was used to visualize the interactions of the mentioned proteins. Furthermore, additional proteins have been visualized which act as nodes. Nodes are proteins not mentioned in the literature but are connected to one or more different proteins that are already in the Visant platform i.e. proteins from the literature. Therefore, nodes serve as bridging molecules between other proteins or can be new proteins within the diagram. In this study, the 4 degrees of separation method is used which means that known proteins can be connected by not more than 4 nodes to be considered. If a node is not bridging two proteins, 4 degrees of separation still applies to it from the original protein.
3. Reactome (Gillespie et al., 2022) is used to confirm or deny the node's involvement in the pathways of interest through the subjection of the node's of interest direct interactors determined by VISANT as a query to the search engine of Reactome. If the overrepresented pathways involve relevant pathways, then the protein is considered as

part of the pathway. Overrepresentation is concluded by a mathematical calculation where the proportion of genes related to the query and subject exceeds the proportion of such genes to be randomly expected (Fabregat et al., 2017).

4. Pathcards (Belinky et al., 2015) are then used to check if the nodes connecting the cell cycle proteins from literature, when queried, do come up with respectable pathways in the results. The pathways of interest are DNA damage, environmental stress, and cell cycle control. If the top relevance score involves either cell cycle, DNA damage control, or stress pathway the protein is not filtered out. Otherwise, it is filtered out. In case pathcards results are vague, NCBI description in Genecards (Stelzer et al., 2016) is considered to judge proteins' involvement in cell cycle, stress, or DNA damage checkpoint regulation.
5. In the final pathway, if any protein contains an interactor that does not bridge into another protein, but is of relevant pathways determined by the tools above, it is included in the diagram. As a result, these nodes are only connected once to another protein in the final pathway diagram.

The reason why proteins involved in cell cycle, stress pathways or DNA damage checkpoint pathways are kept is because these are the main pathways regulating entry into mitosis through the active Cyclin B-CDK1 formation. The proteins (described in literature review) initially subjected to VisANT all stem from any of these 3 pathways. As a result filtering out any protein but not such that is involved in these pathways would hypothetically provide a functional set of interactions.

Below is an example of the workflow described above to find the potential mechanism of KIFC1 involvement in the cell cycle.

The literature presents KIFC1's involvement in the cell cycle (Pannu et al., 2015; Patel et al., 2018; Wei et al., 2019). The proteins of the cell cycle mentioned in the literature review are subjected to VISANT. KIFC1 is also subjected to VISANT.

The figure below portrays KIFC1 with direct interactions:

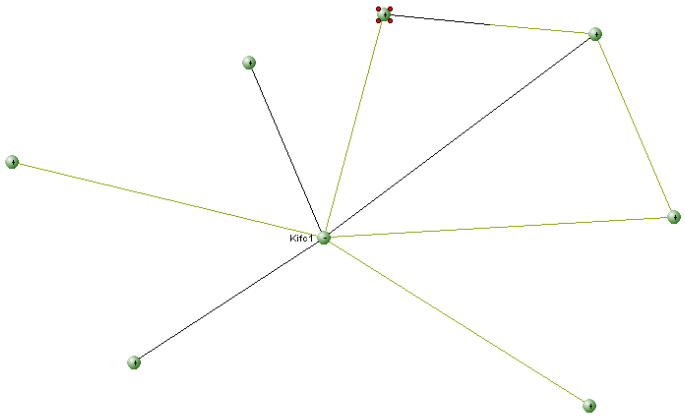

Figure 2.1: **Example output from Visant** (Granger et al., 2016), displaying direct interactors of KIFC1.

Visant shows 4 direct interactions which are recognized in the Pathcards (Belinky et al., 2015) database. The proteins are RNF169, CXXC1, CCDC8, RG9MTD1. As of so far, none of these proteins show direct interactions with cell cycle proteins such as CHK1, CHK2, AURKA, CDC25A, B, C, CCDC1, PLK1, CDC14, etc. However, it is possible that any direct interactor of the KIFC1 direct interactors may connect to one of the aforementioned proteins. One possibility, for example, is KIFC1-CXXC1-EP300-FoxM1. However, it still needs to be tested whether these interactions are meaningful, since for example, coprecipitation experiments cannot assure a pathway from such results.

The direct interactors of KIFC1 and KIFC1 itself are then subjected to the reactome analysis tool. To see if they project into any relevant pathway. Relevant Reactome output consists of Cell-cycle, responses to stimuli. The total number of pathways that were overrepresented was less than 20. The figure below portrays the Reactome output which connects KIFC1 to the cell cycle pathway:

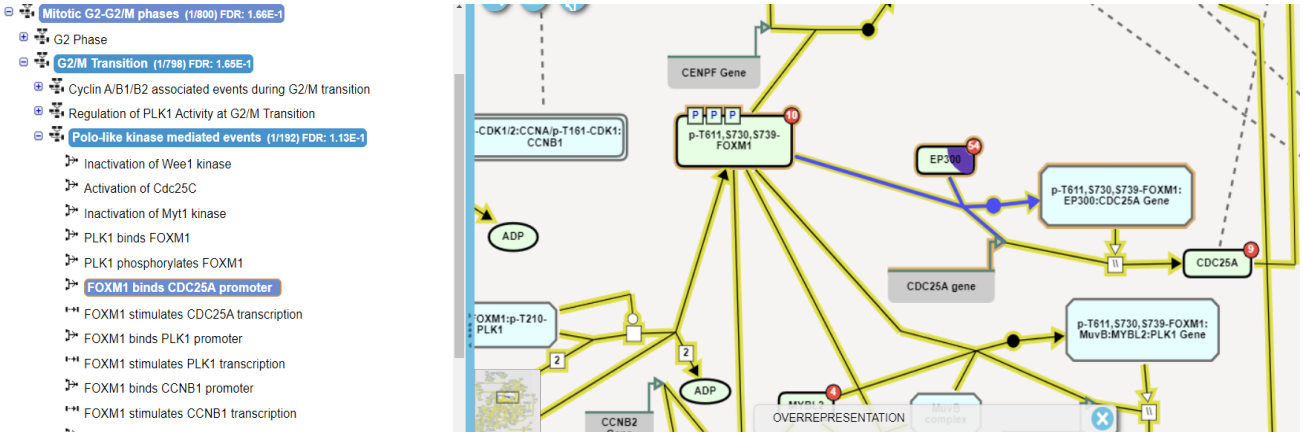

Figure 2.2**: Reactome pathway overrepresentation output** (Gillespie et al., 2022). Reactome output of KIFC1 direct interactors and KIFC1 includes G2/M transition event where FoxM1 transcription factor, which is involved in transcription of cyclin B and is also activated by AURKA and PLK1, binds Cdc25A promoter. Cellular responses to stimuli was also a pathway overrepresented by the direct interactors of KIFC1.

The connection of KIFC1 with FoxM1 goes as mentioned previously: KIFC1- CXXC1 – EP300 – FoxM1. EP300 is an additional node bridging CXXC1 to FoxM1. But now that Reactome has shown an overrepresentation of genes for these pathways, it can be a lot more likely that KIFC1- CXXC1 – EP300 – FoxM1 is a pathway.

Subsequently, Pathcards are used to evaluate the relevance of CXXC1 in the cell cycle, stress, and DNA damage checkpoint pathways. Since these pathways are not mutually exclusive, one of them in the Pathcards output is considered to be a pass, even if the Reactome output included the Cell cycle pathway, but not the environmental stress/cellular responses pathway.

Figure below shows an example output in Pathcards for the protein CXXC1.

7 search results for **CXXC1**

#		SuperPathway Name	Genes Count	Relevance Score
1	+	Gene expression (Transcription)	1546	0.632
2	+	Cellular responses to stimuli	802	0.632
3	+	Unfolded Protein Response (UPR)	94	0.632
4	+	Chromatin Regulation / Acetylation	255	0.632
5	+	Male infertility	52	0.632
6	+	Formation of WDR5-containing histone-modifying complexes	42	0.632
7	+	RNA Polymerase I Promoter Opening	509	0.632

Figure 2.3: The highest relevance score (0,632) involves two relevant pathways: Cellular responses to stimuli and unfolded protein response. Relevance score is also known as the similarity index. It is obtained by calculating the Jaccard coefficient: The number of genes for the protein of interest (CXXC1) which are common with any other pathway outputted divided by the combined number of genes in protein of interest and in the pathway, but without the overlapping genes. It can be depicted as: $\frac{Common\ genes\ for\ protein\ of\ interest\ and\ pathway}{total\ protein\ of\ interest\ genes + total\ pathway\ genes - common\ genes\ for\ both}$ (Belinky et al., 2015).

CXXC1 as a result passes the pathcards filtering to confirm that KIFC1 may be involved in the cell cycle through the CXXC1 protein. Pathcards result for EP300 recognized as P300 shows that it is involved in transcription and transcription regulation. Upon further inspection, GeneCards (Stelzer et al., 2016) describe it as important in many processes, two of which are cellular proliferation (cell cycle) and response to hypoxia (Stress).

The same analysis has been performed for all of the cell cycle, stress, and DNA damage checkpoint proteins to bridge them together or are linking nodes, and form a pathway which is then evaluated by the PathCards database as explained above.

2.2 Cell Culture:

Live cell imaging of the cell cycle using H2B-FUCCI2a stably transfected OMM2.3 cells.

FUCCI construct:

The H2B-FUCCI_2a OMM2.3 are stably transfected with the construct encoding the proteins mCerulean-H2B, mCherry-cdt1, mVenus-geminin. The mCherry is seen red and is bound to the destruction box domain of Cdt1. Cdt1 exists during the G1 phase of the cell cycle and is degraded during the rest of the cell cycle, thus it is seen as red during the G1 phase and represents the cell in the G1 phase. mVenus-geminin, just like geminin, is being synthesized during the S phase and is present until Anaphase, and shows up green under the fluorescent microscope during the period from S phase until anaphase. mVenus is bound to the destruction box domain of geminin. H2B is seen in cerulean color, localises to the nucleus, and is used for marking the cell locations so that the Trackmate plugin can always detect a cell from an H2B-derived channel and track the fluorescence of CDT1 and geminin of that area where cerulean H2B is present. OMM2.3 cells have been stably transfected with this construct. As a result, normal cells express both endogenous and exogenous Cdt1 and Geminin. Detailed explanations and uses of the construct are described by Mort et al., (2014).

H2B_FUCCI2a_OMM2.3 cells (OMM2.3 cells a kind gift from Sarah Coupland, Liverpool. Stable transfections of H2B_FUCCI2a were performed in Fielding Lab, Lancaster) were grown in RPMI media with 10% FBS and 1% penicillin/streptomycin (p/s). To count the cells, they were trypsinized to remove them from the base of the flask and pipetted into a hemocytometer. 200µL cells were put into a hemocytometer with a cover slip on top. A hemocytometer square holds 100nL of liquid. Respective volume has been taken, for example in the case of recording cell cycle lengths, 50 µL was used to obtain 5000 cells within a well. Once the cells had been transferred into the glass-bottomed wells, they were put into an incubator at 37^{o}C , 5% CO2. Cells were left overnight. To confirm that the cells have stuck onto the bottom of the wells, a light microscope has been used. The inhibitor AZ82 at 1µM and the degrader PROTAC at 1µM have been pipetted into the wells just before the start of the recording.

The glass-bottomed wells were supplied with DMSO, PROTAC, and AZ82 as shown below:

5000 cells DMSO	5000 cells PROTAC (1µM)	5000 cells AZ82 (1µM)

Figure 2.4: **The arrangement of cells in a glass bottomed well.** In the 24 well plate, 3 wells have been occupied as shown in the figure. In each of the 3 wells, 3 positions have been recorded using the fluorescent microscope. To each well, 1 milliliter of cell culture media and 1 microliter of AZ82, PROTAC or DMSO was added as shown.

Correleative Live cell and ImmunoFluorescence microscopy:

OMM2.3_H2B-FUCCI2a cells were imaged as a timelapse on a Zeiss LSM880 confocal microscope with a Plan-Apochromat 20x/0.8 M27 objective. Cells were seeded into a glass bottom 24 well plate (P24-1.5P, Cellvis). During imaging, cells were maintained at 37°C and 5% CO2 using the TempModule S1 (800-450000, Pecon) and CO2 Module S1 (810-450001, Pecon). Cells were imaged every 15 minutes in three fields of view per treatment. A Focus Controller 2 (Zeiss) was used to ensure cells stayed in focus over the time series.

After the 70-hour recording has been finished, cells have been fixed with methanol, which both fixes the cells and quenches the fluorsesence of the fluorescent protein conjugates (mCherry-CDT1, mVenus-Geminin and mCerulean-H2B). Subsequently, the cells were labelled for immunorfluoesence imaging, with pericentrin and tubulin antibodies, as described below. The cells were brought back under the microscope, the same fields of view that had been used for live cell imaging retrieved, and were examined for centrosome amplification. The coordinates of each cell have been recorded to ensure that centrosome-amplified cells can be found in the recording file. For chapter 5, a different set of antibodies was used as described below.

Immunofluoresence Microscopy:

OMM2.3_FUCCI2a cells were plated onto 6 (for chapter 5) or 24 (for chapter 4) well plates containing coverslips. The cells were in RPMI supplemented with 10% Fetal Bovine Serum and 1%P/S. From the plates, media were removed and they were rinsed with PBS. Subsequently, 2mL of ice-cold methanol was supplemented to fix and permeabilize cells and then incubated at -20^{o}C. Methanol was removed and 2000µL PBS was added to each well. For the first set of immunofluorescent antibodies, the methanol fixation was done immediately after the live cell imaging has finished.

A blocking solution was made from 5% goat serum in PBS to a 4ml volume. Coverslips from the 6 or 24 well plates have been placed on parafilm in an immuno-fluorescence tray. 200 µL blocking solution has been added to each coverslip and left for 30 minutes. To make the primary antibody solution, 0.2µL of each primary antibody was mixed with 200µL 5% goat serum. Subsequently, the blocking solution was removed from the coverslips and 200µL of primary antibodies were supplied onto each coverslip. The coverslips in the immunofluorescence tray have been incubated for 1.5 hours at room temperature**.** After the incubation, the primary antibodies were removed and coverslips were rinsed three times with PBS.

To prepare the secondary antibodies (goat), 2µL of each secondary antibody was mixed with 1mL 5% goat serum to make a 1/500 dilution. Each antibody combination, containing anti-mouse, anti-rabbit, and anti-rat antibodies was added onto each coverslip (200µL) and incubated at room temperature for 1h in the dark. Then the secondary antibody mix (unbound) was removed and coverslips were washed three times with PBS. 20µL of Mowiol/DAPI mix has been put onto the slides ensuring no bubble formation. Any excess liquids on the coverslips have been removed using a Kimi wipe. Coverslips have then been turned upside down and put onto the slides with DAPI and mowiol to put the cells into contact with DAPI and mowiol. Slides were allowed to dry and were imaged.

Figure below shows the primary antibody combinations.

	1st primary (mouse)	2nd primary (rabbit)	3rd primary (rat)
1	Pericentrin (mo) 1:1000	pAurA (rb) 1:1000	Alpha-Tubulin (rat) 1:1000
2	Pericentrin (mo) 1:1000	pPLK1 (Rb) 1:1000	Alpha-Tubulin (rat) 1:1000
4	Pericentrin (mo) 1:1000	Aurora-A (Rb) 1:1000	gamma-tubulin 1:1000 (rat)

Figure 2.4: **The organisation of primary antibody mixtures for chapter 5.** 3 different combinations of antibodies have been used as shown in the figure. These antibodies have been supplied onto the cover slips held in an immunofluorescence tray.

Antibodies used to determine centrosome status for cells whose cell cycle lengths are known:

	2nd primary (rabbit)	3rd primary (rat)
1	Pericentrin (rb) 1:1000	Alpha-Tubulin (rat) 1:1000

Figure 2.4: **The organisation of primary antibody mixtures for the chapter 4 data collection.** These atibodies have been supplied into 24-well glass bottomed plate, after fixing with methanol.

2.3. Data processing

Measuring the lengths of G1 phase and the S phase to Anaphase period:

To measure the lengths of the cell cycle phases, cells were detected in Fiji using the Stardist plugin. Once they were detected, they were being tracked using the Trackmate plugin. The maximum frame-to-frame linking setting was set to 30 micrometers. After that distance, the cells are considered separate entities. The gap closing, between two cells was set to 30 micrometers. The Max frame gap was set to 5, which means after 5 or more frames of no detection, the cell within 30 micrometers of the previous cell will be considered as a new cell. Track segment splitting – 15 frames. When Trackmate is finished running, the following results window appears:

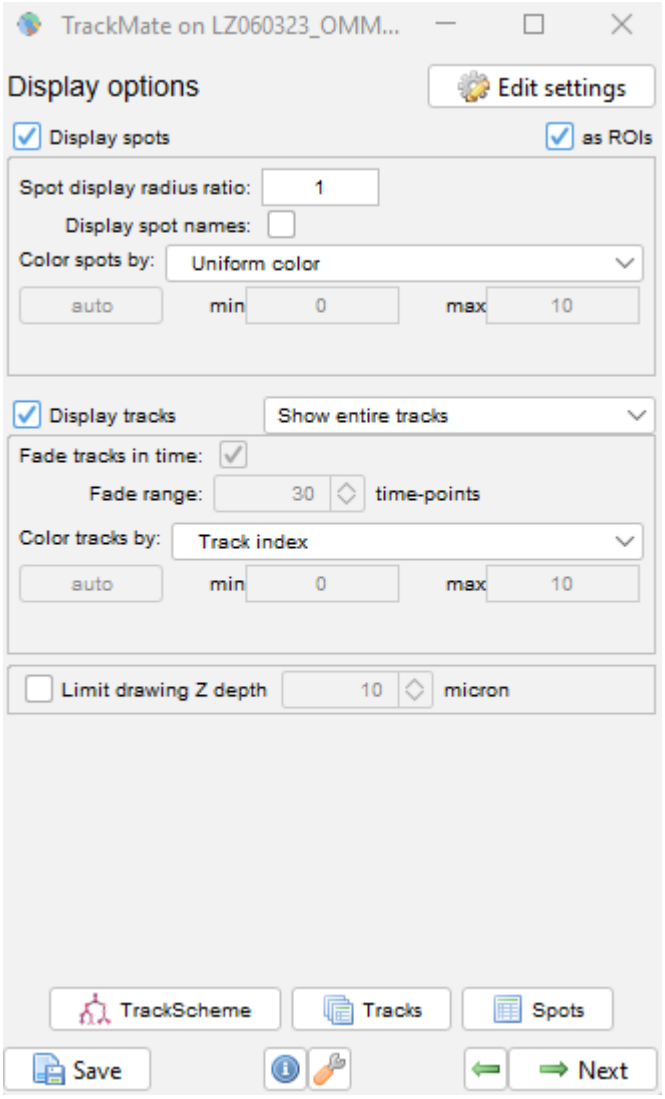

Figure 2.5: **The options window of the recording.** Show entire tracks allows to see the movement of the cell throughout the recording. The “Tracks” option provides quantifiied information about the channels detected. The processing of images and recordings were performed on Fiji (Schindelin et al., 2012).

Upon selecting to show the “Tracks” table, the results show each cell in every frame. The figure below show the output table sorted by cells:

Label	Spot ID	Track ID	Quality (quality)	X (micron)	Y (micron)	Z (micron)	T (sec)	Frame
ID2009	2009	1	0,89	408,32	192,89	0	0	0
ID2073	2073	1	0,88	412,72	188,01	0	898,54	1
ID2113	2113	1	0,9	416,28	188,44	0	1 797,09	2
ID2159	2159	1	0,91	419,15	187,86	0	2 695,63	3
ID2213	2213	1	0,91	420,51	186,36	0	3 594,18	4
ID2286	2286	1	0,86	423,37	186,86	0	4 492,72	5
ID2320	2320	1	0,9	423,81	187,43	0	5 391,27	6
ID2387	2387	1	0,88	424,16	186,39	0	6 289,81	7
ID2448	2448	1	0,87	424,31	186,72	0	7 188,36	8
ID2505	2505	1	0,87	423,54	186,43	0	8 086,9	9
ID2549	2549	1	0,89	423,12	185,74	0	8 985,44	10
ID2602	2602	1	0,89	420,85	184,79	0	9 883,99	11
ID2663	2663	1	0,88	420,78	185,33	0	10 782,53	12

Figure 2.5: **The output table with quantifiable details from each channel.** The details from this window were sorted framewise to obtain the chronological order of fluorescence change from the CDT1 and Geminin derived channels.

Track ID represents an individual cell. The video is sorted by frames. The table also portrays mean fluorescence value of the cell per frame. Figure below shows the output table for signal intensities and a graph where signal intensities are plotted against time.

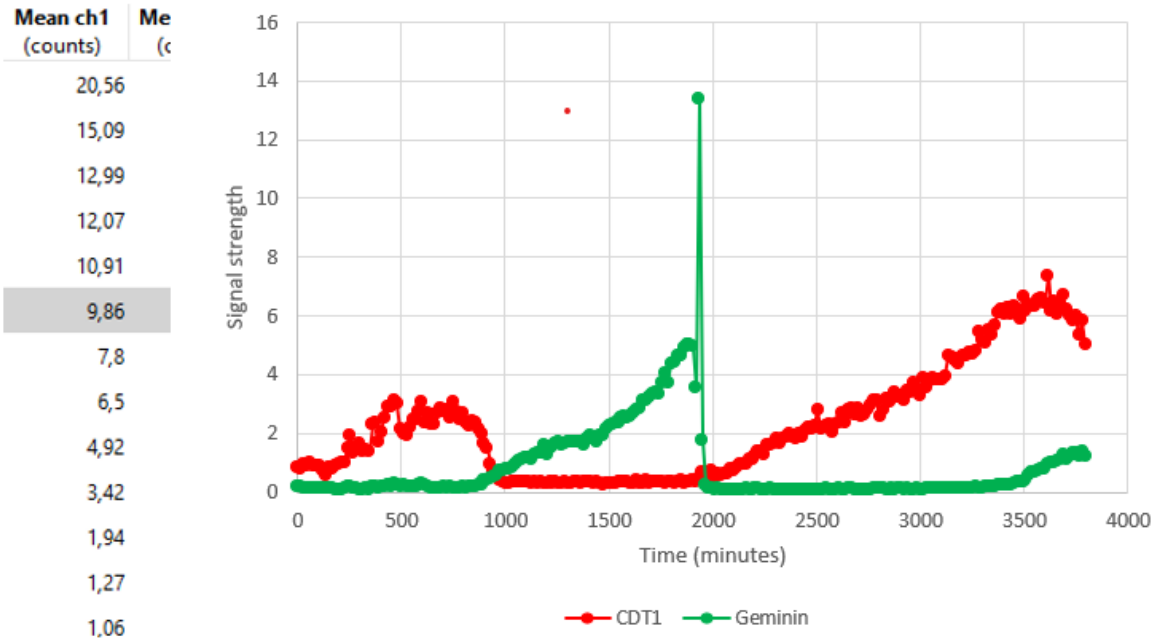

Figure 2.5: **The output table column which represents fluorescence signal strengths and a plot against time.** The signal intensity values have been graphed with respect to time to observe the change in signal intensity. The start of a phase is considered when the fluorescence starts rising, for example from Geminin fluorescence, S phase begins at around minute 900 and ends at around minute 1950.

Ussually, the plotted data may contain an outlier as seen from the figure above. Outlier is ignored if it does not affect the general trend obtained in the plot.

Quantifying the fluorescence area of a channel :

The acquisition is set to portray separate channels in separate windows. Figure 2.7 shows the green (pericentrin) channel, (figure 2.7, (1)). To deduce the area over which the channel covers the image, thresholding has been used. For every acquisition, a consistent thresholding setting has been utilized. The thresholding method is default, set to cover 0,75% of the pixels with value, the resulting pixels are shown in figure 2.7 (2).

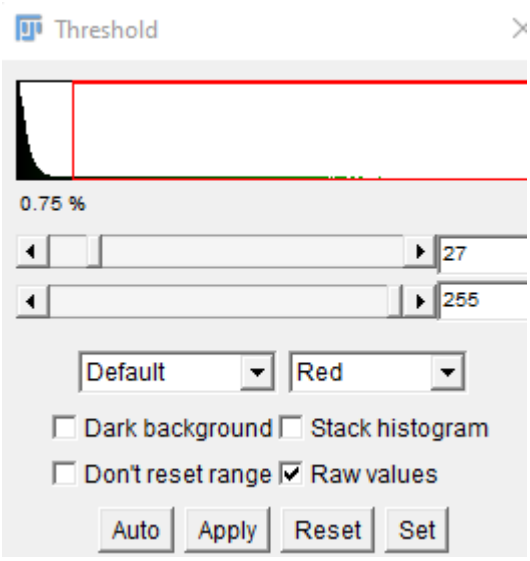

Figure 2.6: **The thresholding setting.** This setting has been used on every image to capture the signal that only represents centrosomal signal.

Subsequently, the thresholded area is selected and a mask is created (figure 2.7 (3)). Binary operations have been processed on the image in this order: Dilate, erode, open, fill holes, dilate, close, despeckle, and remove noise (> 10 pixels), (figure 2.7 (4)). The following mask has been used to create a selection of its area over the original image by edit – create selection on the mask and subsequently: edit–restore selection on the original image (figure 2.7 (5)).

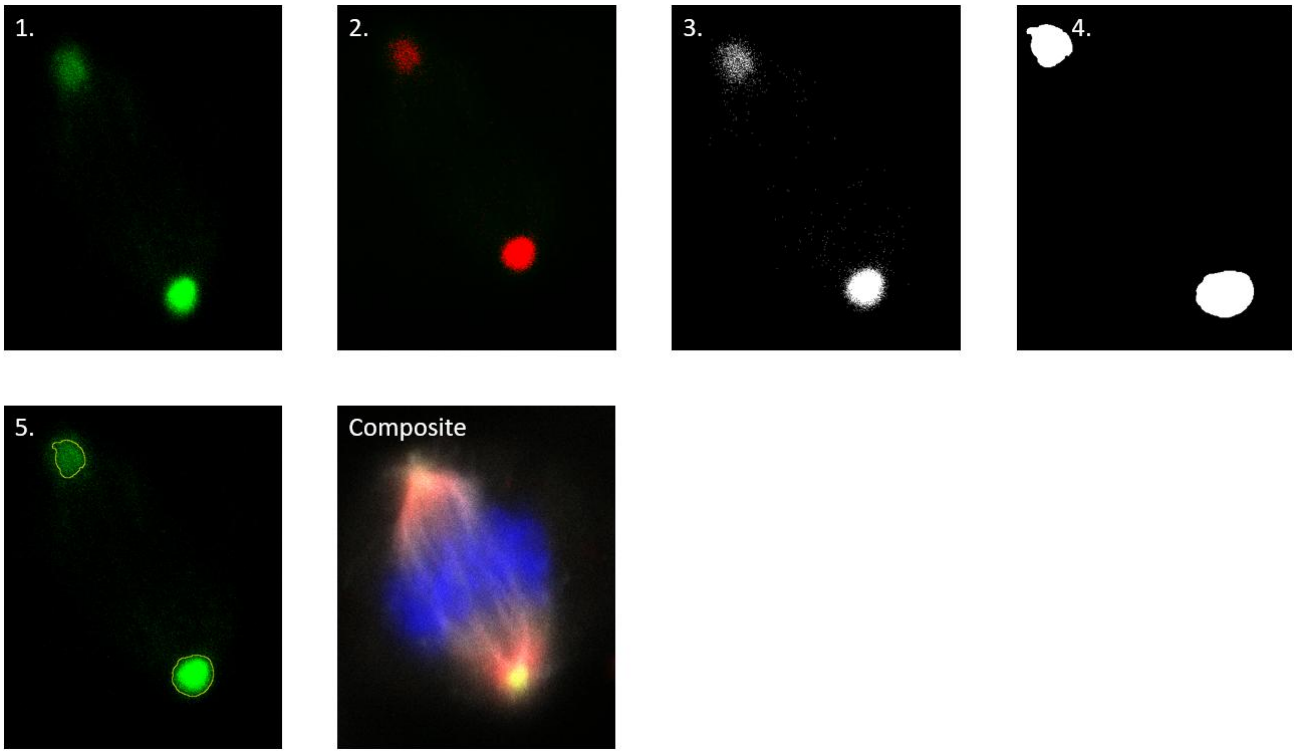

Figure 2.7: **Example workflow of obtaining the area for which parameters are calculated.** To count centrosomes, as done for chapters 4 and 5, no image editing was required, as centrosomes are seen as discrete structures of respective fluorescent colour.

Now that the centrosome boundaries are set, the following quantifications have been performed on the original image: Area, mean gray value and integrated density.

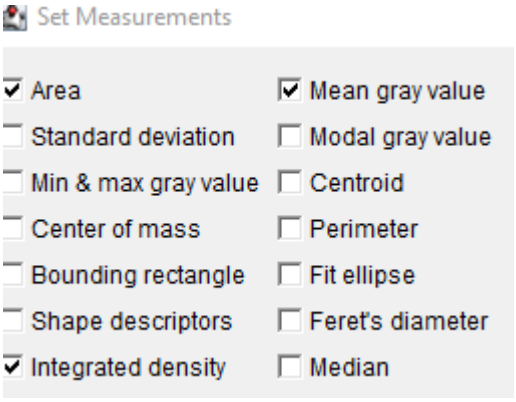

Figure 2.8: **The output parameter choices.**

The same operations have been made for any other tested channel, for example, AURKA (red channel) of this acquisition. To deduce the area of other channel fluorescence, for example, AURKA area coverage, the same method has been utilized, just on the respective channel.

Chapter 3 Results:

G2/M Pathway analysis: identifying centrosomal G2/M signalling indicators

3.0 Introduction

The purpose of the G2/M pathway construction is to understand the regulatory proteins of the pathway. The visualisation of the pathway allows to judge each protein's functions and compare it with that of others. Once the key regulatory molecules are filtered out, their link with centrosomes is examined through the databases outlined in the method section and with the aid of literature. The pathway constructed here is branched into three parts as shown in the figure below. PLK1 and AURKA are two of the few proteins inclusive of all parts. 14-3-3 and the different variants are also involved in many pathways, but due to their lack of participation in centrosome dynamics, they were not chosen to set up antibodies against them. For the chosen proteins, the antibodies have been set up to examine their relationship with pericentrin. Polo-like Kinase-1 (PLK1) and Aurora Kinase-A (AURKA), in addition to their phospho-forms were the central proteins.

The following figure portrays the G2/M pathway after expanding the pathway from literature review by using the systemic tools.

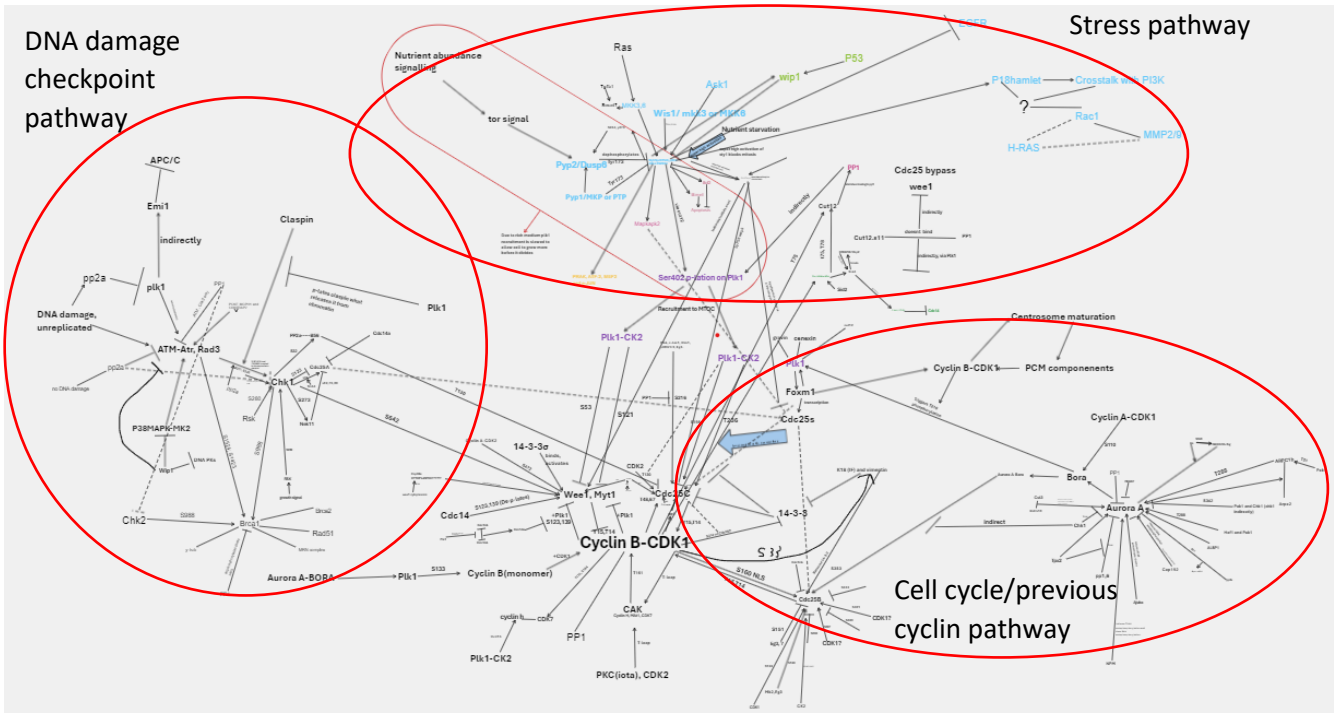

Figure 3.10: **The expanded G2/M transition pathway**. The pathway can be divided into cell cycle machinery, stress, and DNA damage checkpoint control parts. Portrayed on Microsoft Whiteboard (Microsoft Corporation, 2023)..

3.1 Overview of the pathway:

PLK1 and AURKA function in the cell cycle homeostatic machinery, as described below.

Aurora Kinase-A and PLK1 are essential proteins in the G2/M transition (Bruinsma et al., 2015). Both of these proteins function in multiple common pathways of the activation of the Cyclin-B-CDK1 complex. The pathway culminates with CDK1 being dephosphorylated by Cdc25C on T14 and Y15 (Gheghiani et al., 2017). Plk1 phosphorylates Cdc25C to remove 14-3-3, which acts in a positive feedback loop with cyclin B-Cdk1, opposing the actions of Wee1 and Myt1 kinases. While Cdc25B does not act in the positive feedback loop, most likely it acts only in the initial activation of CDK1 which then sets off the positive feedback loop with Cdc25C (Lindqvist et al., 2005; Bulavin et al., 2003; Vazquez-Novelle et al., 2010). pPLK1 phosphorylates Cdc25C on S198 after 14-3-3 has been removed (Schmucker and Sumara, 2014) since it hinders this site and subsequently, Cdc25C can move into the nucleus to activate Cdk1 (Bulavin et al., 2003). Cdc25B is activated by phospho-Aurora Kinase A (Cazales et al., 2005). PLK1 also initiates cyclin-B activation. PLK1 phosphorylates it on S133 on centrosomes initiating autophosphorylations for full cyclin B activation (Jackman et al., 2003). Schmucker and Sumara (2014) explain that PLK1 is expressed only after the completion of the S phase. Aurora Kinase-A phosphorylates S137 and T210 on PLK1 releasing the kinase domain from the polo domain allowing the kinase to interact with other substrates, thus activating PLK1 allowing to perform the aforementioned functions. AURKA itself is activated by the events of the previous CDK, which is cyclin A-CDK1.

Other than cell cycle events occurring on centrosomes, there are other events occurring on centrosomes – the environmental stress response pathway and the DNA replication checkpoint pathway.

The stress pathway is described below.

Environmental condition changes such as lack of nutrients result in Pyp2 activity drops avoiding Sty1 phosphorylation and thus inhibition. This results into Sty1 activation which phosphorylates Plo1 (plk1 homologue) on Serine 402 (Hagan, 2008). The phosphorylation of Plo1/PLK1 results in its recruitment to the yeast SPB/centrosome (Kowalczyk et al., 2013). For example, when there is nutrient stress, TOR signalling is reduced, and Pyp2 activity drops, leaving more Sty1 activity. This results in a more frequent division as it allows cells to divide at smaller sizes due to nutrient

deficiency through the recruitment of PLK1 to the centrosome (Kowalczyk et al., 2013). Another yeast protein Cut12 (Stf1 homologue) is responsible for the recruitment of Plo1 to the spindle pole body in mitosis (Maciver et al., 2003). This recruitment is dependent on nutrient availability to match the rate of cell divisions (Petersen et al., 2005). Cha et al., (2007) state that P38MAP kinases phosphorylate Cdc25B on centrosomes resulting in 14-3-3 inhibitory binding. The P38MAPK pathway is active in response to environmental stress and inflammation (Boutros et al., 2007). The phosphorylation site is Serine 309 which is associated with 14-3-3 inhibitory binding, preventing association with PLK1 (Gardino and Yafe, 2011). Aurora Kinase-A is also involved in stress response pathways. Cubillos-Ruiz et al., (2017) explain that cancer cells create many different types of stress in cells activating respective pathways which leads to an accumulation of unfolded proteins in the endoplasmic reticulum. (Lu et al., 2022) have shown that Aurora kinase-A is essential in mediating the unfolded protein response in cancer cells. It is also known that AURKA is involved in the p38MAPK stress response pathway because inhibition of AURKA using Alisertib downregulates the p38MAPK pathways (Li et al., 2015).

Aurora Kinase A and PLK1 are both involved in the DNA checkpoint pathways to mediate cell cycle transitions once the replication checkpoints have been passed.

PLK1 activatory T210 phosphorylation occurs on centrosomes and is dependent on AURKA (Vigneron et al., 2018). AURKA can be activated by BORA which is activated by Cyclin A-CDK1 phosphorylating it on S110. However, Aurora Kinase-A is not fully activated until Checkpoint kinase 1 (Chk1) activity drops. Once the checkpoint has been passed, T288 is phosphorylated on AURKA (Bruinsma et al., 2015; Cazales et al., 2005). The activation of PLK1 by AURKA results in FoxM1 transcription factor activation which is responsible for G2/M transition genes such as cyclin B transcription (Laoukili et al., 2005). The cellular localisation of Wee1 kinase is controlled by Chk1 and PLK1 (Gooijer et al., 2017). phosphoPLK1 associates with pAURKA and phosphorylates Wee1 on S53 targeting it for degradation in a Chk1-dependent manner, where Chk1 activity must be low for the latter to occur. Reducing Chk1 activity is a result of the DNA replication completion. In response to Chk1 activity drop Aurora A kinase is activated and phosphorylates Cdc25B on S353 (Cazales et al., 2005) which is one of the requirements for the protein to become active.

Chk1 can relay the signal to mitotic proteins directly, without bridging through AURKA and PLK1 which both mainly localise to centrosomes (Asteriti et al., 2015), altough PLK1 and AURKA cross-talk to recruit Chk1 (Asteriti et al., 2015). For example, Zhao et al., (2002) have shown that the

DNA damage system directly relays inhibitory signals to the cell cycle machinery, as Chk1 can phosphorylate Cdc25A on S123 to target it for degradation. Melixetian et al., (2009) have also shown other pathways through which Chk1 negatively regulates mitosis commitment. However, it is unlikely that the positive control of mitosis can proceed without AURKA and PLK1. Either way, the recruitment of Chk1 to the centrosome is essential for the arrest of the cell cycle after DNA damage has been detected (Lin et al., 2022) and its recruitment is dependent on AURKA and PLK1 (Asteriti et al., 2015). Kramer et al., (2004) have shown that an early inhibition of Chk1 results in early centrosome separation and Cdk1 activation, showing that Chk1 must remain active until the cell is ready to enter mitosis. Since centrosome-associated Chk1 controls the activation of Cdc25B (Kramer et al., 2004), it can thus be said that Chk1 is essential to initiate the feedback loops between Cdc25 phosphatases and Cdk1, which are also dependent on phosphorylated AURKA and PLK1. Chk1 can also phosphorylate 14-3-3 binding sites on Cdc25B which are presented by Boutros et al., (2008), what masks PLK1 binding site. That shows that Chk1 controls PLK1-Cdc25B interaction through 14-3-3. The inactivation of 14-3-3 binding to Cdc25B occurs passively by Chk1 activity drop since PP1 and PP6 are able to dephosphorylate the 14-3-3 binding sites on Cdc25B (Lucie et al., 2016). Tibelius et al., (2009) have shown that the absence of pericentrin results in loss of Chk1 from centrosomes leading to early activation of the mitotic CDK, and pericentrin accumulation is dependent on pAURKA (Jana, 2021).

Overall, it appears that multiple pathways – stress, DNA damage, and the perpetual cell cycle pathway (previous CDK activating the next one) converge to the PLK1-AURKA dependent Cyclin-B CDK1 activity regulation, which happens on centrosomes.

The next figure shows the initial pathway before utilisation of systemic tools:

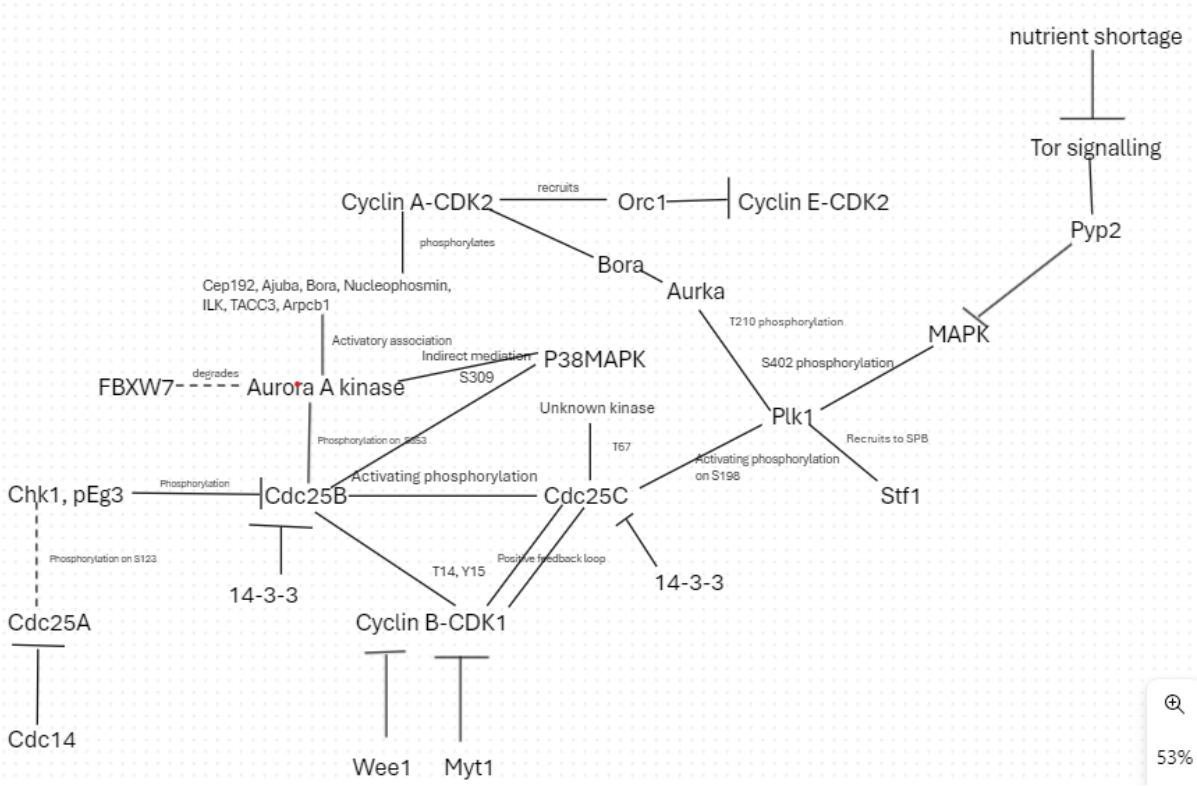

Figure 3.2: **The initial unexpanded pathway of the G2/M transition**. This set of protein interactions was used as described in section 2.1. Additional proteins could have been used, but were excluded do to the complexity of using a large number of molecules with the method described. Each protein in this pathway has been expanded in terms of interactions it contains in VisANT (Granger et al., 2016). If the interactors (nodes) then connect to another protein in this pathway, and are not filtered out it, they were shown in the previous figure. 4 nodes can be the most nodes bridging the proteins shown here. Portrayed on Microsoft Whiteboard (Microsoft Corporation, 2023). In this figure it is seen that the 4 direct interactors of cyclin B-CDK1 regulate the two main phosphosites of CDK1 – T14 and Y15. It appears that the activatory (dephosphorylation of T14 and Y15) pathway layer contains much more pathway control, suggesting that the CDK1 activation is controlled through the control of activatory pathway and not the inhibitory pathway. Cdc25B, Cdc25C and Plk1 contain the most interactors. Plk1 only appears to mediate stress-dependent control. Cdc25B – DNA damage, stress and and perpetual cell cycle machinery (mediated by Cyclin A-CDK1) pathway control. Cdc25C – Stress pathway and is downstram of Cdc25B.

After the pathway expansion, the 3 pathways of cell cycle/previous cyclin, stress response and DNA damage checkpoint, have become more mutually exclusive. It appears that as the pathways merge closer into Cyclin B-CDK1 activation, a lot more common proteins mediate the pathways towards cell cycle control. For example, 14-3-3 is involved p38MAPK signal, CHK1 signal and cyclin A-CDK1 signal where CDK1 phosphorylates keratins which then compete for 14-3-3 binding with its other substrates (Ku et al., 2002),

As mentioned in the introduction, Aurora kinase-A and PLK1 appear to be the regulatory proteins of centrosome growth and G2/M transition pathways. These two proteins are not mutually exclusive from all of the 3 pathways, and unlike 14-3-3, they are involved in earlier stages of the pathways and also centrosome growth.

Aurora Kinase A is upstream of PLK1 as it phosphorylates T210 activating it. Aurora Kinase-A is activated by multiple proteins including ARPC1b, Hef1, Pak1 and indirectly by Cyclin A-CDK1.

As a result, AURKA and PLK1 antibodies were chosen to be tested to see how the parameters of these two proteins differ upon centrosome amplification. Additionally, the phosphorylated forms of these proteins were tested too, since looking at this chapter, it appears that once the phosphorylations are added (T210 on PLK1) and Thr288 on AURKA, they begin exerting the effects on the cell cycle control. These phosphorylations are activatory phosphorylations (Schmucker and Sumara, 2014; Dodson and Bayliss, 2012).

Chapter 4: Results. Investigating the relationships between KIFC1, centrosomes and the cell cycle rates.

Chapter 4.0: Introduction

This chapter investigates the relationships of KIFC1-centrosome amplification, KIFC1 – cell cycle rate and cell cycle rate-centrosome amplification. The latter is proposed in Figure 1.1. Here, it is hypothesized that both KIFC1 and amplified centrosomes increase the rate of the cell cycle. However, assuming KIFC1 does increase the rate of the cell cycle, a question remains whether it was affected by the amplified centrosome number. Therefore, to identify the contribution of KIFC1 to cell cycle kinetics (independent of centrosome clustering) it also needs to be established whether centrosome amplification itself affects the cell cycle. The relationship between centrosome amplification and the cell cycle is an interesting question and has not been directly tested until now. Therefore, KIFC1-cell cycle and centrosome-cell cycle links have been examined separately. Firstly, it is examined whether KIFC1 affects centrosome number in our model system. KIFC1 depletion would be expected to decrease the proportion of cells with amplified centrosomes, as KIFC1 is required for the clustering of supernumerary centrosomes in mitosis, and hence the survival of cells displaying centrosome amplification. KIFC1-PROTAC and AZ82 effective concentrations have been determined using cell survival assays, with 1µM being an effective concentration without significant cell death.

Chapter 4.1: Examining the relationship of KIFC1 and centrosome number.

To find this relationship, OMM2.3_H2B-FUCCI2a cells were treated with either solvent control (DMSO),1µM KIFC1-PROTAC or an equal concentration of the KIFC1 inhibitor, AZ82 in glass-bottomed 24-well plates. 1µM KIFC1-PROTAC was chosen as this is the lowest concentration at which the lab has seen consistent, robust degradation of KIFC1 (by both Western blotting, flow cytometry and immunofluroesence microcopy; Fielding lab, unpublished data). As an additional control, the inhibitor on which the PROTAC is based, AZ82, was included at the same concentration as the PROTAC. Previous data would suggest that AZ82 is significantly less potent than the KIFC1-PROTAC in phenotypic assays, and 1µM is expected to have little to no effect on cells. These cells were then placed in the live-cell imaging chamber and a time-lapse of H2B_FUCCI

was taken, with images acquired every 15 minutes for 69 hours, capturing 3 positions in each of the 5 wells. Immediately after the final frame's acquisition, cells were removed from the microscope, fixed with methanol and stained for immunofluorescence microscopy. DAPI stain was used to measure the total cell count. Pericentrin stain was used to count centrosomes and assign the cell to either normal or centrosome amplified. Figure 4.1.1 below portrays the experimental setup and results output format.

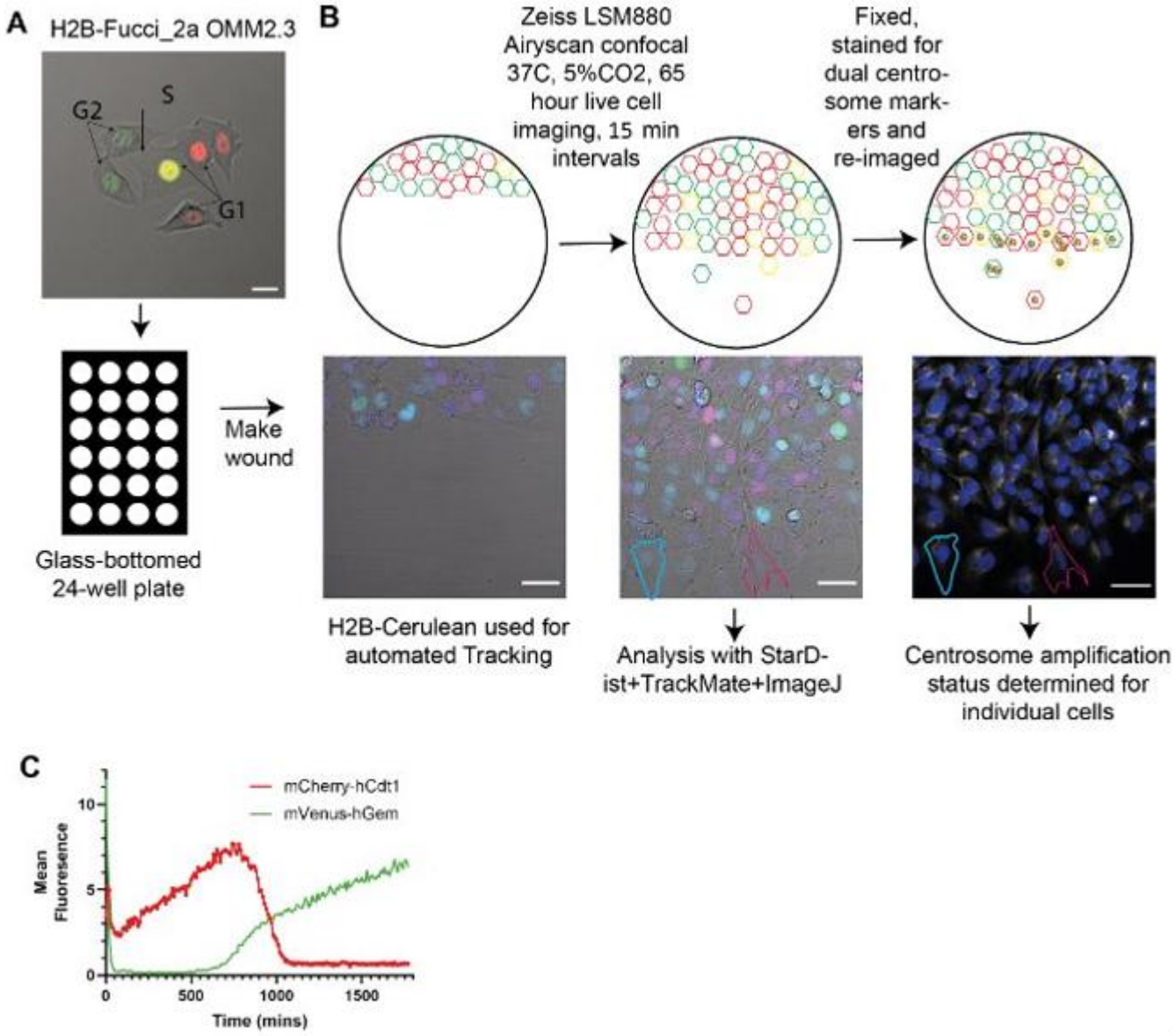

Figure 4.1.1: **A brief overview of the experimental setting and the output format (C).** The workflow was as follows: Panel A shows the fluorescent cells and the 24 well plate in which they were imaged. Panel B shows live cell imaging, and fluorescent antibody detection. Panel C shows example output of live cell imaging data.

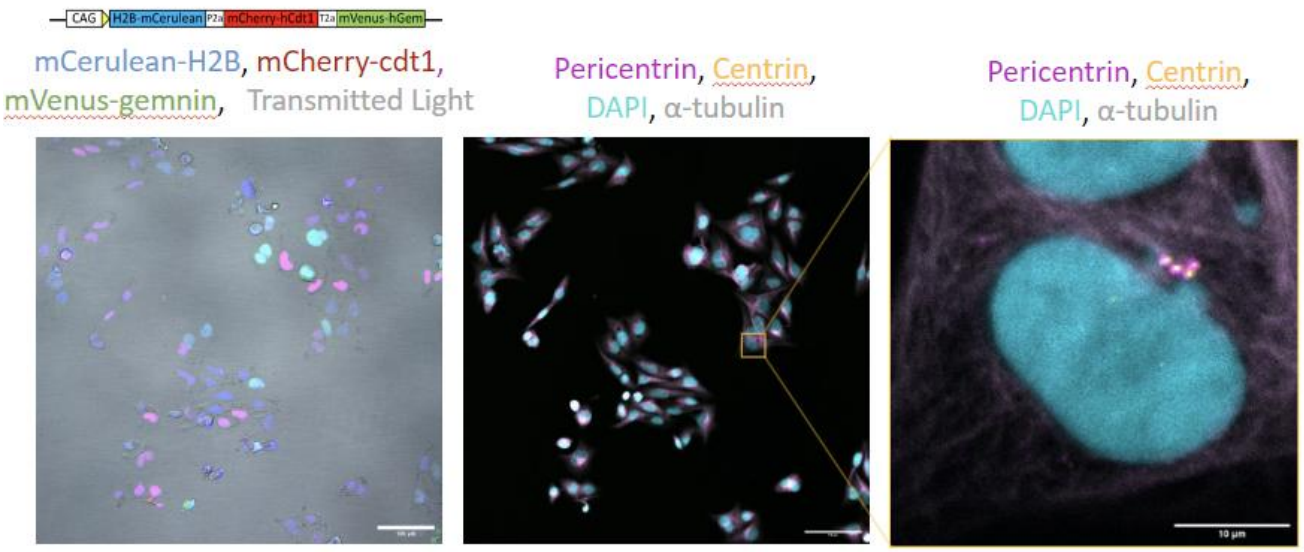

Figure 4.1.2: **Correlative live (FUCCI) and immunfluoresence imaging. The left panel shows the final timepoint of a field of view live imaged for H2B_FUCCI2a.** Cerulean channel was used to detect the cell nuclei, while the other two channels were quantified at the area of cerulean fluorescence. Subsequent to the final image of the FUCCI live cell imaging being captured, cells were then fixed and stained for immunofluorescence with anti-pericentrin, centrin and alpha-tubulin antibodies, plus DAPI. The plate was then returned to the confocal and the same field of view imaged, allowing the centrosome amplification status of live-tracked cells to be determined.

Following immunofluorescence staining, the plate was returned to the same microscope and the fields of view corresponding to the 9 points imaged in the live-cell experiment were imaged. The methanol fixation prior to the immunofluorescence staining ablated the FUCCI-fluoresence, allowing the antibody staining to be visualised. The cerulean-H2B from the live cell image and DAPI from the immunofluorescence image were compared to ensure the same fields of view were captured for both the live and fixed imaging. For each picture, the number of cells with amplified centrosomes was counted. The number was then taken as a proportion of the total cell count in that picture as measured with Stardist (Figure 4.1.4). As there were images of 3 fields of view per condition, numbers of cells with centrosome amplification were added and then the averages were calculated.

It is important to consider that cells with two centrosomes at the early phases of the cell cycle (before G2) are likely to be abnormal, as in theory, it should have 1 centrosome by then. As a result, based on the fluorescence of Cdt1 (a marker of G1 phase), cells with two centrosomes

could be assigned to still have centrosome amplification. Cdt1 fluorescence level is easily seen when the brightness values of each channel (channel 1 in the case of Cdt1 and channel 2 for geminin) for each cell are graphed and compared. Based on the fluorescent values of each channel at the last time point, the cell cycle phase for that cell when pericentrin stain has been recorded, can be deduced. The following figure portrays Cdt1 and Geminin fluorescence for a full cell cycle. Geminin and Cdt1 fluorescence is further analysed later.

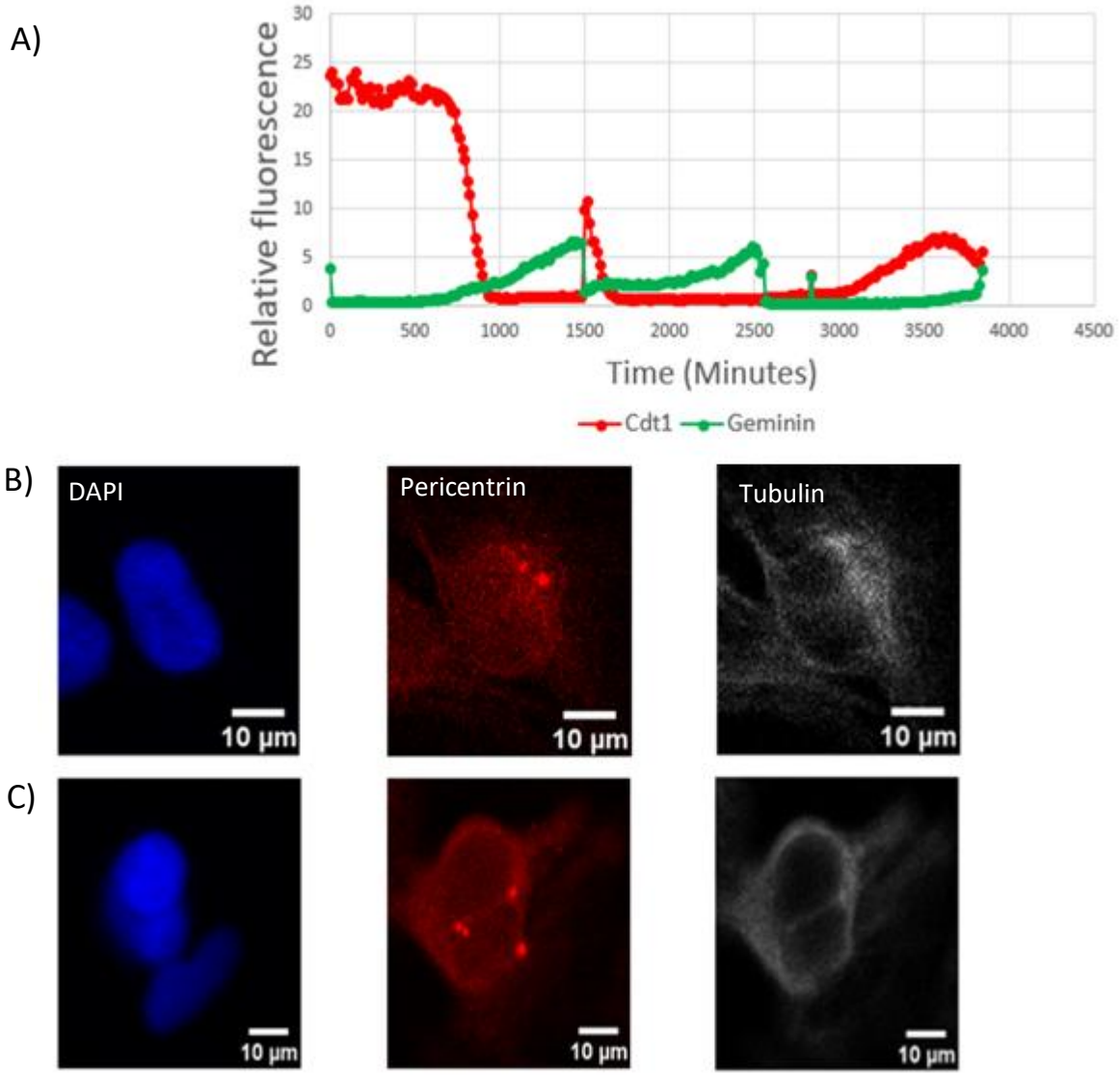

Figure 4.1.3: A: Example of FUCCI trace for cell in G1 at the end of the timelpase. The live recording, followed by fixed cell imaging of OMM2.3_H2B-FUCCI2a cells was performed. Trackmate, with StarDist plugin, in FIJI, was used to quantify fluorescence of mCherry-cdt1 and mVenus-Geminin in individual cells across the 69 hour timecourse. An example trace of this quantification from one cell, that is in G1 phase at the end of the timecourse, is shown, where Cdt1 is still abundant. **B: Example acquisition of cells with centrosome amplification (this acquisition showcases a cell with two centrosomes during G1).** OMM2.3_H2B-FUCCI2a cells were treated with either solvent control (DMSO), KIFC1-PROTAC or the KIFC1 inhibitor, AZ82 in glass-bottomed 24-well plates. These cells were firstly subjected to a live-cell imaging experiment, followed by fixing and staining for immunofluorescence microscopy. DAPI was used to measure total cell count. Pericentrin stain was used to count centrosomes and assign the cell to either normal or centrosome amplified. **C: Example acquisition of cells with centrosome amplification.** The pericentrin channel (red) was used to determine the centrosome number in the cell.

The percentages of cells with clearly amplified centrosomes, with 2 centrosomes during the G1 phase were counted. In other words, all cells with centrosome amplification were included in the calculation. The calculation has been performed on each well (condition). The figure below portrays the latter.

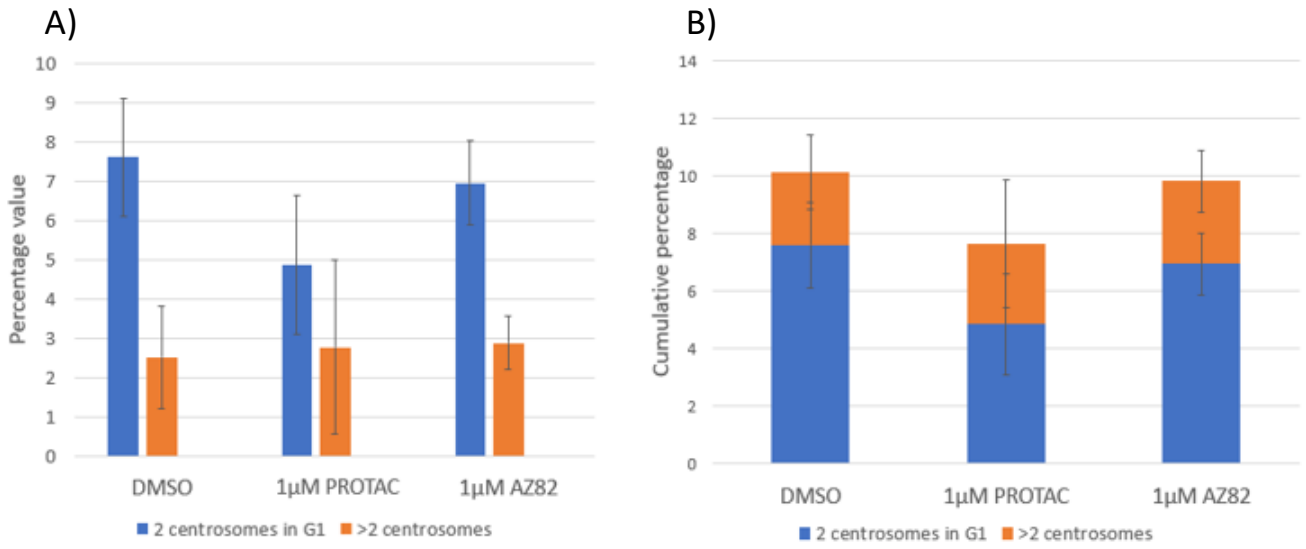

Figure 4.1.4: A: the percentages of cells with centrosome amplification split into two categories: "2 centrosomes in G1" and ">2 centrosomes. Refer to figure 4.1.3 for experimental explanation. DMSO: cells with 2 centrosomes during G1: 15 (7.58%) (SE 1,49%); cells with more than 2 centrosomes 5 (2,53%) (SE 1,30%). 1µM PROTAC: Cells with 2 centrosome during G1: 7 (4,86%) (SE 1,76%); Cells with more than 2 centrosomes: 4 (2,78%) (SE 2,21%). 1µM AZ82: Cells with 2 centrosomes during G1: 29 (6,95%) (SE 1,07%); cells with more than 2 centrosomes: 12 (2,88%) (SE 0,69%).

B: The cumulative proportions of cells with indicated abnormality with respect to the total cell number. Significant differences have not been calculated for this figure as standard deviation is not applicable for a bar that is a sum of the different data sets.

Significant differences have been obtained through Unpaired t-test with Welch's correction. Between the different conditions, the signficantly different comparisons for the "2 centrosomes during G1" category are "1µM PROTAC" vs "1µM AZ82" with a P value of 0,0462 and "1µM PROTAC" vs "DMSO" with a P value of 0,0247. No significant differences have been picked up within the ">2 centrosomes" category between the different conditions.

From Figure 4.1.4A, above it is seen that cells with 2 centrosomes during G1 are the most prevalent abnormality, there appears to be fewer cells with more than 2 centrosomes. Under 1µM PROTAC, the cells have a significantly lower number of centrosome amplification in the form of 2 centrosomes during the G1 phase of the cell cycle. Meanwhile, the number of cells with more than 2 centrosomes is indifferent to every condition. Wells with DMSO and AZ82 also have a signficantly lower number of cells with more than 2 centrosomes than cells with 2 centrosomes in G1. Figure 4.1.4B shows cumulative values of centrosome amplification for each condition. It appears that cells under PROTAC show the lowest value, but it is hard to draw conclusions since standard deviations have not been calculated. As a result, it appears, that KIFC1 has a weak effect on centrosome amplification in current model system. However, it is apparent that KIFC1 increases the probability of a cell having 2 centrosomes in the G1 phase of the cell cycle, as seen in figure 4.1.4A.

Chapter 4.2: Examining the link between KIFC1 and the cell cycle length.

Next, the link between KIFC1 and cell cycle length has been analysed. Cell cycle lengths have been measured for the G1 phase (mCherry-Cdt1 fluorescence) and for the S to Anaphase phases (mVenus-Geminin fluorescence). Figure 4.2.1 gives example images acquired at the beginning and end of the 70 hour timecourse.

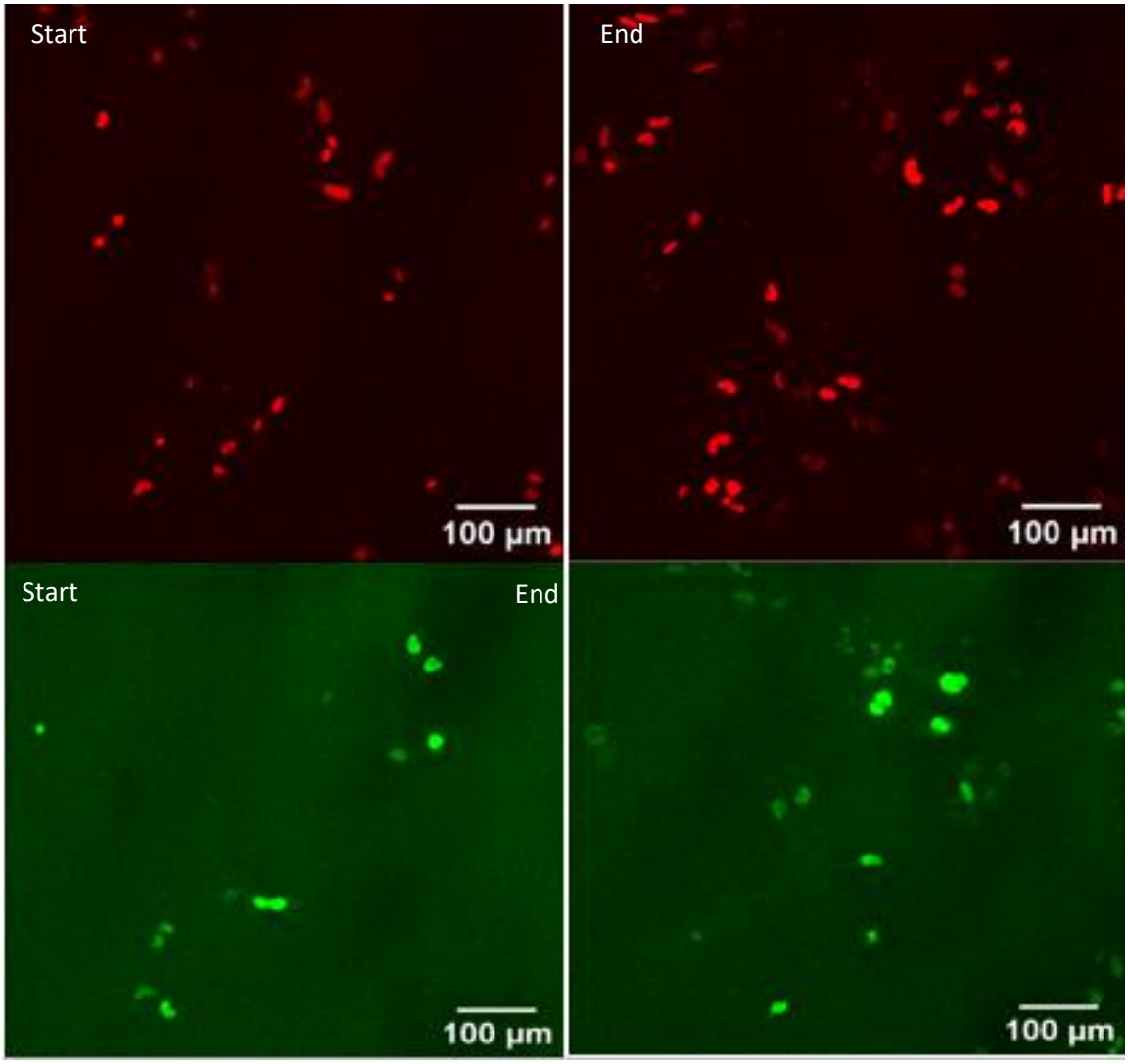

Figure 4.2.1: **Acquisitions of OMM2.3_H2B-FUCCI2a cells at the start of the recording and at the end of the recording (70h).** Refer to figure 4.1.3 for experimental explanation. The drugs KIFC1-PROTAC and AZ82 were both used at 1µM, to degrade or inhibit KIFC1, respectively. Cell cycle lengths were then analysed under the conditions of certain inhibitors/degraders and their concentrations. Green channel represents geminin and red channel represents Cdt1 fluorescence. All 4 captures are done on DMSO well (see method section). "Start" denotes captures from first frame and "End" denotes the captured picture at 261st frame which is the last frame of the recording that is 70 hours long.

The recording was then used to graph the quantity-dependent fluorescence of Cdt1 and Geminin in every cell. Trackmate with Stardist plugin in Fiji allows for selection of cells and creates a table with fluorescent data. Both channels have been recorded at once, thus the fluorescent data was graphed for both mCherry-tagged Cdt1 and mVenus-tagged Geminin, for selected cells. At least 15 cells were used from each position to obtain the fluorescent values and later calculate averages, where possible.

Figure below portrays some of the graphs created from fluorescence data tables in Fiji for both proteins.

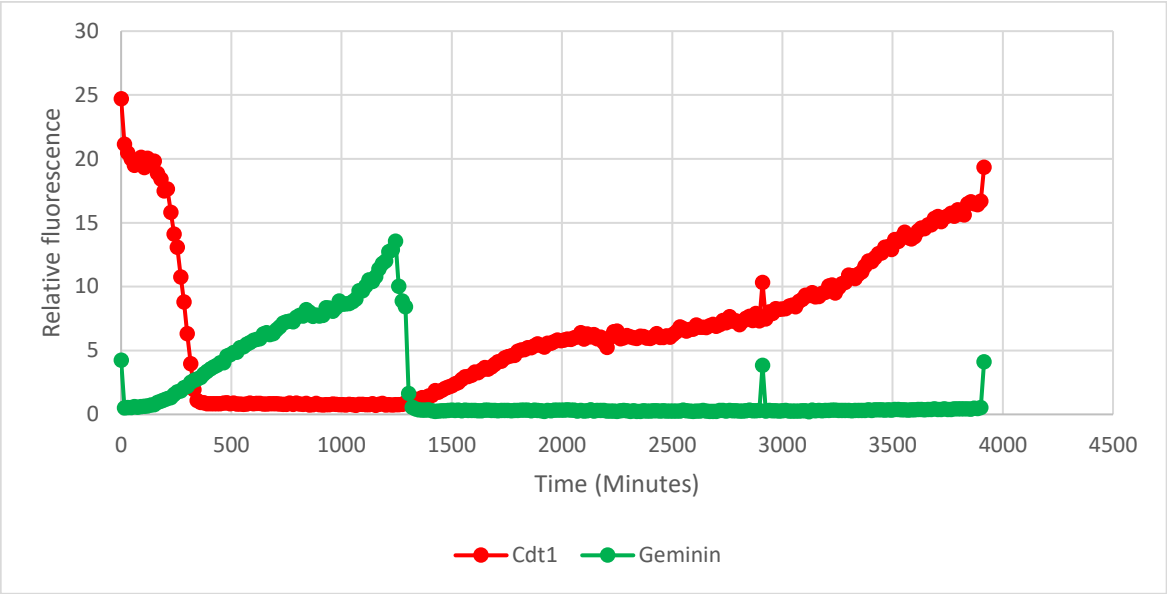

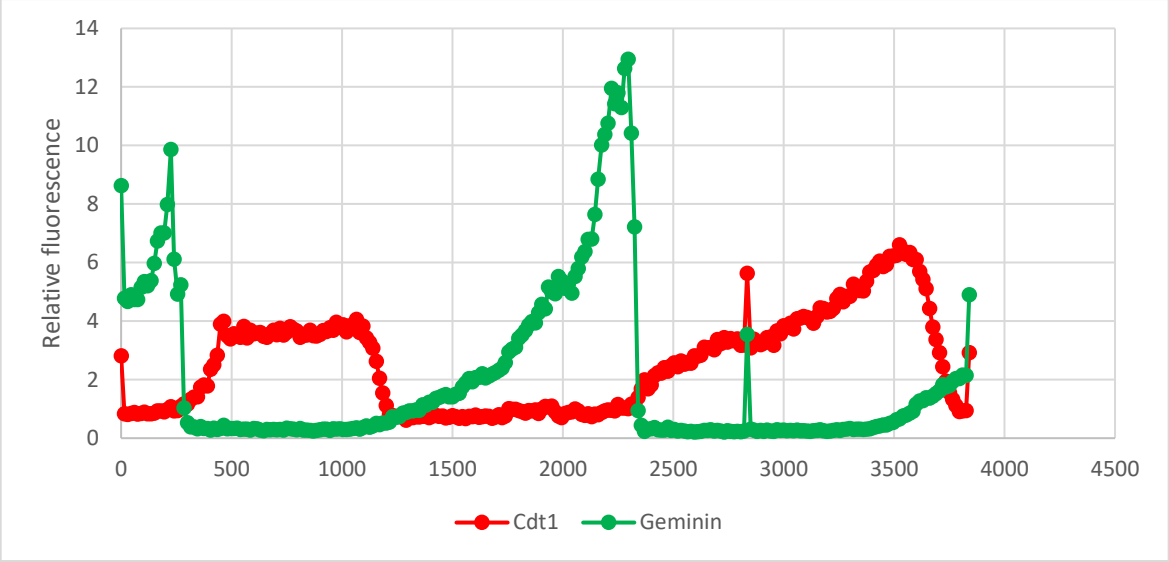

Figure 4.2.2: **Example of FUCCI trace of Cdt1 and geminin fluorescence levels timelapse.** The fluorescence intensity represents the relative levels of the respective protein quantities. The live, followed by fixed cell imaging of OMM2.3_H2B-FUCCI2a cells, described in section 2.3 was performed. Trackmate, with StarDist plugin, in FIJI (Schindelin et al., 2012), was used to quantify fluorescence of mCherry-cdt1 and mVenus-Geminin in individual cells across the 69 hour timecourse.

The following graphs portray the average cell cycle lengths for (A): all types of cells, (B): centrosome amplified cells only, and (C) normal cells only. All types refer to normal cells and centrosome amplified cells. The figure below shows the average length of G1 and S to Anaphase periods for all the cells for which cell cycle phase lengths have been recorded.

A) <u>All cells</u>

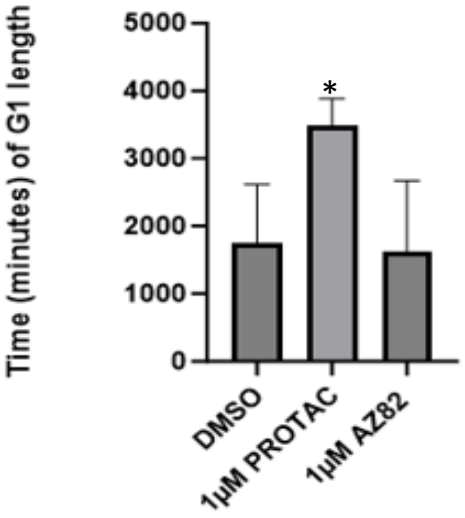

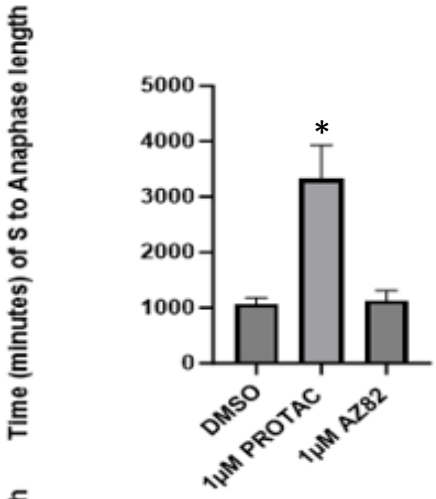

B) **<u>Centrosome amplified cells</u>**

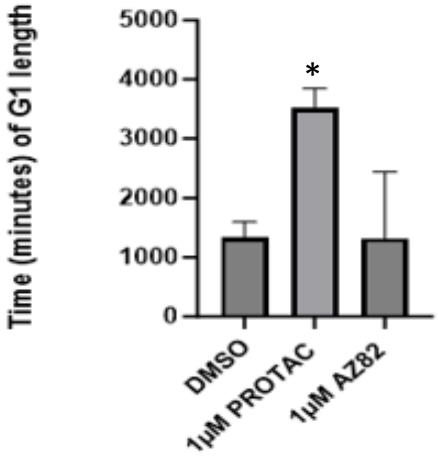

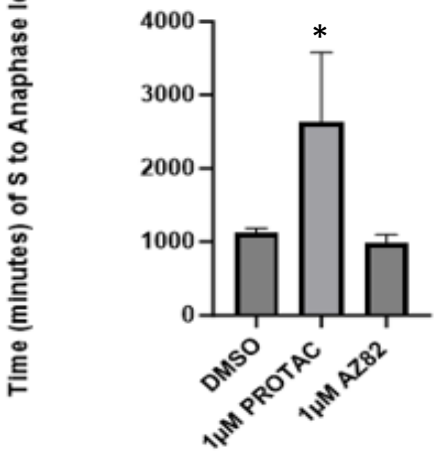

C) **<u>Normal cells</u>**

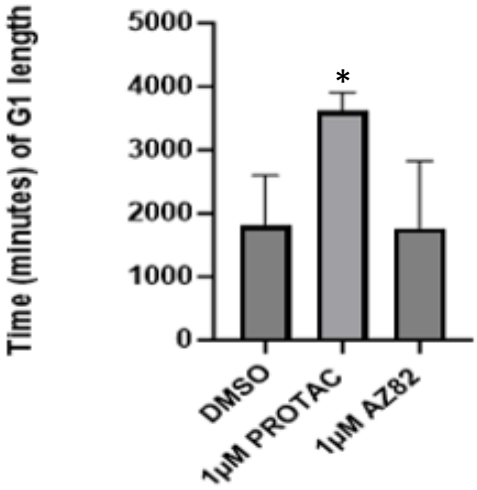

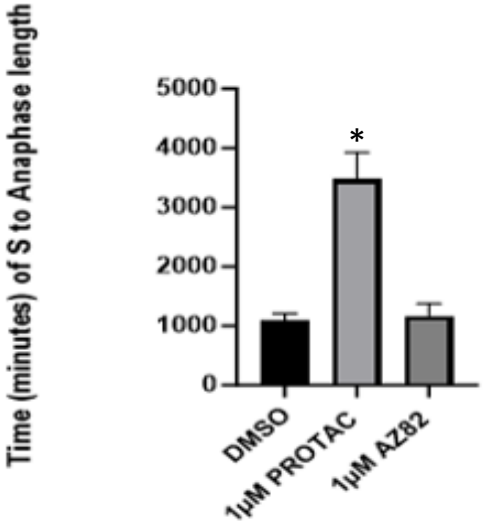

Figure 4.2.3: KIFC1 ablation affects cell cycle lengths under high concentrations of PROTAC degrader for all cells overall, for normal cells, and for cells with centrosome amplification. Refer to figure 4.1.3 for experimental explanation. Statistical test used was one-way ordinary Anova with Tukey's multiple comparison test. G1 phase data of part A comparisons: Significant differences occurred between: DMSO vs. 1μM PROTAC (P value < 0.0001); 1μM PROTAC vs. 1μM AZ82 (P value < 0.0001). S to Anaphase phase data of part A comparisons: Significant differences occurred between DMSO and 1μM PROTAC (P value < 0.0001); 1μM PROTAC and 1μM AZ82 (P value < 0.0001). G1 phase of part B comparisons:DMSO vs. 1μM PROTAC (P value < 0,0001); 1μm PROTAC vs. 1μM AZ82 (P value < 0,0001). S to Anaphase data comparisons of part B: DMSO vs. 1μM PROTAC (P value < 0.0001); 1μM PROTAC vs. 1μM AZ82 (P value < 0.0001). Comparisons for G1 phase data of part C : DMSO vs. 1μM PROTAC (P value 0,0262); 1μM PROTAC vs. 1μM AZ82 (P value 0,0199). S to Anaphase phase data of part C comparisons: 1μM PROTAC and 1μM AZ82 (P value 0,0206) and DMSO vs 1μM PROTAC (P value 0,0284). Refer to figure 4.3.2 for citation of software for statistical analyses of software for statistical analyses.

Figure 4.2.3A above shows that the PROTAC category is different from the other two categories, DMSO and 1μM AZ82. Thus, the cell cycle is significantly longer for cells treated with the KIFC1-PROTAC, suggesting KIFC1 is required for normal cell cycle progression, as in these cells KIFC1 has been degraded by the PROTAC. Under the same concentration of the KIFC1-inhibitor AZ82, the lengths are not significantly different from the DMSO-conditioned well, supporting previous data from the lab suggesting it has little to no activity at this concentration. As a result, this provides some information about the effects of KIFC1 on the cell cycle: the absence of KIFC1 prolongs the length of the G1 phase of the cell cycle. As for the S to Anaphase fraction of the cell cycle, the same can be said as it shows a significantly prolonged S to Anaphase phase of the cell cycle under the degradation of KIFC1.

Figure 4.2.3B also only shows the same significant differences for both phases as figure 4.2.3A. This further shows that the degradation of KIFC1 is most effective using this drug and the latter results in a significantly prolonged G1 phase of the cell cycle under the conditions tested. AZ82 on the other hand, does not show such a result and it appears that inhibition of KIFC1 at this concentration does not alter the length of either phase. This is further discussed later.

Figure 4.2.3C only involves cells with a normal centrosome number- that is 1 centrosome during G1 or 2 centrosomes during later phases of the cell cycle. However, the obtained pattern is exactly the same as for the other cell types. During the G1 phase of the cell cycle, only the degradation of KIFC1 with 1μM PROTAC prolongs the cell cycle. As a result, it can be said that during the G1 phase of the cell cycle, KIFC1 accelerates its progress independently of centrosome amplification or clustering, as this sample did not involve such abnormalities. The S to Anaphase part of the cell cycle has shown the same results and the same conclusion can be drawn, except that the S to Anaphase phase appears to be slightly more sensitive to KIFC1 as the distance between the standard deviation bars is larger.

Lastly, the percentage increase in cell number has been compared for all 5 conditions. The number of cells during frame 1 of the recording is considered as the base cell count. The number of cells in the last frame is the final cell count. The difference between the two is calculated and expressed as a percentage of the base cell count. The figure below portrays the latter.

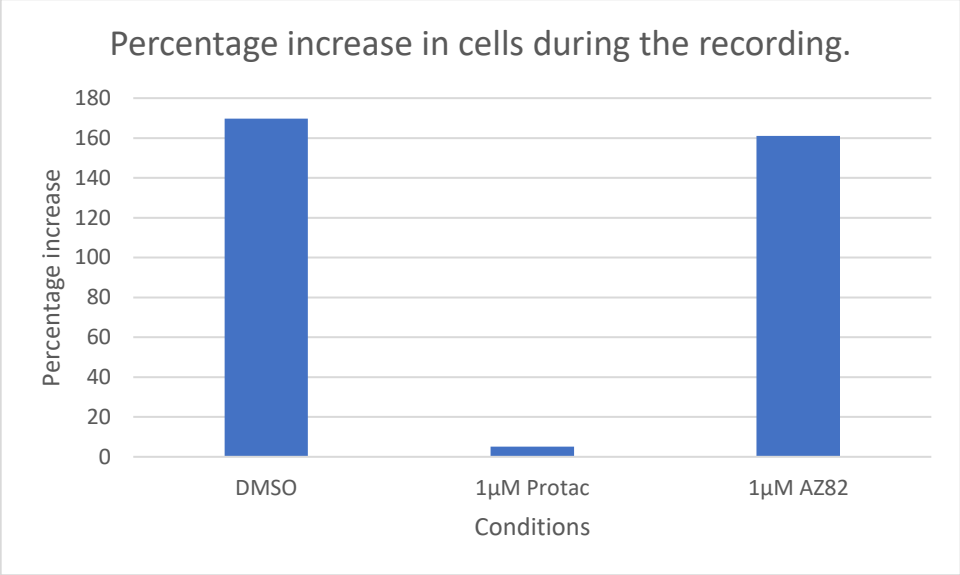

Figure 4.2.4A: The percentage increase in cell numbers of cells under each condition affecting KIFC1. Refer to figure 4.1.3 for experimental explanation. Under PROTAC the reduction in cells it is seen the continued fluorescence of cells but never an observed splitting. This suggests that it is an inhibition of the cell cycle rather than cell cycle under the assumption that the presence of fluorescence represents a living cell. This suggests a cytotostatic mechanism of the drug. Further studies could be done to detect cell death during a timelapse.

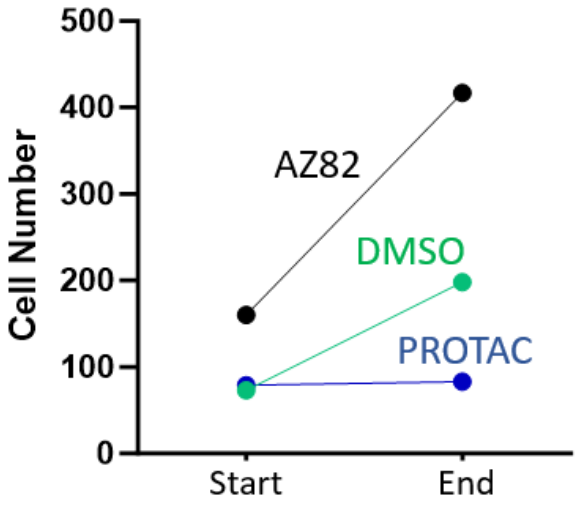

Figure 4.2.4B: The increase in cell number from start of the recording to the end of the recording uder each condition. Refer to figure 4.1.3 for experimental explanation.

Looking at Figures 4.2.4A and 4.2.4B, it is apparent that the PROTAC degrader is the most potent molecule when it comes to halting the division of cells. As a result, it can be said that KIFC1 degradation results in slower or less frequent cell division. On the other hand, the inhibition of KIFC1 does not show such results, which leaves room for speculation that the presence of KIFC1, even with inactive ATPase domain, still allows some cell cycle function to be performed.

Chapter 4.3: Examining the link between centrosomes and the cell cycle length.

For this analysis, the pericentrin stain was used to count the centrosome number per cell and then cells were grouped into having a normal number of centrosomes or amplified centrosomes. The figure below portrays examples of the respective types of cells concerning the centrosome status that were put into categories in this study. Cells can have a normal number of centrosomes if they contain 1 centrosome during the G1 phase or 2 centrosomes during the rest of the cell cycle.

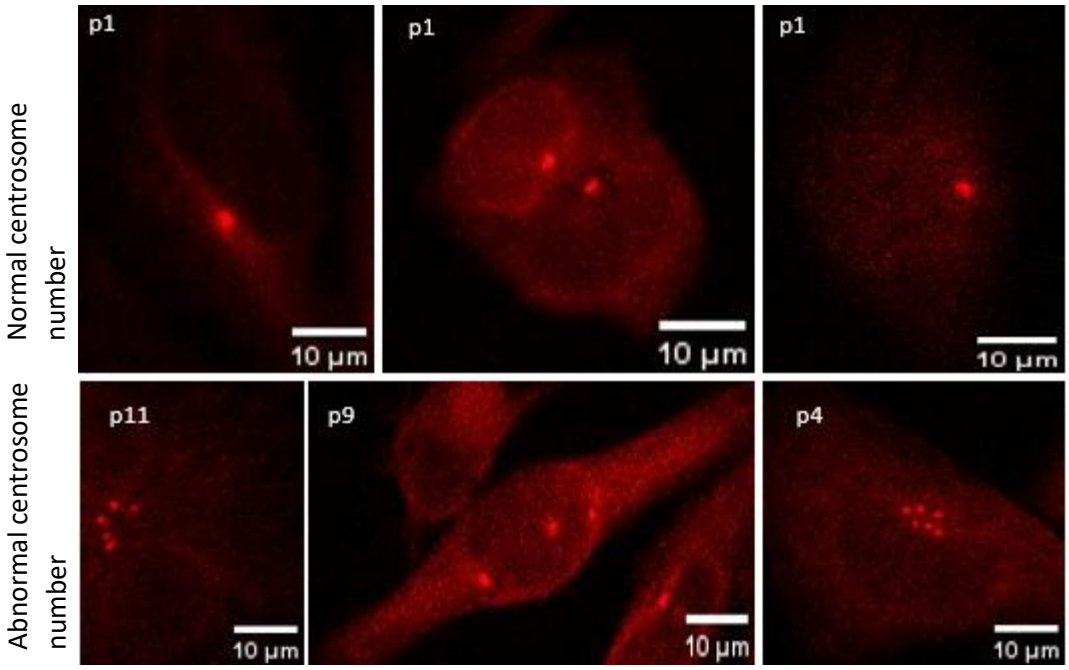

Figure 4.3.1: **Examples of cells with normal and amplified centrosomes**. Refer to figure 4.1.3 for experimental explanation. The upper 3 cells (images) portray cells with normal centrosome number, while the bottom 3 cells (images) portray centrosome amplification through the pericentrin fluorescence.

The following set of figures portrays the lengths of G1 and S to Anaphase phases of the cell cycle. ”CA+” stands for cells with centrosome amplification, and “no CA” stands for cells with a normal centrosome number. The data is portrayed as a graph per condition i.e. 3 graphs each having measurements for the aforementioned abnormalities.

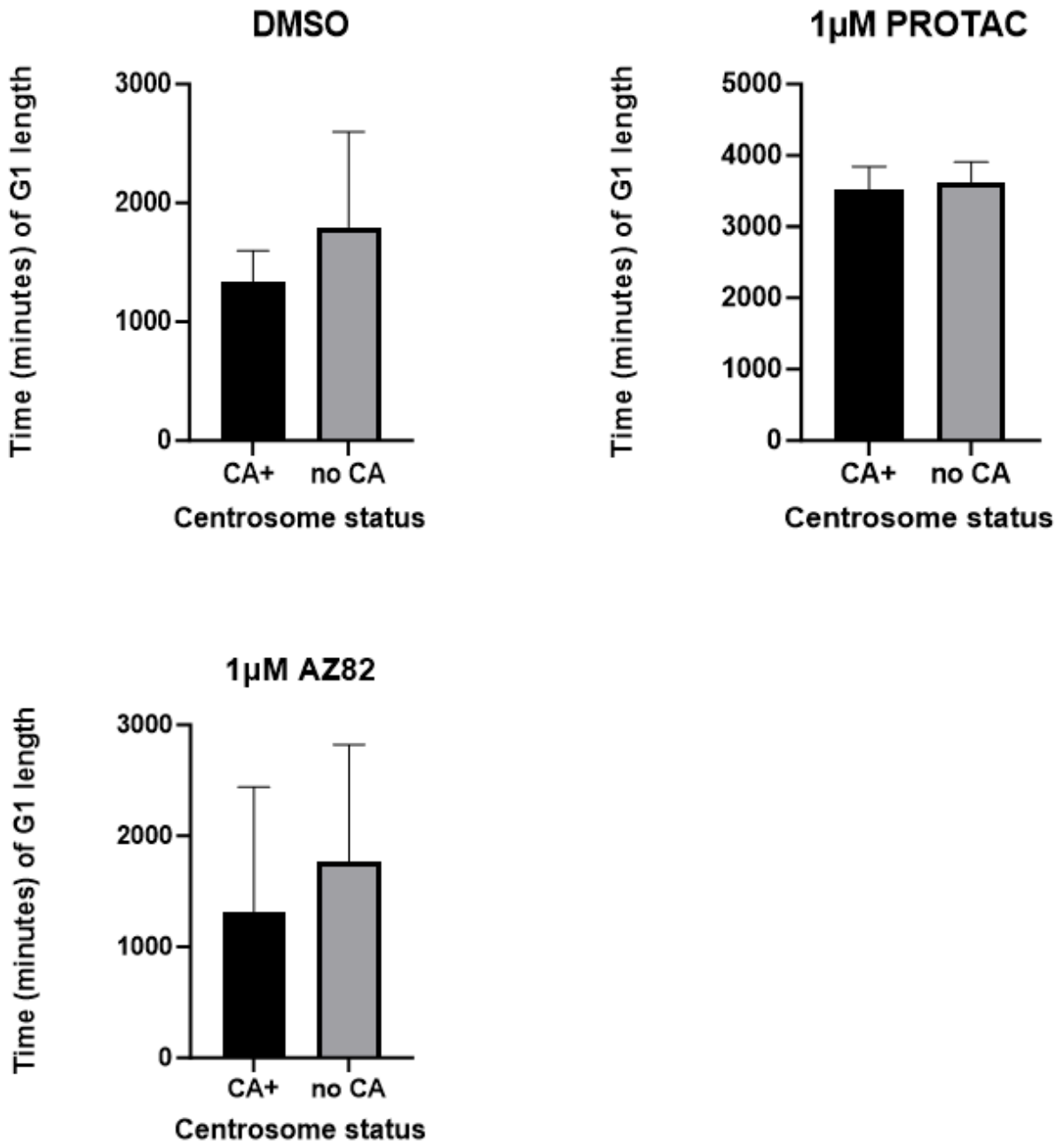

Figure 4.3.2: **Length of the G1 phase for the normal (no CA) or centrosome amplified cells (CA+) which are subjected to the indicated conditions.** Refer to figure 4.1.3 for experimental explanation. Significant differences have been obtained through Unpaired t-test with Welch’s correction. DMSO: variables are insignificantly different: CA+ vs no CA (P value 0,237). 1µM PROTAC: variables are insignificantly different: CA+ vs no CA (P value 0,726). 1µM AZ82: variables are insignificantly different: CA+ vs no CA (P value 0,3456). Calculations, statistics and comparative tests have been done through the GraphPad prism version 9.0.0, GraphPad software, Boston, Massachusetts,USA, www.graphpad.com.

Figure 4.3.2 above contains 2 different bar charts each for each condition, comparing the cell cycle lengths of the indicated abnormalities. Under all the conditions, whether KIFC1 is present or not, it appears that G1 length is consistent for the two compared abnormalities as no significant differences have been picked up. As a result, it can be said that in the presence or absence of KIFC1, the length of the G1 phase of the cell cycle is not affected by the different abnormalities of centrosomes. In other words, it appears that the number of centrosomes in a cell does not directly affect the time that takes a cell to complete the G1 phase of the cell cycle.

The following set of results portrays the length of S to Anaphase (Geminin) for cells with centrosome amplification, and without centrosome amplification.

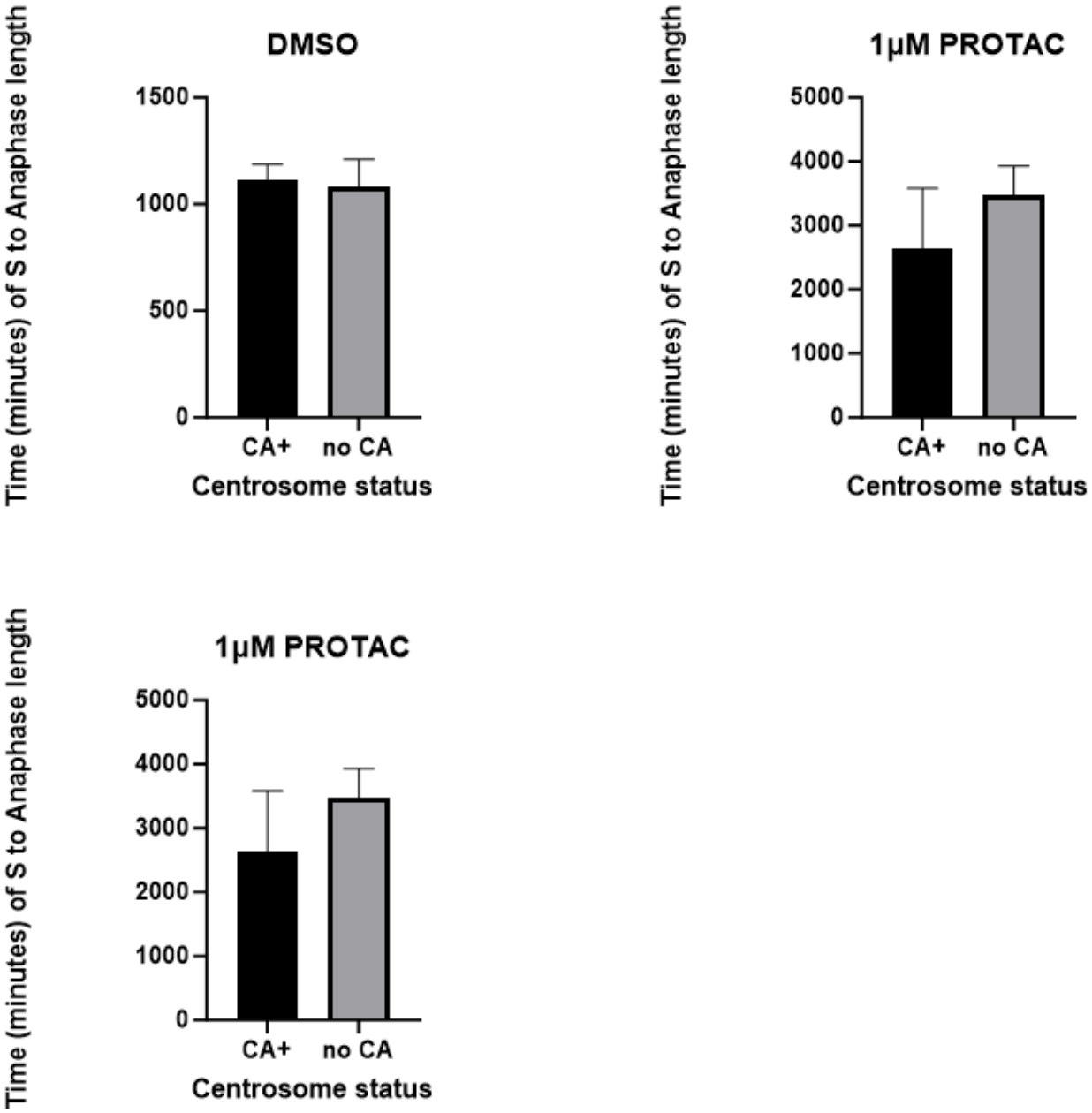

Figure 4.3.3: **Length of the S phase to anaphase period of the cell cycle for normal (no CA) or centrosome amplified cells (CA+) which are subjected to the indicated conditions**. Significant differences have been obtained through Unpaired t-test with Welch's correction. DMSO:Variables are insignificantly different: CA+ vs no CA (P value 0,6866). 1µM PROTAC: Variables are insignificantly different: CA+ vs no CA (P value 0,1629). 1µM AZ82: variables are insignificantly different: CA+ vs no CA (P value 0,374). Refer to figure 4.3.2 for citation of software for statistical analyses.

Figure 4.3.3 shows no significant differences in any of the 3 charts. As a result, it can be said that the length of S to Anaphase period of the cell cycle is not affected by any form of centrosomal abnormality tested.

Chapter 4.4: Chapter 4.1 Discussion:

The relationship between KIFC1 and the centrosomes in the cell:

Overall, it is well-proven that KIFC1 causes centrosome clustering (Sabat-Pospiech et al., 2019). However, when looking for a direct link between the amplification of centrosomes and KIFC1, the evidence is moderate. Figure 4.1.4 Part A shows that when KIFC1 is degraded by the KIFC1-PROTAC, the number of cells with 2 centrosomes during G1 is lower, compared to when it is present. The only reason why 2 centrosomes can exist during G1 is due to the inheritance of previously clustered centrosomes, since centrosomes duplicate only during the S phase. As a result, it can be said that centrosome amplification after mitosis becomes less prevalent without KIFC1. This suggests of a new mechanism of generation of amplified centrosomes: inheritance of more than one centrosome during mitosis. Such process would render one cell not viable while the other with a potential for carcinogenesis through the multiple inherited centrosomes. A reasonable explanation could be that the absence of KIFC1 results in declustered centrosomes during mitosis, resulting in mitotic arrest or death of cells with centrosome amplification, resulting in the reduced number of cells with amplification of centrosomes during the G1 phase of the cell cycle.

Another observation from Figure 4.1.4 part A is that cells with more than 2 centrosomes remain at the same proportions irrespective of the presence or absence or inhibition of KIFC1. It is hard to discuss such observation, but ultimately it can be said, that KIFC1 does not participate in the amplification of centrosomes, but only in clustering. A counterargument for the latter statement exists however: without the clustering of centrosomes, cells with amplified centrosomes die or undergo a mitotic arrest, thus ultimately the absence of KIFC1 should reduce the number of cells with amplified centrosomes. However, a cell in mitotic arrest could still leave a cell appearing the same way in the fixed images studied here as a cell alive with centrosome amplification and thus would be counted as another cell with amplified centrosomes.

For Figure 4.1.4, part B, the expected trend is that the cells subjected to DMSO would show the highest cumulative percentage, while the wells with 1µM of KIFC1-PROTAC would show the lowest. AZ82 would be second to PROTAC as PROTAC completely degrades the protein while AZ82 only inhibits it, so here we speculate PROTAC to be a more efficient molecule to prevent KIFC1-mediated effects. There was no software with which ANOVA testing could be done on cumulative

charts (composed of different variable percentages), but looking at the error bars of the charts, it appears that the PROTAC samples are lower.

Overall, it appears that the figures of chapter 4.1 support the fact that KIFC1 is required for maintainace of centrosome amplification. More apparently its degradation does suggest of the consequences having amplified centrosomes with the inability to cluster them.

Chapter 4.5 Chapter 4.2 discussion.

The relationship between KIFC1 and the length of cell cycle phases.

Figure 4.2.3, part A shows the lengths of the G1 phase and S to Anaphase periods of all cells (including normal and centrosome amplified). Overall, it appears that specifically, the degradation of KIFC1 lenghtens the phases of the cell cycle. Inhibition with AZ82 gives a length that is not significantly different to the DMSO sample lengths. It can be speculated that the inhibition of KIFC1 leaves the protein with the ability to function elsewhere despite the inability to move along the microtubules, hence no changes in the lengths of the G1 phase under AZ82. Likewise, AZ82 is also less potent than KIFC1-PROTAC. However, the degradation of KIFC1 also prevents centrosome clustering, thus it is unclear whether the effects on cell cycle length seen are centrosome clustering independent. On the other hand, AZ82 should also prevent centrosome clustering, yet no change in cell cycle lengths was seen under the effect of AZ82. To conclude this figure, it can be said that the presence of KIFC1 results in a shorter cell cycle overall.

Figure 4.2.3, part B shows the same results as figure 4.2.3A, but only for cells with amplified centrosomes. It appears that the G1 phase of such cells is enlengthened when PROTAC is applied. As a result, it appears that the absence of KIFC1 slows the G1 phase compared to when it is present (DMSO), independent of the number of centrosomes, because the well with KIFC1 present (DMSO) shows a significantly faster rate normalised to the number of centrosomes (both have amplified unclustered). AZ82-bearing wells are not significantly different from the DMSO wells, hence it can be said that inhibition, but not degradation of KIFC1 is insufficient to prevent cell cycle acceleration. Looking at the data only for the S to Anaphase period of the cell cycle, it appears that this phase is as responsive to the degradation of KIFC1 as the G1 phase for the cells with unclustered, amplified centrosomes. Overall, this figure shows the same results as the previous

figure, but the same conclusion can be drawn confidently: centrosome clustering or amplification could still be the factors affecting cell cycle rate.

Figure 4.2.3, part C shows the lengths of the two phases for healthy cells i.e. those with a normal centrosome count. The PROTAC samples are the only ones significantly different from the DMSO comparatives, for G1 and S to Anaphase data. Thus, a conclusion can be made that in cells bearing a normal centrosome count, the degradation of KIFC1 enlengthens the cell cycle. This figure (4.2.3 A,B,C) proves that KIFC1 exhibits effects on the cell cycle in a centrosome clustering-independent mechanism in two ways, (1): these cells only have a normal centrosomal phenotype so centrosome clustering or amplification could not be the other reason why cell cycle length is shortened, (2): AZ82-bearing wells are not significantly different from the DMSO well what means that the presence of KIFC1 allows the phase to be shortened (Applies to parts A,B and C of figure 4.2.3). As a result, it can be said that KIFC1 does accelerate the cell cycle in a centrosome clustering-independent pathway in normal cells. For both phases, the 1µM PROTAC samples appear to be significantly different from the AZ82 comparatives, further proving that KIFC1 is functioning elsewhere than just to cluster centrosomes, because the presence of KIFC1 maintains the cell cycle length similar to that of under DMSO. In other words, the only difference between PROTAC and AZ82 wells is that the latter still contains KIFC1, and as observed, it maintains a faster cell cycle rate.

Figure 4.2.4 shows that overall, the cell numbers have increased only when KIFC1 is present whether inhibited or not. DMSO and AZ82-bearing wells have shown similar numbers concerning the percentage increases in cell count over the 70-hour period. Contrastingly, the PROTAC-bearing well has shown the lowest increases. Overall, this figure strongly supports the hypothesis that KIFC1 functions in the cell cycle.

Overall, there is plenty of evidence proving that KIFC1 does function in the cell cycle despite functioning in centrosome clustering. Figures 4.2.3 and 4.2.4 portray data to support this hypothesis in two different ways. Firstly, in Figure 4.2.3 part C where only a specific set of cells with respect to their centrosomal status are compared under the 3 different conditions, the enlegthened G1 or S to Anaphase periods under the degradation of KIFC1 (PROTAC comparatives)

can only be explained due to single reason – the absence of KIFC1 prevents cell cycle acceleration. Centrosome amplification is not a factor (figure 4.2.3 part C) as such cells have been excluded. Secondly, the cell cycle phase lengths in AZ82-containing wells have not been significantly different from the cell cycle phase lengths of cells in the DMSO wells. AZ82 does not degrade KIFC1 which can justify that the presence of KIFC1 may perform a cell cycle function, most likely through some nuclear transport pathways.

Furthermore, it has been found in chapter 4.3 that centrosome amplification does not affect the length of cell cycle phases giving further support for the argument that KIFC1 accelerates cell cycle in centrosome-clustering independent mechanisms. Even though cells under AZ82 do not show shorter cell cycle phases, this inhibitor is not as potent as the PROTAC degrader and potentially allows some centrosome clustering to occur. Also, it is difficult to see if a cell contains amplified centrosomes, as it is only present in mitosis. In this study, a small number of cells have been detected with clustered centrosomes in mitosis for which cell cycle data has been also available.

Chapter 4.6: Chapter 4.3 Discussion.

The relationship between centrosomes and the length of cell cycle phases.

Looking at Figure 4.3.2, it appears that under no subjected conditions the cells show a significantly different length of G1 phase. As a result, it can be said the centrosome amplification by itself does not change the rate of the G1 phase of the cell cycle. The rate of the G1 phase is also not affected by centrosome amplification irrespective of the presence (DMSO), absence (1µM PROTAC) or the inhibition (1µM AZ82) of KIFC1. The latter means that whether clustering of centrosomes occurs or not, centrosome amplification will have no effect on the G1 phase of the cell cycle.

Looking at Figure 4.3.3, under all the conditions tested, the length of the S to Anaphase period is unaffected by centrosome amplification in the same way as for the G1 phase of the cell cycle from the previous figure. Here the ability or inability of cells to cluster centrosomes also has no effect on the comparison of cell cycle phase length between cells with centrosome amplification and normal cells.

Chapter 4 of this study shows that centrosome amplification does not affect the rate of the cell cycle. However, it is still unclear whether centrosomes by themselves have a direct impact on the

pathways of the cell cycle. For example: whether clustering affects the cell cycle or if any signals within the cell cycle pathway occur differently, despite the rate being unaffected. It is also unclear whether the process of centrosome clustering distorts the signalling on centrosomes as they are a scaffold for cell cycle machinery. Additional analysis has been done in chapter 5 of this study to test the effects of centrosome amplification on the specific parameters of cell cycle proteins rather than lengths of phases. Chapter 5 also provides data with larger sample numbers allowing to draw conclusions more accurately. In the next part of this study, there will be a few example pictures of clustered centrosomes during mitosis provided. As a result, the centrosomal parameters will be compared with cell cycle parameters computationally.

It is hypothesized here that in the cells which contain centrosome amplification and centrosome clustering that occurs during mitosis, the events of the cell cycle will be altered because centrosomes are a scaffold for cell cycle machinery. Chapter 4 of this study did not provide any data to support the latter, but the number of samples with centrosome amplification is low. As a result, in the next section, it is attempted to look for any correlations between centrosome parameters and cell cycle protein parameters. In addition to the correlation patterns between changes in centrosome parameters and cell cycle proteins' parameters, the average values of cell cycle parameters and centrosomal parameters were compared.

Chapter 5: Results: Comparing the centrosomal parameters with cell cycle parameters:

Chapter 5.1 Introduction.

The reason for this chapter is to further investigate the relationship between the centrosomes and the cell cycle. The results of this thesis so far demonstrate that KIFC1 increases the rate of certain cell cycle phases in centrosome clustering independent pathways and that centrosome amplification does not result in faster cell cycle rates. Despite the latter, there were three reasons to continue with the current investigation:

1. Due to the low number of cells and many insignificant results obtained for the past analyses, it is hard to deduce the effects of centrosome amplification on cell cycle kinetics. As a result, Fluorescent labelling of cell cycle proteins was used next. The proteins assessed here are Aurora-A kinase and Polo-Like Kinase 1, in addition to the phosphorylated, active forms of these key centrosome-localised cell cycle kinases.

2. The effect of centrosome amplification on the individual proteins that govern the cell cycle is analysed as opposed to cell cycle lengths.

3. The effect of centrosome amplification on the relationships/correlations between cell cycle parameters and centrosomal parameters has been tested. This shows whether centrosome amplification disturbs the pathways connecting the cell cycle and centrosome dynamics and thus provides implications of how centrosome amplification may affect the cell cycle events with changing centrosomal parameters. Correlation coefficient (R^2) has been considered as satisfactory with a value above or equal to 0.5. Therefore, R^2 values will be considered different only if one of them is above the 0.5 threshold and the other one is not. For exampe, two data sets with values 0.01 and 0.45 are both considered as showing no correlation, meaning the trend is indifferent for the two data sets.

Centrosomal parameters are considered to be well represented by pericentrin protein since it is located on centrosomes and represents centrosome development directly. Thus centrosome parameters were quantified using the pericentrin-derived fluorescence. The centrosomal parameters derived from pericentrin fluorescence are centrosome size (judged by pericentrin fluorescence area) and centrosome maturity (judged by the relative quantity of pericentrin on the centrosomes, determined by its integrated density via Fiji). Integrated density is calculated by multiplying the mean gray value of the selected area within the acquisition by the selected area.

The units of integrated density are grayscale value*μM^2. Grayscale value is the same as mean gray value which is the strength of the signal in an area, directly proportional to the concentration of the protein in the area of interest. The units of mean grey value are not specified. Cell cycle parameters are the quantifiable properties of the three proteins tested here: mean grey value (concentration or density), Integrated density (relative quantity/molecule count) and lastly, the area of the fluorescence of the protein until a certain threshold. The threshold limit is important since there is always some minor background fluorescence potentially representing false positives. Tubulin state has been used to determine the mitotic status of the cells. Fang et al., (2017) have utilised integrated density for protein quantitation and here this method has been employed.

Pericentrin stain has been utilised to mark the centrosomes in a cell and assign the cell's centrosomal status which was either centrosome amplified-"CA" or normal – "normal". Subsequently, the other channel which has appeared red stemming from rabbit antibodies has been used to portray a cell cycle protein – either AURKA, pAURKA, PLK1 or pPLK1. There were 3 combinations of antibodies used in this part of the study: 1 – MoPer, RbAURKA, RatTub. 2 – MoPer, RbpAURKA, RatTub. 3 – MoPer, RbpPLK1, RatTub. Every set also contained a DAPI-stained DNA. Mo stands for Mouse, Rb for Rabbit, and Rat for Rat. Per stands for Pericentrin, AURKA for Aurora kinase A, PLK1 for Polo-like kinase 1 and a prefix p for a phosphorylated state of the protein. Pericentrin has been used as a marker for the centrosomes while AURKA, pAURKA, pPLK1 and PLK1 have been used as the tested cell cycle proteins. AURKA, pAURKA and pPLK1 can also be used as alternative markers for centrosomes. Once the parameters have been calculated and cell centrosomal statuses assigned, two analyses have been done for each comparison of centrosomal vs. cell cycle parameters. The first one was comparing the relationship between the two i.e. correlation and how it changes with centrosome amplification (portrayed in a scatter plot). The second one was done by comparing the average values and standard deviation, in the form of a bar chart.

Mouse, showing green, antibodies were such: anti-pericentrin, and anti-PLK1. Rabbit, showing red, antibodies were such: anti-pAURKA, anti-pPLK1, anti-AURKA, anti-pericentrin. Rat antibodies, showing grey, were such: anti- alpha-tubulin and anti-gamma tubulin.

In the following set of example acquisitions, pericentrin is the centrosome marker and Aurora A kinase is the protein of interest (cell cycle protein). The acquisitions below are examples of pictures, not all of the acquired pictures are shown below. In further analysis, all of the pictures

were be used. Every acquisition has been performed for cells in the mitotic phase, seen from tubulin-derived fluorescence and DAPI stain.

Figure below shows example acquisitions of a mitotic cell with centrosome amplification.

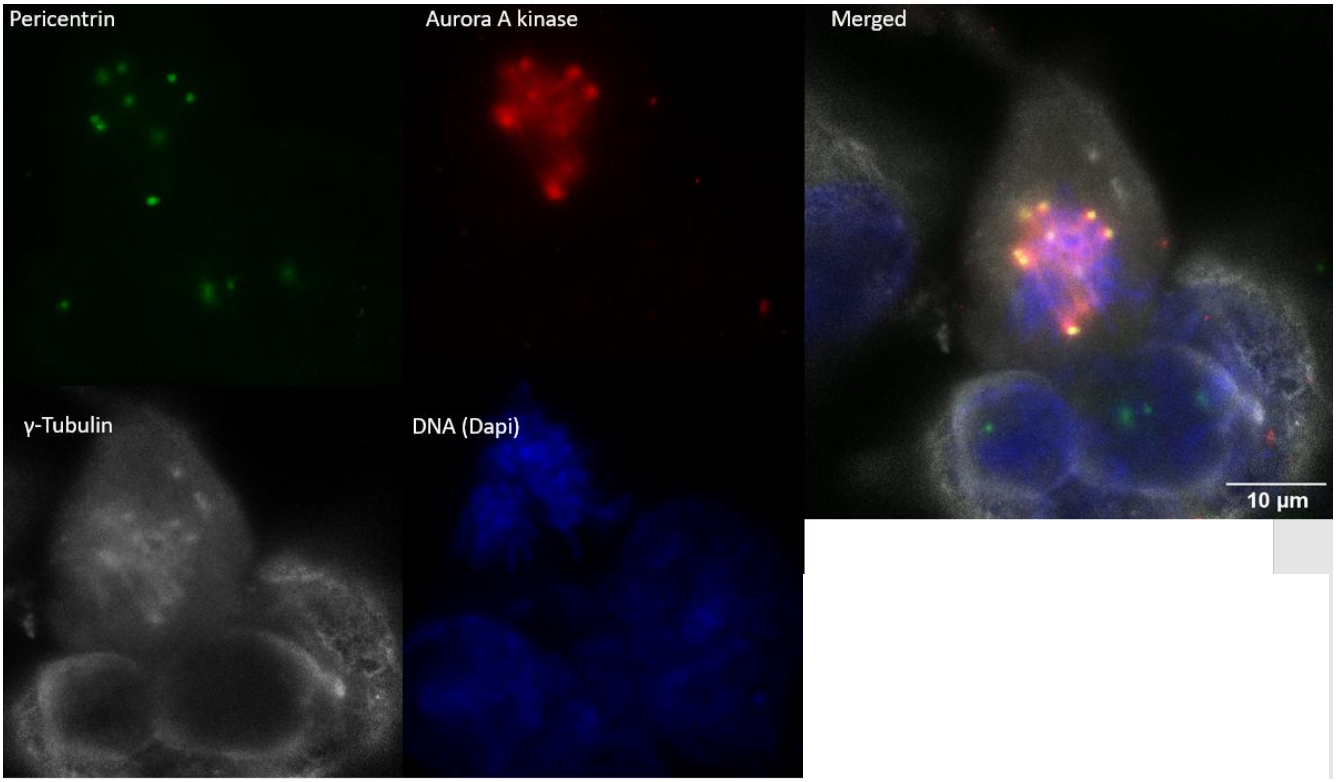

Figure 5.1.1: **Example acquisition of centrosome amplification in OMM2.3_H2B-FUCCI2a cells through the 4 channels**. OMM2.3_H2B-FUCCI2a were stained with primary antibodies and subsequently with goat secondary antibodies as explained in the methods section in Chapter 2. Green channel represents mouse primary antibody, red channel represents rabbit primary antibody, gray channel represents rat primary antibody. Dapi was mixed with Mowiol ant naturally assimilated into the DNA due to high affinity. The 4 channels portray the fluorescence derived from these proteins: Green (top left) – pericentrin; Red (top right) -Aurora Kinase- A; Gray (bottom left) – tubulin; blue (bottom right) – DNA. Merged: The 4 types of fluorescence acquired from the following antibodies: Pericentrin, Aurora A kinase, tubulin. DAPI was used to visualise DNA. The visualised cell shows a composite image of the 4 channels. Acquisitions processed via Fiji (Schindelin et al., 2012).

Looking at the figure above, it can be seen that Pericentrin, Aurora Kinase-A and gamma-Tubulin all outline centrosomes and can be used to justify centrosome amplification for this cell.

The figure below shows a second example acquisition of a cell which is in mitosis and contains centrosome amplification, this time with clustered centrosomes.

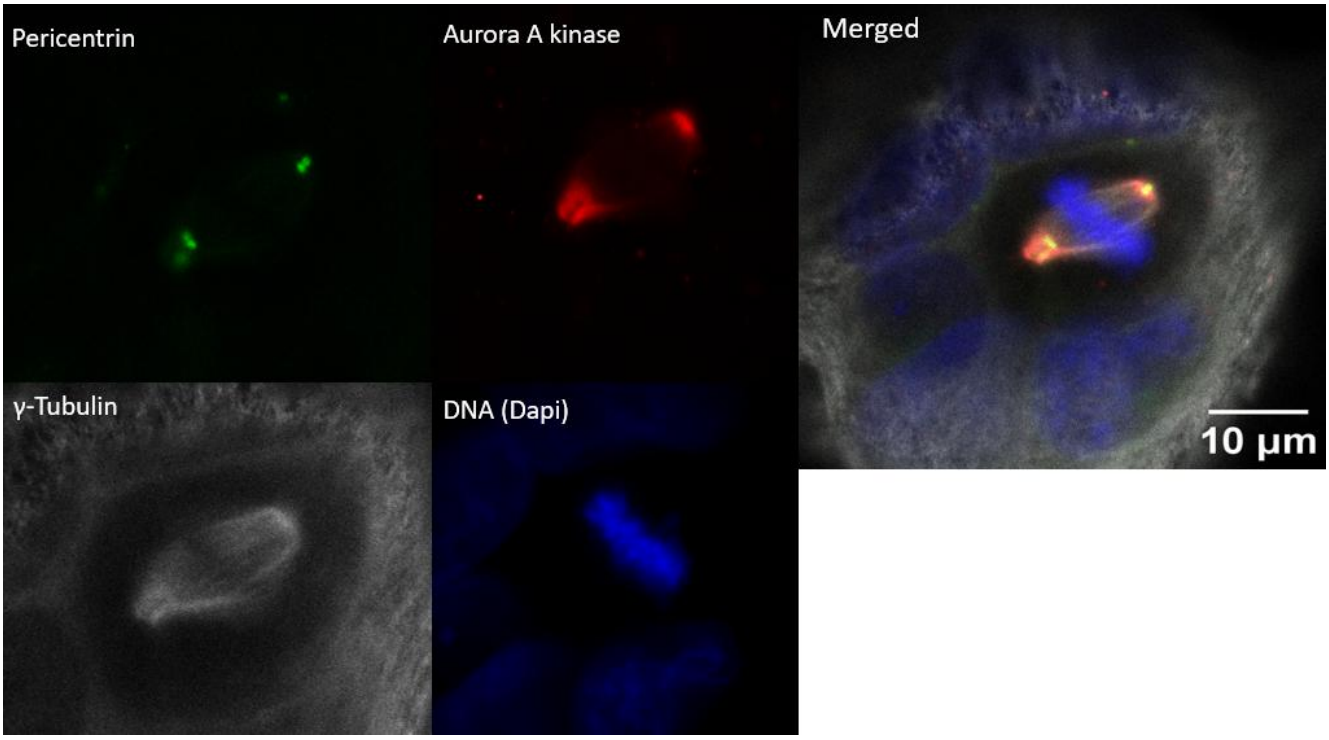

Figure 5.1.2: **Example acquisition of centrosome amplification in OMM2.3_H2B-FUCCI2a cells through the 4 channels**. Refer to figure 5.1.1 for experimental explanation. The 4 types of fluorescence acquired from the following antibodies: Pericentrin, Aurora A kinase, tubulin. DAPI was used to visualise DNA. Image on the right shows all channels merged. Acquisitions processed via Fiji (Schindelin et al., 2012).

In the acquisition above it can be seen that the cell contains at least 3 centrosomes with at least two positioned to one side of the cell, better seen through the Aurora Kinase-A channel.

The figure below portrays a cell which contains a normal number of centrosomes.

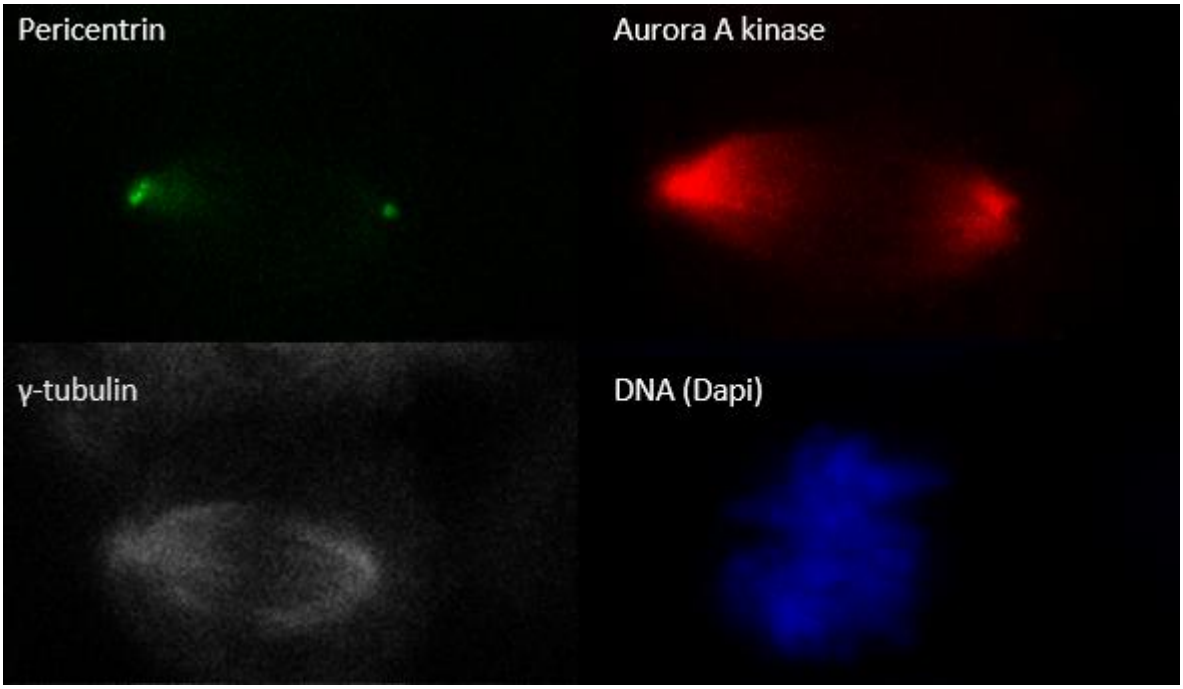

Figure 5.1.3: **Example acquisition of OMM2.3_H2B-FUCCI2a cells through the 4 channels** Refer to the figure 5.1.1 for experimental method outline. Acquisitions processed via Fiji (Schindelin et al., 2012).

The acquisition in Figure 5.1.3 it is seen that cells are in mitosis due to chromosomes aligning at the metaphase plate, microtubules forming as seen from AURKA and tubulin channels and centrosomes being at the opposite poles of the cell. This cell does not have centrosome amplification.

The next set of figures portrays acquisitions of cell images with the same DAPI and pericentrin stains, but with a rabbit phospho-PLK1 stain and alpha-tubulin. As a result, the red channel will correspond to the pPLK1 protein in the following set of images. This protein is considered to closely resemble centrosome localisation.

The following figure shows a single cell for the 4 afforementioned channels, but a Z stack image has been taken. Z stack refers to the 3rd dimension of depth. As a result, 3 slices arise for each channel, thus 12 images are portrayed below for the cell.

The figure below shows an acquisition of a cell with centrosome amplification.

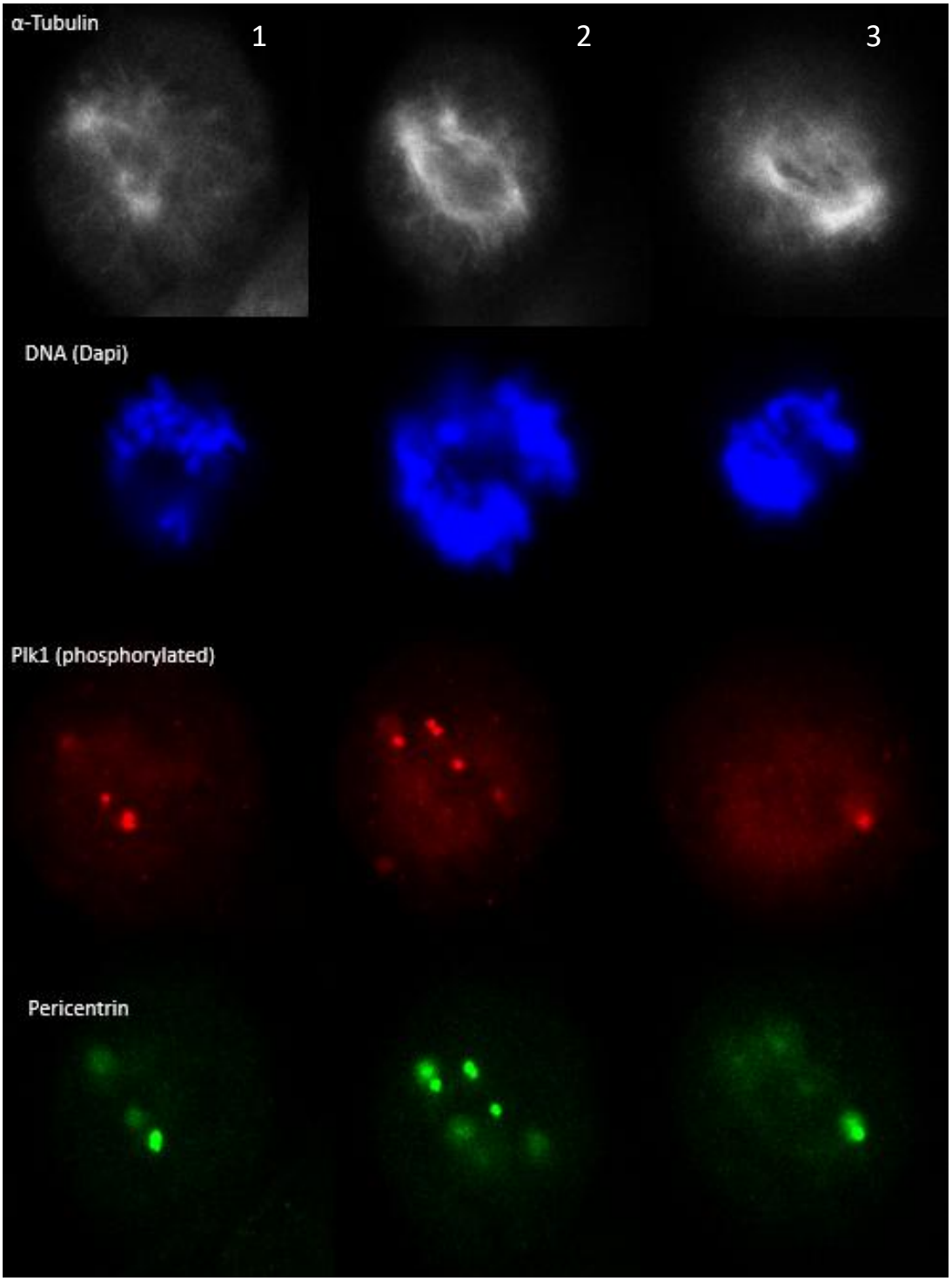

Figure 5.1.4: **Example Z-Stack acquisition of centrosome amplification in OMM2.3_H2B-FUCCI2a cells through the 4 channels**. Refer to the figure 5.1.1 for experimental method outline and antibody setup. Pericentrin channel (green) has been used to assign this cell to have amplification. 3 different slices through the depth of each channel have been acquired for this figure. Acquisitions processed via Fiji (Schindelin et al., 2012).

The cell shown above in Figure 5.1.4 contains amplified centrosomes judged by pericentrin and phospho-PLK1 derived fluorescence.

The next acquisition is a one dimensional picture of the 4 channels.

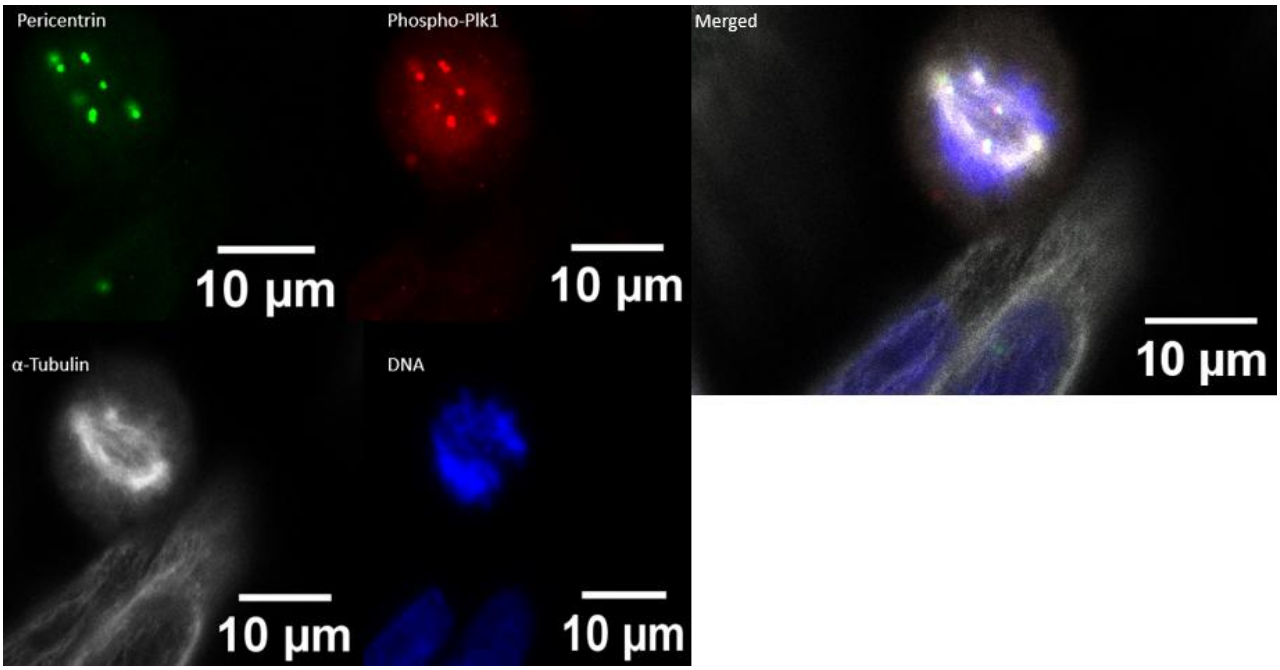

Figure 5.1.5: **Example acquisition of centrosome amplification in OMM2.3_H2B-FUCCI2a cells through the 4 channels**. Refer to the figure 5.1.1 for experimental method outline. Pericentrin channel (green) has been used to assign this cell to have amplification. Merged image on the right side of the figure portrays 4 channels in one picture. Acquisitions processed via Fiji (Schindelin et al., 2012).

Looking at the cell above, it can be seen that the cell contains amplified centrosomes from the pericentrin and pPLK1-derived fluorescence.

The next set of pictures shows acquisitions of cell images with the stains for the following proteins: DAPI for DNA (blue), Alpha-tubulin (grey), pericentrin (green), and pAURKA (red). The cell contains a normal centrosome count.

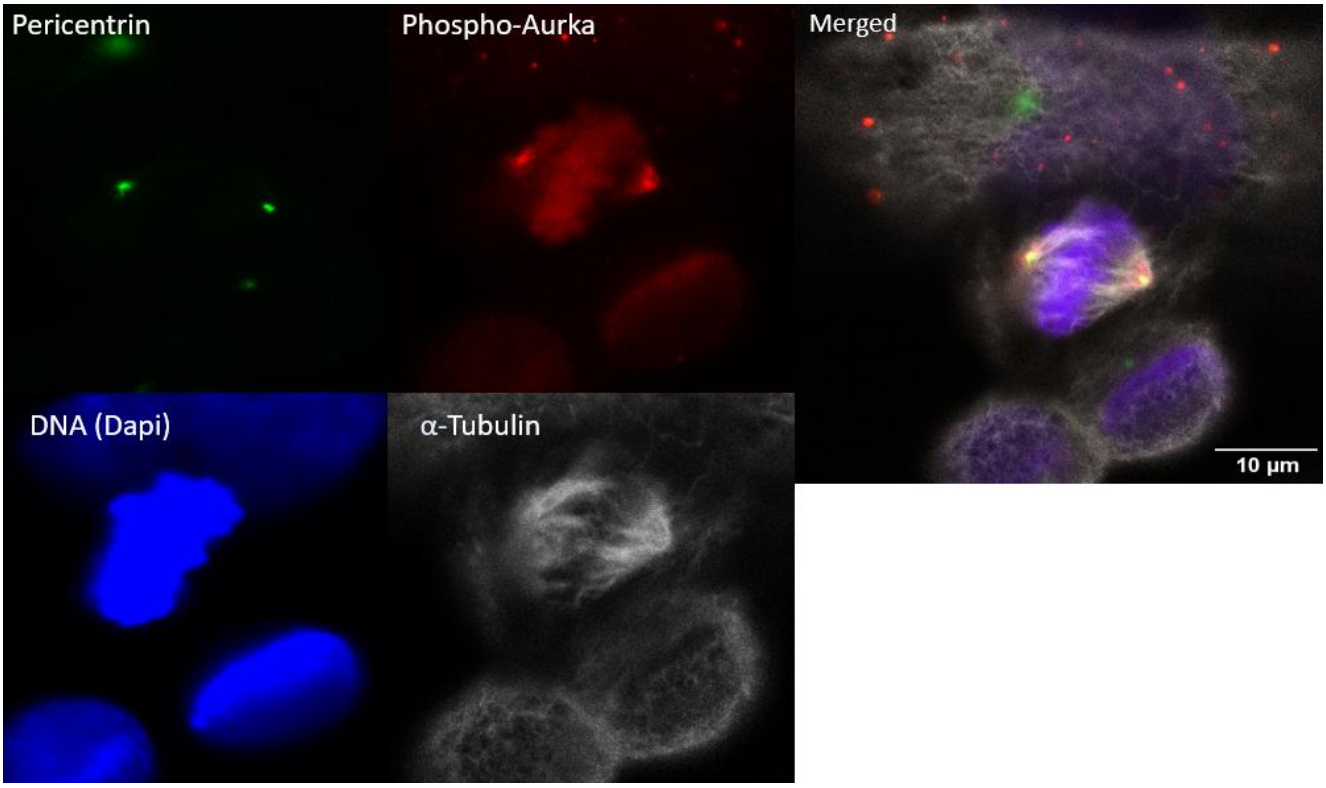

Figure 5.1.6: **Example acquisition OMM2.3_H2B-FUCCI2a cells through the 4 channels**. Refer to the figure 5.1.1 for experimental method outline. The shown cell has been assigned mitotic through the tubulin and phospho-aurora A channels. Image on the right side of the figure shows the four channels merged. Acquisitions processed via Fiji (Schindelin et al., 2012).

From the figure above it is seen through pericentrin and pAURKA derived fluorescence that the cell contains two centrosomes. From tubulin and pAURKA channels it is apparent that the cell is in the mitotic stage.

The following acquisition is a Z stack with 2 slices for each channel (8 pictures total).

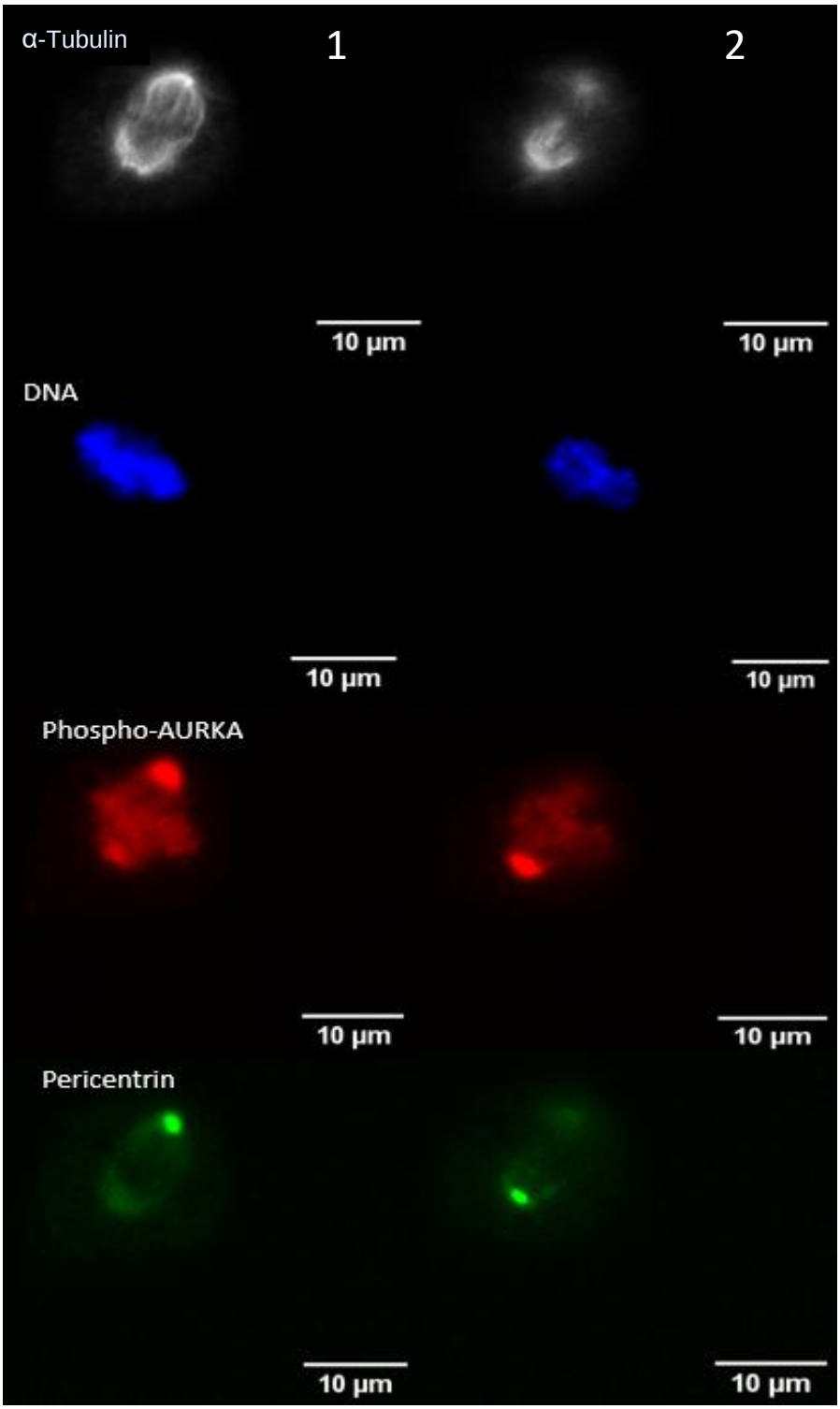

Figure 5.1.7: **Example Z-stack acquisition OMM2.3_H2B-FUCCI2a cells through the 4 channels**. Refer to the figure 5.1.1 for experimental method outline. The shown cell has been assigned mitotic through the tubulin and phospho-aurora A channels. This figure shows a two-dimesnional image of a mitotic cell. Acquisitions processed via Fiji (Schindelin et al., 2012).

Chapter 5.2: Results: Cell cycle parameter comparisons with centrosome parameters.

To analyse the above images and the rest, DAPI and tubulin stains were used to visualise the boundaries of the cell and to judge whether it is in mitosis. The other two stains are used for finding the relationship between centrosomes and the cell cycle. Every combination of primary antibodies contained one bound to a cell cycle protein which will be analysed with respect to the other stained protein which is a centrosomal marker (pericentrin). Two parameters of pericentrin have been compared: its fluorescence area corresponding to the area of centrosomes and the integrated density of pericentrin, corresponding to the total quantity of centrosomal pericentrin. The centrosome area parameter refers to the total area of all the centrosomes in that cell, it is not an average area of one centrosome. The same applies to all the other parameters. These parameters were graphed on a scatter plot for normal and for centrosome amplified cells, where each point/dot represents data from a different cell. Subsequently, every parameter's average value for normal and centrosome amplified cells has been graphed on a bar chart to compare the difference between the values rather than the difference in the relationships/correlations.

The following set of figures shows the relationships between the Centrosome area and the indicated parameters of Aurora Kinase-A.

The figure below compares the centrosome area with the integrated density of AURKA on centrosomes.

A)

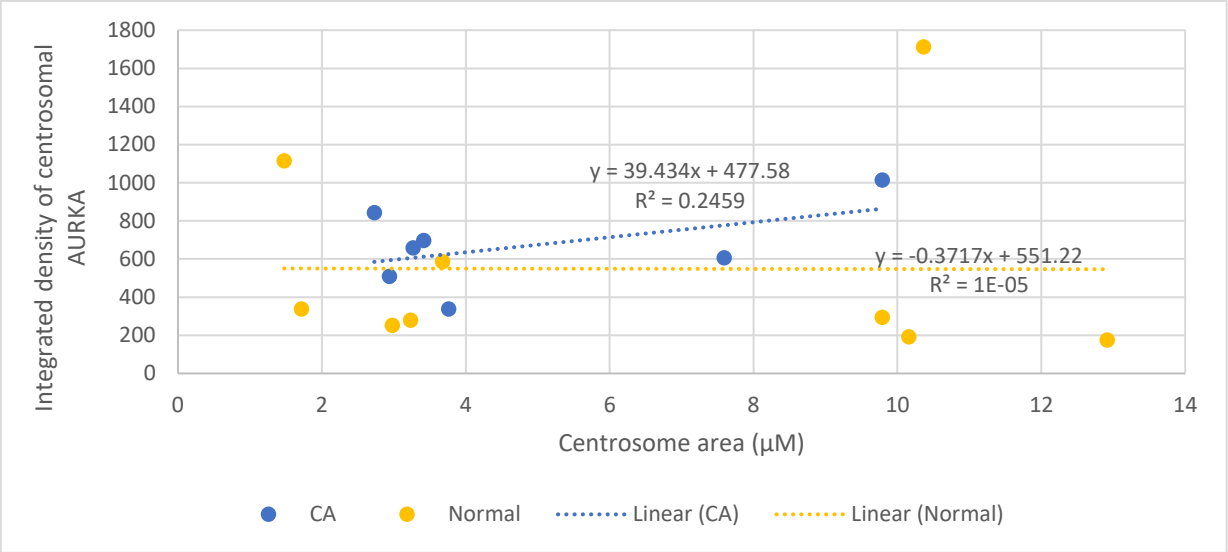

B)

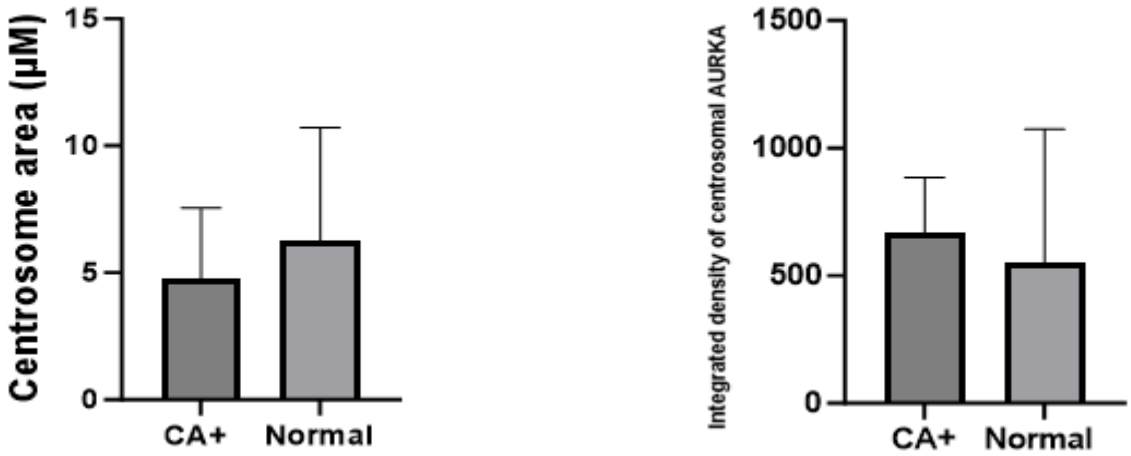

Figure 5.2.10, part A**: The centrosome area against the Integrated density of AURKA on centrosomes**. Lines of best fit and correlation coefficients for the different comparatives: CA: y = 39,434x + 477,58; R^2 = 0,2459. Normal: y = -0,3717x + 551,22; R^2 = 1E-05. Figure 5.2.10, part B: **The comparison of data distribution of the indicated parameters.** Significant differences have been obtained through Unpaired t-test with Welch's correction**.** Statistics for Centrosome area: CA+: range 7,063; mean: 4,785. Normal: range: 11,44; mean 6,256. The two categories are insignificantly different (P value 0,432). Statistics for integrated density of AURKA on the centrosome area: CA+ range: 676; mean: 666,3. Normal range: 1537; mean 548,9. The two tested categories are not significantly different (P value 0,55). Refer to figure 4.3.2 for citation of software for statistical analyses .

The scatter in figure 5.2.10A shows no relationship between the centrosome area and the integrated density of centrosomal Aurora Kinase-A, as correlation coefficients are below the 0,5 threshold, for both normal and centrosome amplified cells.

Figure 5.2.10B shows that the centrosome area and the integrated density of centrosomal AURKA are indifferent for normal cells and cells with amplified centrosomes.

The figure below compares the centrosome area with the Mean Gray value of Aurora Kinase-A on the area of centrosomes.

A)

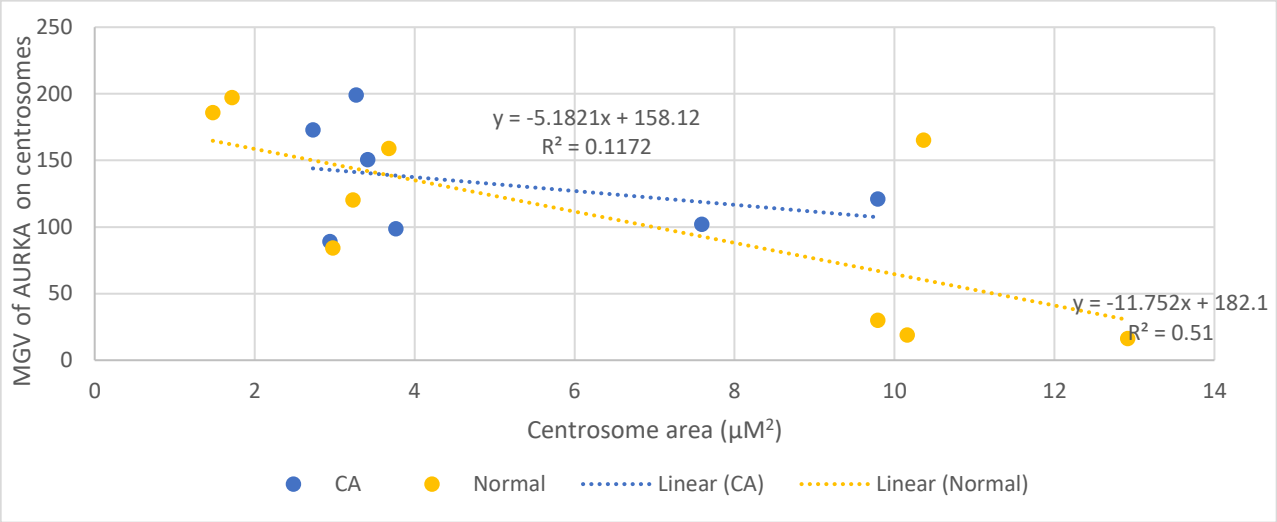

B)

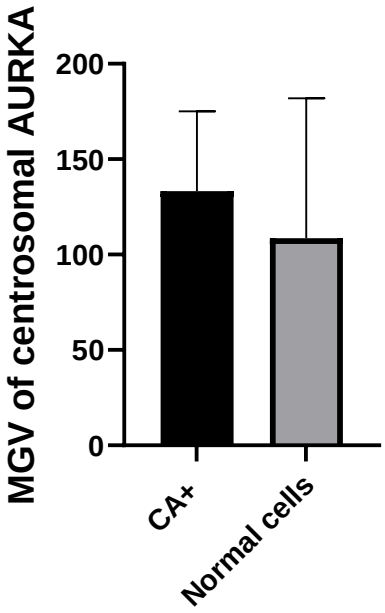

Figure 5.2.11, Part A: **The Mean gray value of Aurora Kinase A on centrosomes against the area of centrosomes**. The data obtained for area, MGV and integrated density has been done via Fiji (Schindelin et al., 2012) as described in chapter 2 methods section. CA: Line of best fit equation: y = -5,1821x + 158,12; R^2 = 0,1172. Normal: Line of best fit equation: y = -11,752x + 182,1; R^2 = 0,51.

Figure 5.2.11, Part B: **The Mean gray value of Aurora Kinase A on centrosomes for the two data categories**. Significant differences have been obtained through Unpaired t-test with Welch's correction. Statistics: CA+: range: 110; mean: 133,3. Normal cells: range: 180,9; mean 108,6. The two data categories are insignificantly different (P value 0,4108). Calculations and comparative tests have been done through the GraphPad prism version 9.0.0, GraphPad software, Boston, Massachusetts,USA, www.graphpad.com.

Looking at figure 5.2.11A, only the “Normal” category has shown a correlation coefficient over 0,5 indicating a correlation for normal cells between the centrosome area and the mean grey value of centrosomal Aurora Kinase-A. Looking at figure 5.2.11B, it can be said that the mean grey value of AURKA on centrosomes is independent of whether cells contain a normal or an amplified centrosome number.

The next figure portrays the relationship between the centrosome area and the area of the fluorescence of Aurora Kinase-A.

A)

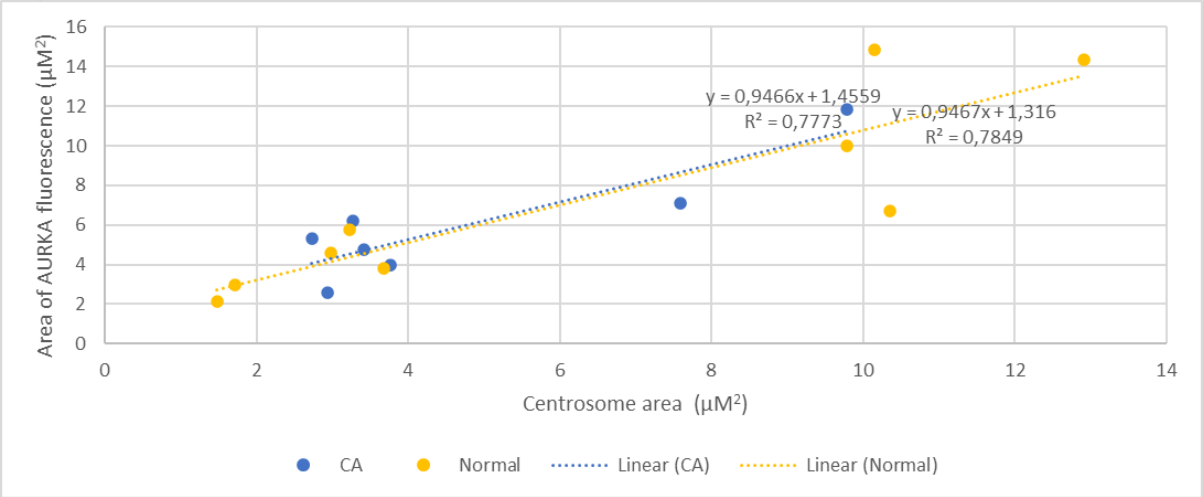

B)

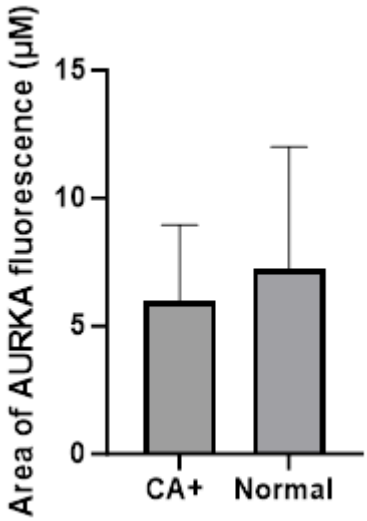

Figure 5.2.12 Part A: **The area of Aurora kinase-A fluorescence against the centrosome area**. Lines of best fit and correlation coefficients for the different comparatives: CA: y = 0,9466x + 1,4559; R^2 = 0,7773. Normal: y = 0,9467x + 1,316; R^2 = 0,7849.

Figure 5.2.12 Part B: **The average Area of AURKA fluorescence for normal and centrosome amplified cells**. Significant differences have been obtained through Unpaired t-test with Welch's correction. CA+: range 9,223; mean: 5,986. Normal: range: 12,71; mean: 7,238. Data sets are not significantly different (P value 0,5301). Calculations and comparative tests have been done through the GraphPad prism version 9.0.0, GraphPad software, Boston, Massachusetts,USA, www.graphpad.com.

The scatter plot (figure 5.2.12A) shows that the centrosome area correlates well with the area of Aurora Kinase-A fluorescence for both normal and centrosome-amplified cells. Figure 5.2.12B shows that the area of AURKA fluorescence is indifferent between normal and centrosome-amplified cells.

The figure below compares the centrosome area with the mean gray value of phospho-Aurora Kinase-A on centrosomes.

A)

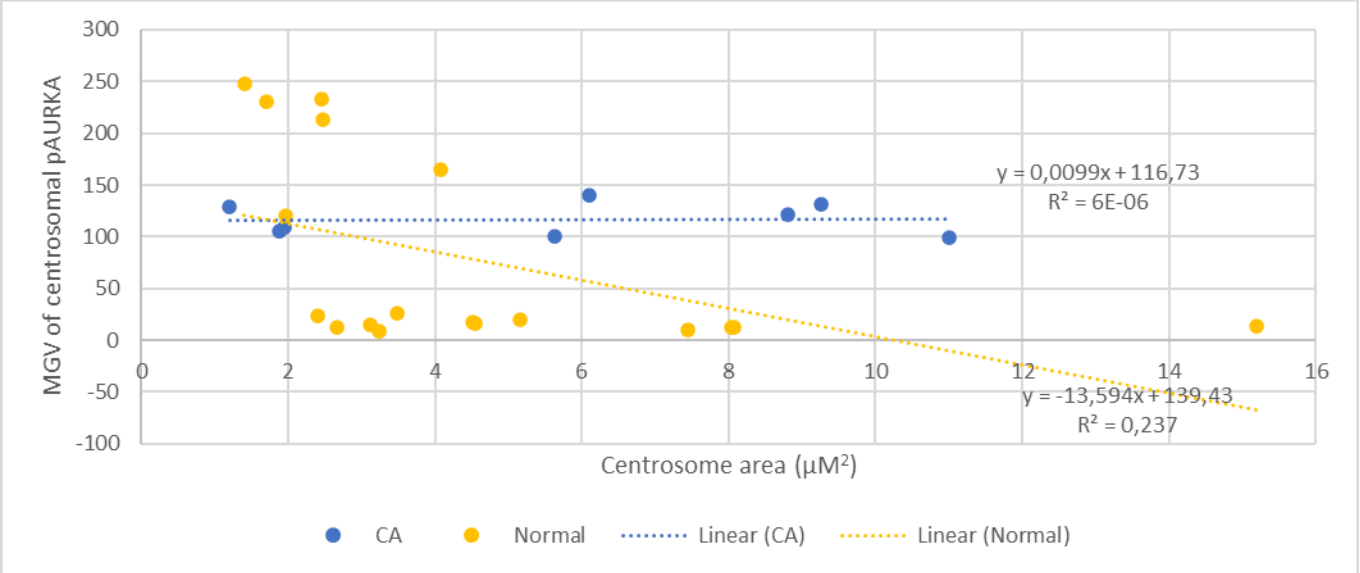

B)

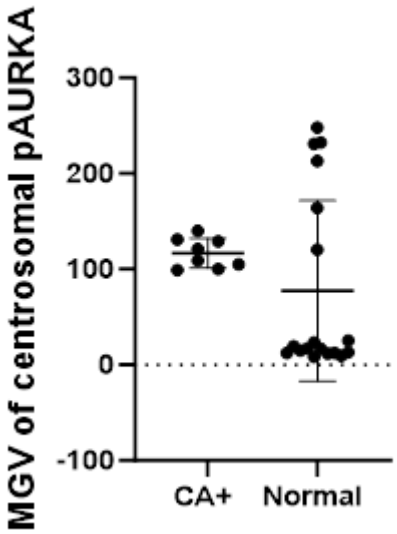

Figure 5.2.13 A: **The Mean gray value of phospho-Aurora Kinase A on centrosomes against the area of centrosomes**. CA: Line of best fit equation: y = 0,0099x + 116,73; R^2 = 6E-06. Normal: Line of best fit equation: y = -13,594x + 139,43; R^2 = 0,237.

Figure 5.2.13 B: **The average mean gray value of Aurora Kinase A on centrosomes for the two data categories**. Significant differences have been obtained through Unpaired t-test with Welch's correction. Statistics: CA+: range: 43; mean 119,3. Normal: range: 180,9; mean: 85,6. The comparatives are not significantly different (P value 0,4108). Calculations and comparative tests have been done through the GraphPad prism version 9.0.0, GraphPad software, Boston, Massachusetts,USA, www.graphpad.com.

From the scatter plot in figure 5.2.12A, it can be seen that neither for normal nor centrosome amplified cells the centrosome area correlates with the MGV of centrosomal pAURKA. The bar

chart shows that the MGV of centrosomal pAURKA is consistent for normal and centrosome amplified cells.

The next figure shows the relationship of centrosome area and the integrated density of pAURKA on the area of centrosomes.

A)

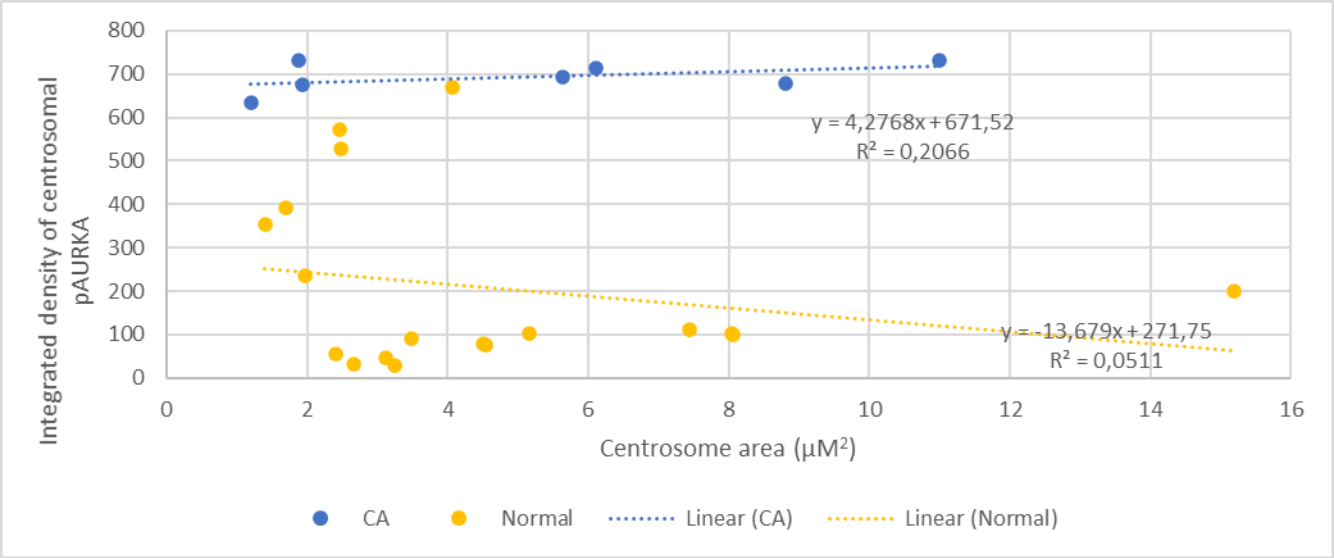

B)

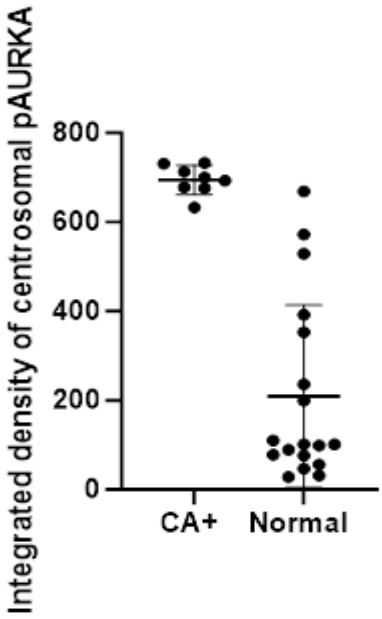

Figure 5.2.14 A: **The Integrated density of pAURKA on centrosomes against the area of centrosomes**. Line of best fit equations. CA: y = 4,2768x + 671,52; R^2 = 0,2066. Normal: Line of best fit equation: y = -13,679x + 271,75; R^2 = 0,0511. An outlier has been removed from the "CA+" category.

Figure 5.2.14 B: **Average integrated density of centrosomal pAURKA for normal and centrosome amplified cells**. Significant differences have been obtained through Unpaired t-test with Welch's correction. Statistics: CA+: range: 100; mean 694,6. Normal: range: 640,8; mean 209,5. The variables are significantly different (P value < 0,0001). Calculations and comparative tests have been done through the GraphPad prism version 9.0.0, GraphPad software, Boston, Massachusetts,USA, www.graphpad.com.

Looking at the scatter from figure 5.2.14A, it can be said that neither for normal or centrosome amplified cells, the two parameters are dependent, as seen from the low correlation coefficients.

From the bar chart above it can be said that in cells with centrosome amplification, there are significantly more pAURKA molecules scaffolded on centrosomes than in normal cells.

The next figure shows the relationship between the pAURKA fluorescence area and centrosome area.

A)

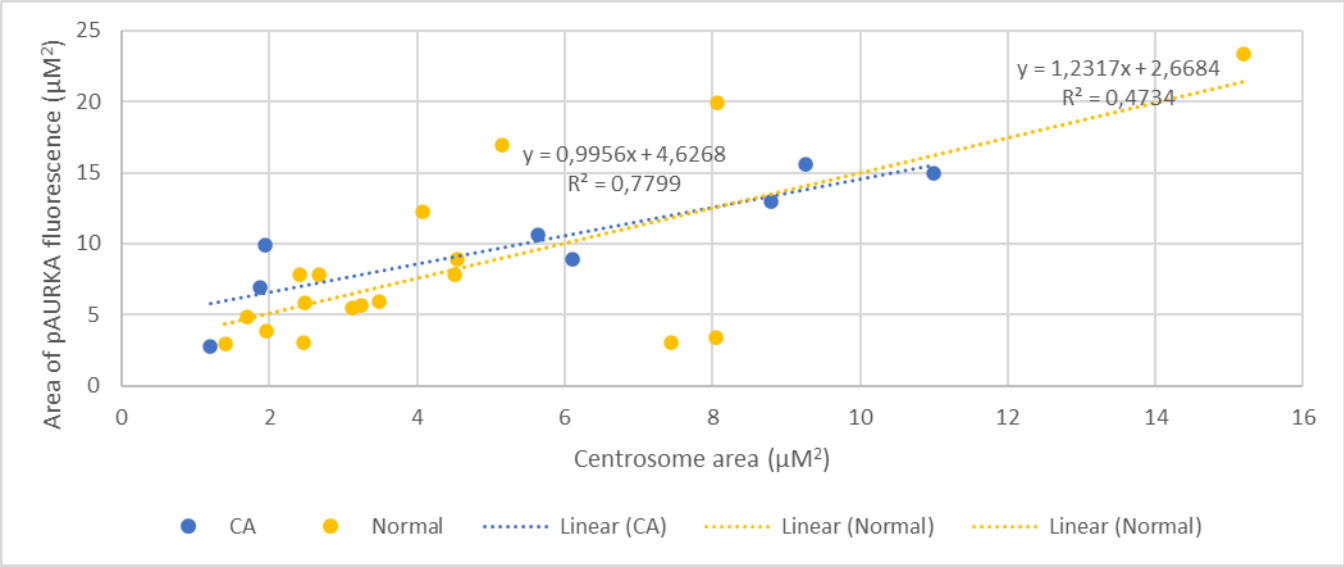

B)

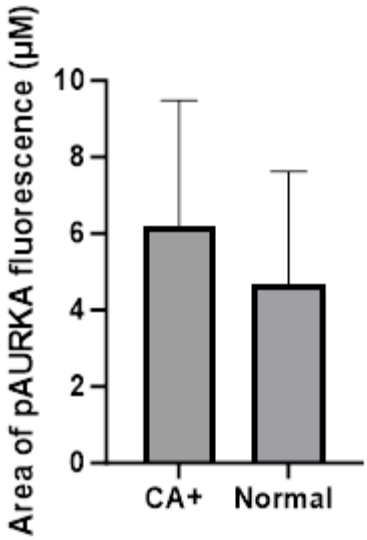

Figure 5.2.15A: **Area of pAURKA fluorescence against the area of the centrosomes**. CA: Line of best fit equation: y = 0,9956x + 4,6268; R^2 = 0,7799. Normal: Line of best fit equation: y = 1,2317x + 2,6684; R^2 = 0,4734.

Figure 5.2.15B: **Average area of phospho-Aurora Kinase-A fluorescence for normal and centrosome amplified cells**. Significant differences have been obtained through Unpaired t-test with Welch's correction. CA+: Range: 10; mean: 6,191. Normal: range: 8,36; mean: 4,692. Not significantly different (P value 0,289). Calculations, statistics and comparative tests have been done through the GraphPad prism version 9.0.0, GraphPad software, Boston, Massachusetts,USA, www.graphpad.com.

Figure 5.2.15A above shows that the area of centrosomes coincides well with the area of pAURKA fluorescence, as for both categories the correlation coefficients are relatively high. Figure 5.2.15B

shows that normal and centrosome amplified cells are not different concerning their pAURKA fluorescence area.

The figure below shows the relationship of centrosome area with the mean grey value of centrosomal pPLK1.

A)

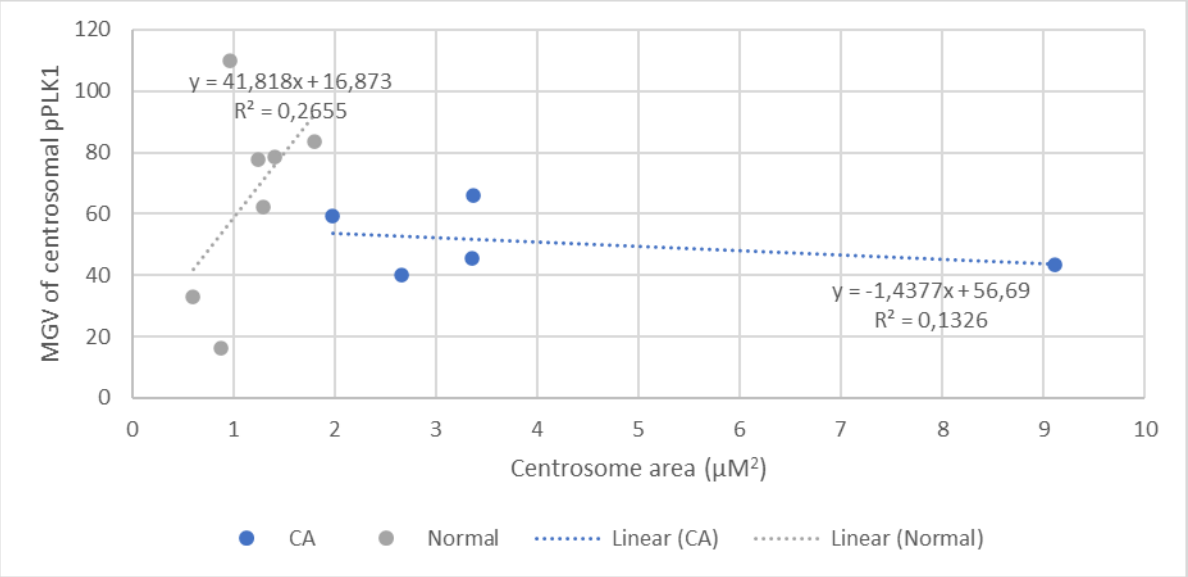

B)

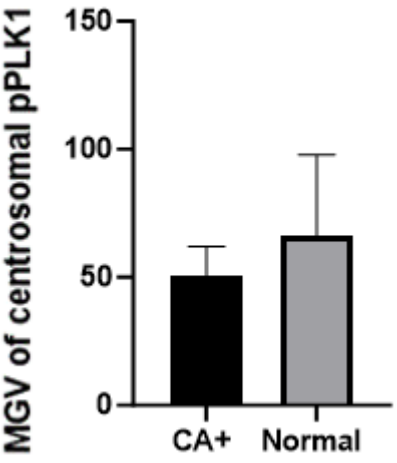

Figure 5.2.16 A: **The mean gray value of pPLK1 on centrosomes versus the area of centrosomes**. CA: Line of best fit equation: y = -1,4377x + 56,69; R^2 = 0,1326. Normal: Line of best fit equation: y = 41,818x + 16,873; R^2 = 0,2655.

Figure 5.2.16 B: **The average Mean gray value of pPLK1 on centrosomes for normal cells and centrosome amplified cells**. Significant differences have been obtained through Unpaired t-test with Welch's correction. CA+: range: 26,17; mean: 50,81. Normal: range: 93,7; mean: 65,87. The two sets of data are not significantly different (P value 0,2831). Calculations, statistical tests and comparative tests have been done through the GraphPad prism version 9.0.0, GraphPad software, Boston, Massachusetts,USA, www.graphpad.com.

In figure 5.2.16A, none of the lines of best fit shows a good enough correlation for it to be considered a dependency. From the bar chart in figure 5.2.16B, it can be said that the mean grey value of centrosomal pPLK1 is independent of the centrosome amplification.

The figure below shows the relationship of centrosome area with the Integrated density of centrosomal pPLK1.

A)

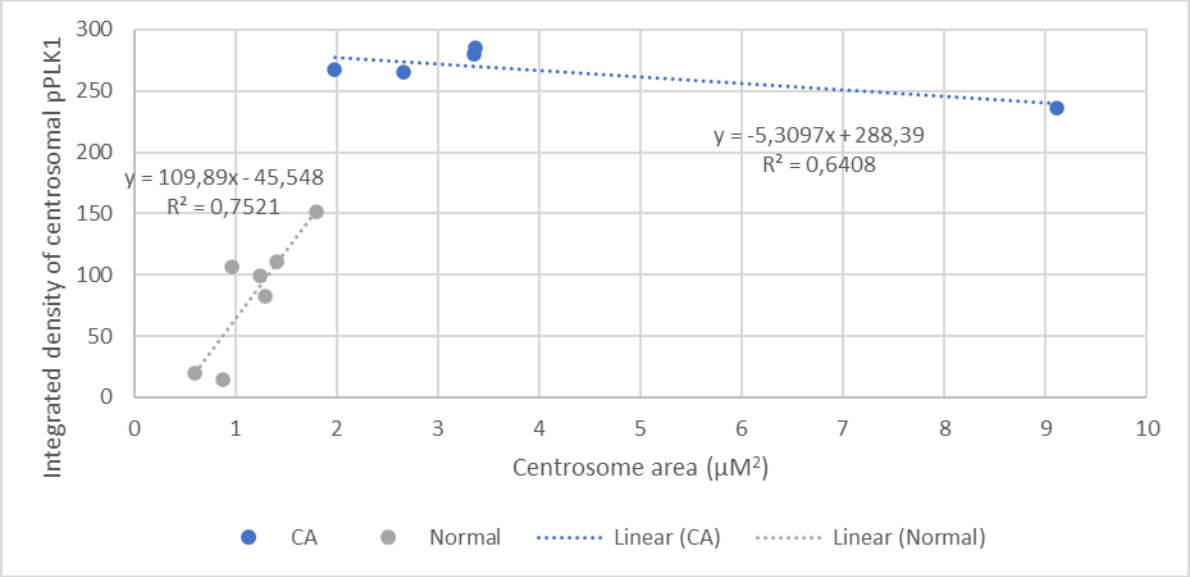

B)

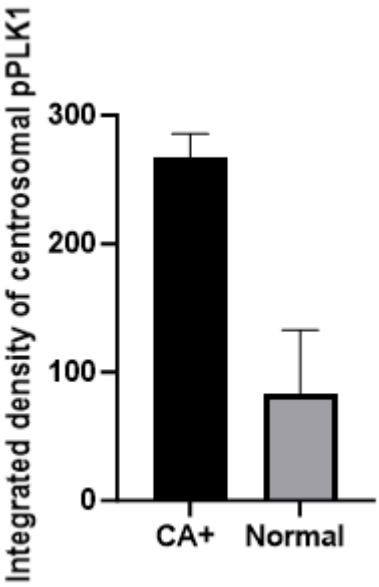

Figure 5.2.17 A: **The Integrated density of pPLK1 on centrosomes against the area of centrosomes**. CA: Line of best fir equation: y = -5,3097x + 288,39; R^2 = 0,6408. Normal: Line of best fit equation: y = 109,89x - 45,548; R^2 = 0,7521.

Figure 5.2.17 B**: Average integrated density of pPLK1 on centrosomes for normal and centrosome amplified cells**. Significant differences have been obtained through Unpaired t-test with Welch's correction. CA+: range: 48,7; mean: 266,7. Normal: range 136,8; mean 83,21. The data sets are significantly different (P value < 0,0001). Calculations and comparative tests have been done through the GraphPad prism version 9.0.0, GraphPad software, Boston, Massachusetts,USA, www.graphpad.com.

From the figure 5.2.17A above it appears that both sets of data show a good correlation with the coefficients above the 0,5 threshold.

The bar chart in figure 5.2.17B shows that for normal cells the quantity of pPLK1 is much lower than for cells with amplified centrosomes.

The next figure compares the centrosome area to the area of pPLK1 fluorescence.

A)

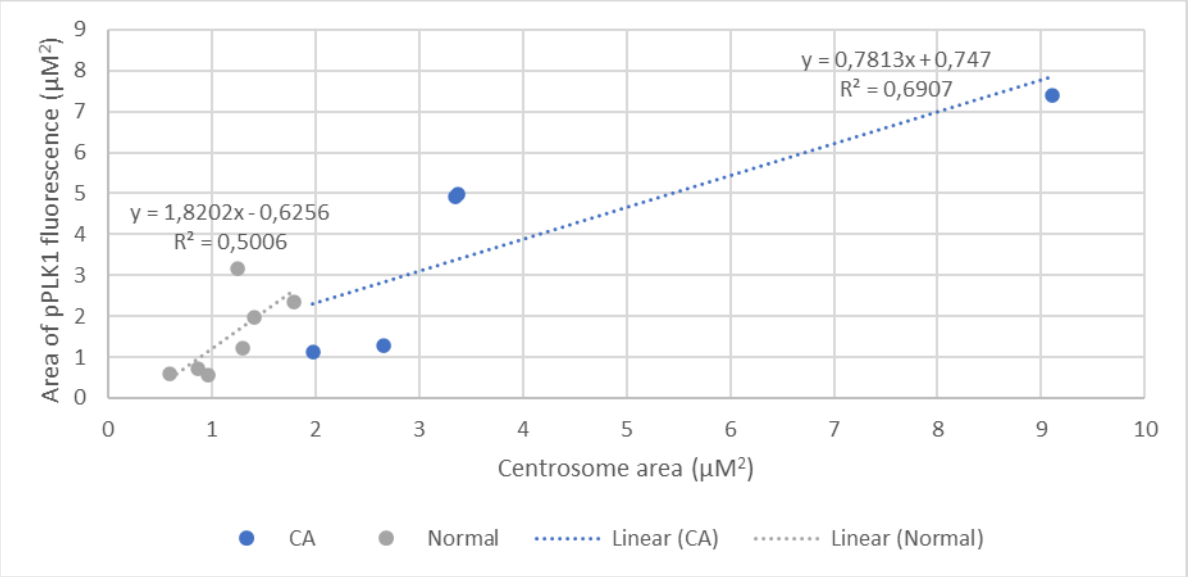

B)

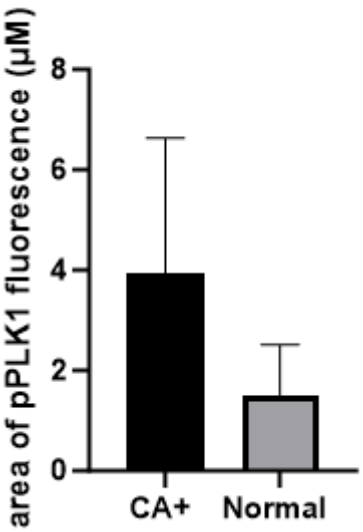

Figure 5.2.18 A: **The area of pPLK1 fluorescence againt the area of centrosomes**. CA: Line of best fit: y = 0,7813x + 0,747; R^2 = 0,6907. Normal: Line of best fit: y = 1,8202x - 0,6256; R^2 = 0,5006.

Figure 5.2.18 B: **Average area of pPLK1 for normal and centrosome amplified cells**. Significant differences have been obtained through Unpaired t-test with Welch's correction. Statistics: CA+: range: 6,263; mean 3,945. Normal: range: 2,610; mean 1,507. Variables not significantly different (P value 0,1134). Calculations and comparative tests have been done through the GraphPad prism version 9.0.0, GraphPad software, Boston, Massachusetts,USA, www.graphpad.com.

Centrosome area correlates well with the pPLK1 location, as seen from the correlation coefficients for both data sets in figure 5.2.18A. Figure 5.2.18B shows that the area of pPLK1 fluorescence does not change when centrosomes are amplified.

The following set of figures portrays data comparing the centrosomal integrated density from pericentrin fluorescence against Aurora Kinase-A, phospho-Aurora Kinase A and phospho-Polo-like Kinase 1.

A)

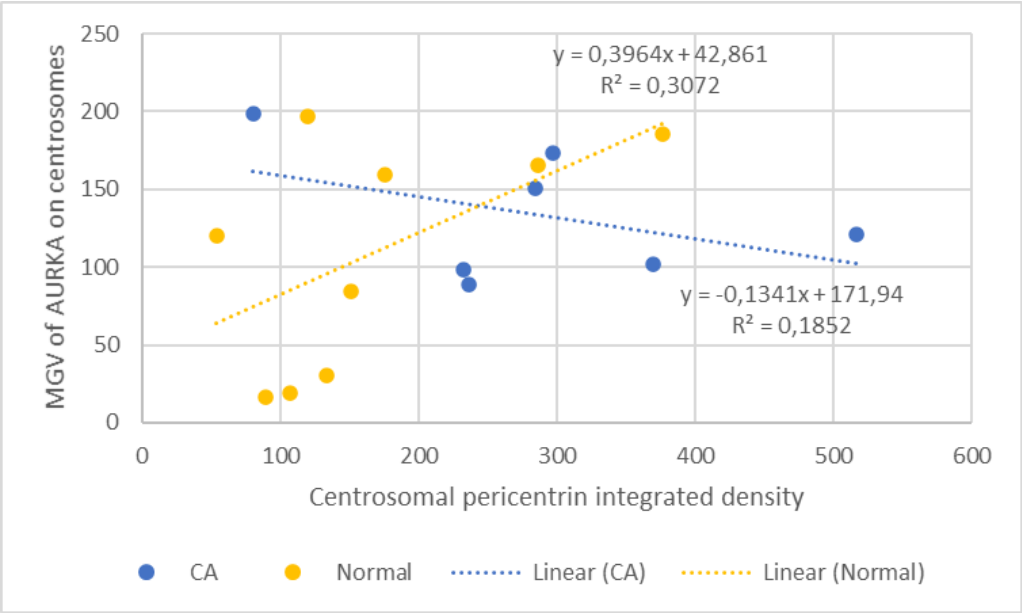

B)

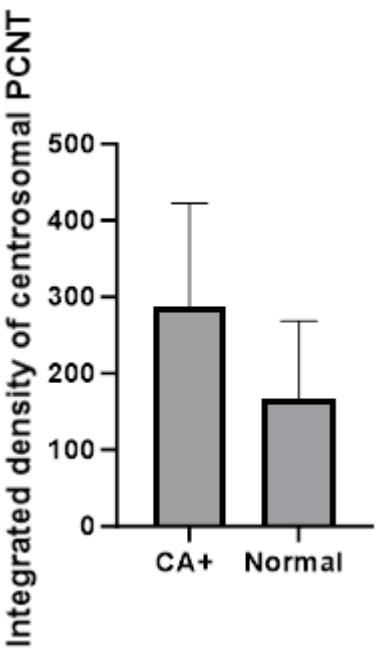

Figure 5.2.19 A: **The MGV of Aurora kinase-A on centrosomes against the integrated density of centrosomal pericentrin**. Line of best fit equations: CA: y = -0,1341x + 171,94; R^2 = 0,1852. Normal: y = 0,3964x + 42,861; R^2 = 0,3072.

Figure 5.2.19 B: **The average Integrated density of AURKA of normal and centrosome amplified cells**. Significant differences have been obtained through Unpaired t-test with Welch's correction. Statistics: CA+:range: 436,7; mean: 288,0. Normal: range: 288,8; mean: 165,8. Comparatives not significantly different (P value 0,0712). Calculations and comparative tests have been done through the GraphPad prism version 9.0.0, GraphPad software, Boston, Massachusetts,USA, www.graphpad.com.

The scatter plot in figure 5.2.19A shows that neither data category shows any dependence between the two parameters. Figure 5.2.19B shows that the integrated density of centrosomal pericentrin is the same for normal and centrosome-amplified cells.

The next figure shows the relationship between the Integrated density of Aurora Kinase-A on centrosomes and the integrated density of centrosomal pericentrin.

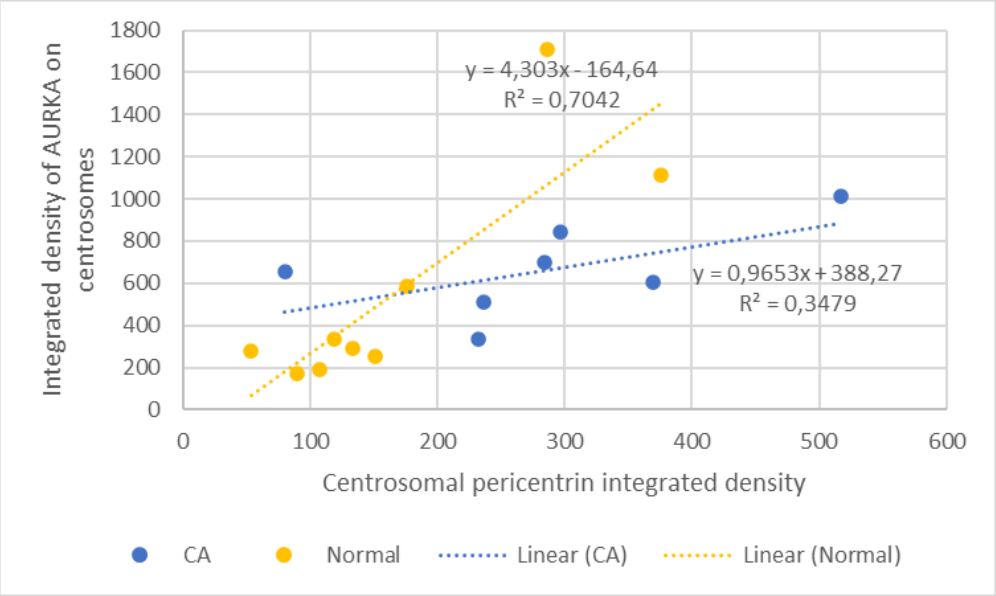

Figure 5.2.20: **The Integrated density of centrosomal AURKA against the integrated density of centrosomal pericentrin**. Line of best fit equations: CA: y = 0,9653x + 388,27; R^2 = 0,3479. Normal: y = 4,303x - 164,64; R^2 = 0,7042.

Figure 5.2.20 shows that only for normal cells there is a sufficient positive correlation between the tested parameters.

The following figure portrays the relationship between the area of Aurora Kinase-A fluorescence and the integrated density of centrosomal pericentrin.

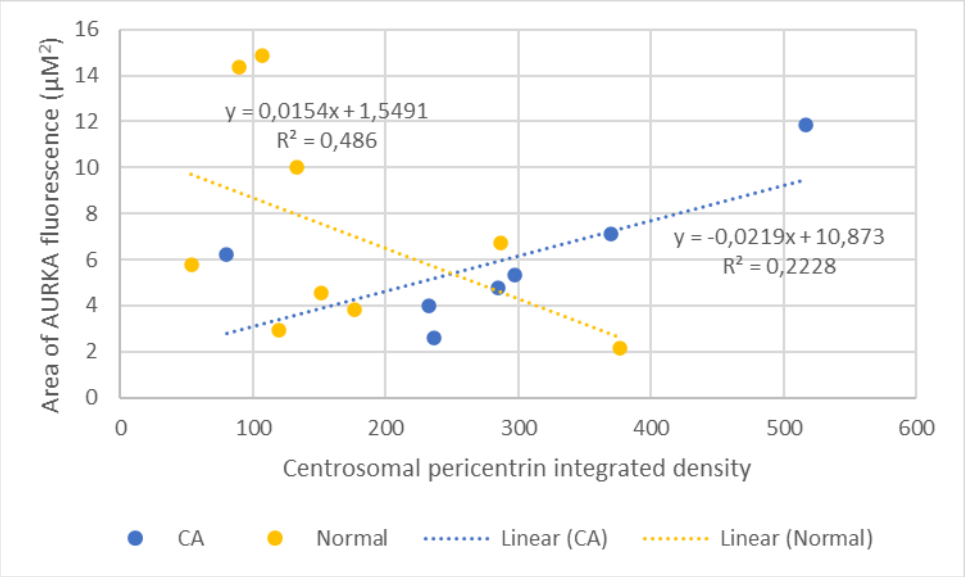

Figure 5.2.21: **The area of AURKA fluorescence against the integrated density of centrosomal pericentrin**. Line of best fit equations: CA: y = y = 0,0154x + 1,5491; R^2 = 0,486. Normal: y = y = -0,0219x + 10,873; R^2 = 0,2228.

Figure 5.2.21 shows that there is no relationship between the two parameters for normal and centrosome-amplified cells.

The figure below shows the relationship between the mean grey value of phospho-Aurora Kinase-A on centrosomes and the integrated density of centrosomal pericentrin.

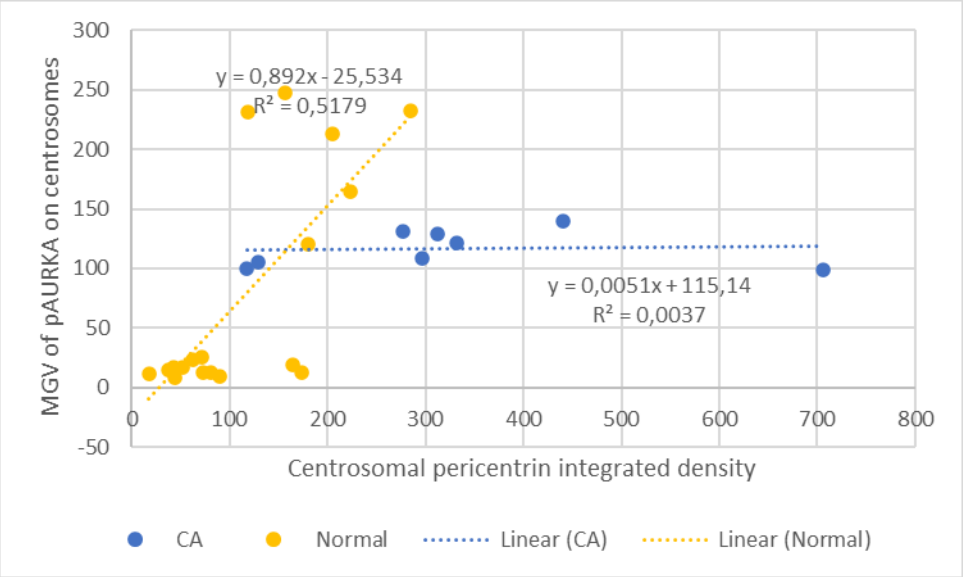

Figure 5.2.22: **The MGV of centrosomal pAURKA against the integrated density of centrosomal pericentrin**. Line of best fit equations: CA: y = 0,0051x + 115,14; R^2 = 0,0037. Normal: y = 0,892x - 25,534; R^2 = 0,5179.

Figure 5.2.22 shows that only in normal cells there is a relationship between the two tested parameters.

The figure below shows the relationship between the Integrated density of centrosomal phospho-Aurora Kinase-A and the integrated density of centrosomal pericentrin.

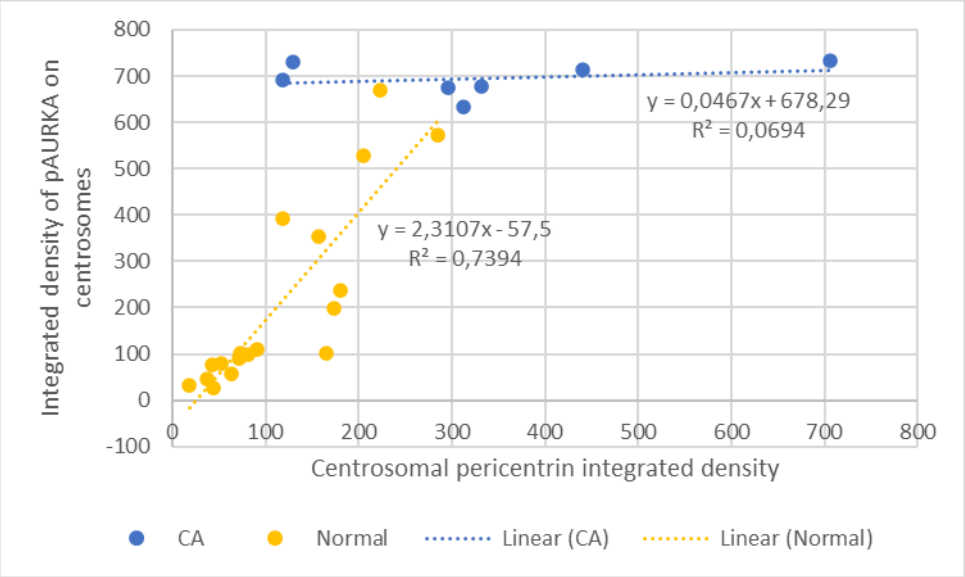

Figure 5.2.23: **The Integrated density of centrosomal pAURKA against the integrated density of centrosomal pericentrin**. Line of best fit equations: CA: y = 0,0467x + 678,29; R^2 = 0,0694. Normal: y = 2,3107x - 57,5; R^2 = 0,7394.

The figure 5.2.23 portrays that only in normal cells there is a positive relationship between the tested parameters.

The next figure portrays the relationship between the area of phospho-Aurora Kinase A derived fluorecence and the integrated density of centrosomal pericentrin.

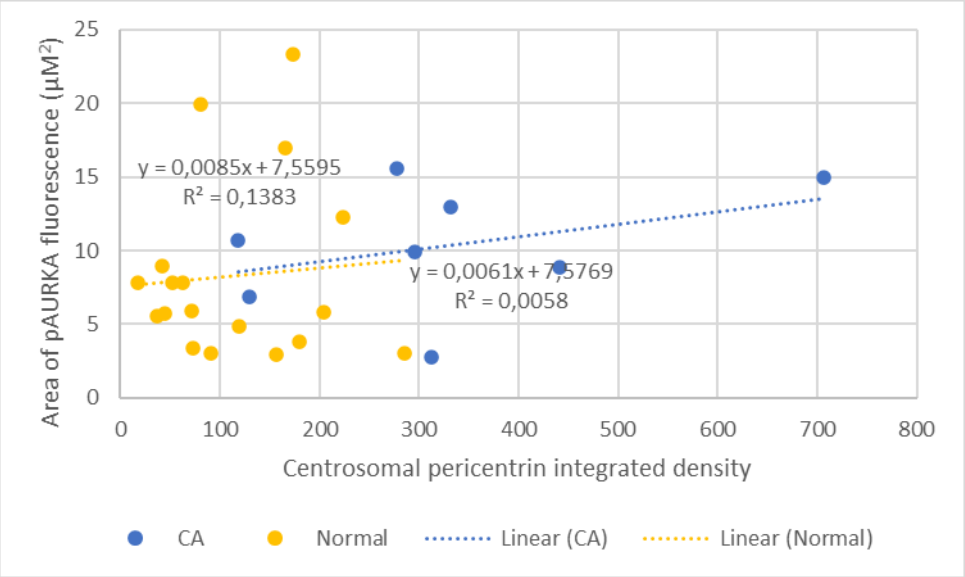

Figure 5.2.24: **The area of pAURKA derived fluorescence against the integrated density of centrosomal pericentrin**. Line of best fit equations: CA: y = 0,0085x + 7,5595; R^2 = 0,1383. Normal: y = 0,0061x + 7,5769; R^2 = 0,0058.

From figure 5.2.24 it can be seen that the two parameters do not depend on each other in either cell type.

The following graphs show the scatter plots concerning the pPLK1 parameter's relationship with the integrated density of centrosomal pericentrin.

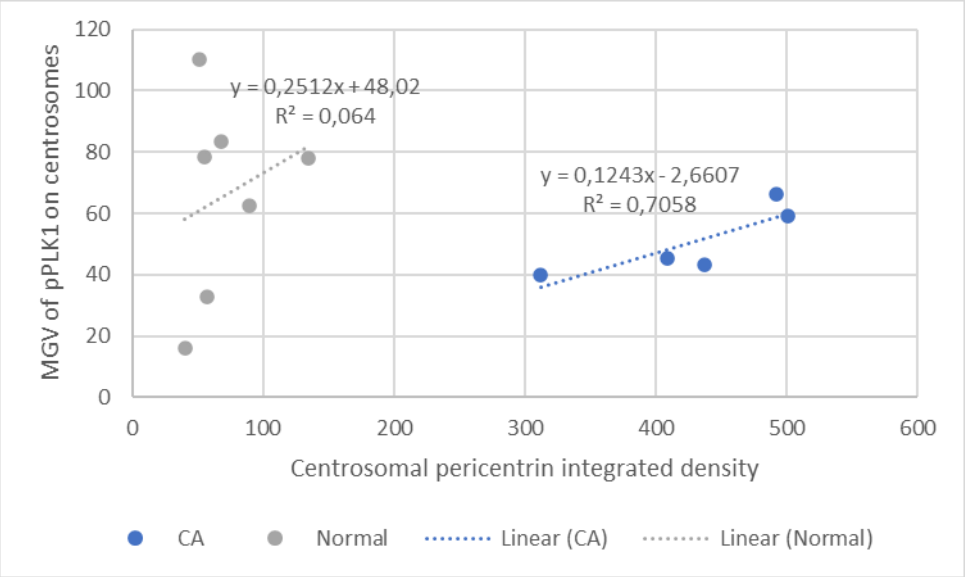

Figure 5.2.25: **The mean gray value of centrosomal pPLK1 against centrosomal pericentrin integrated density**. Line of best fit equations: CA: y = 0,1243x - 2,6607; R^2 = 0,7058. Normal: y = 0,2512x + 48,02; R^2 = 0,064.

Looking at figure 5.2.25 it can be said that a positive correlation between the two parameters exists only for the cells with centrosome amplification

The following figure shows the integrated density of centrosomal pPLK1 versus the integrated density of centrosomal pericentrin.

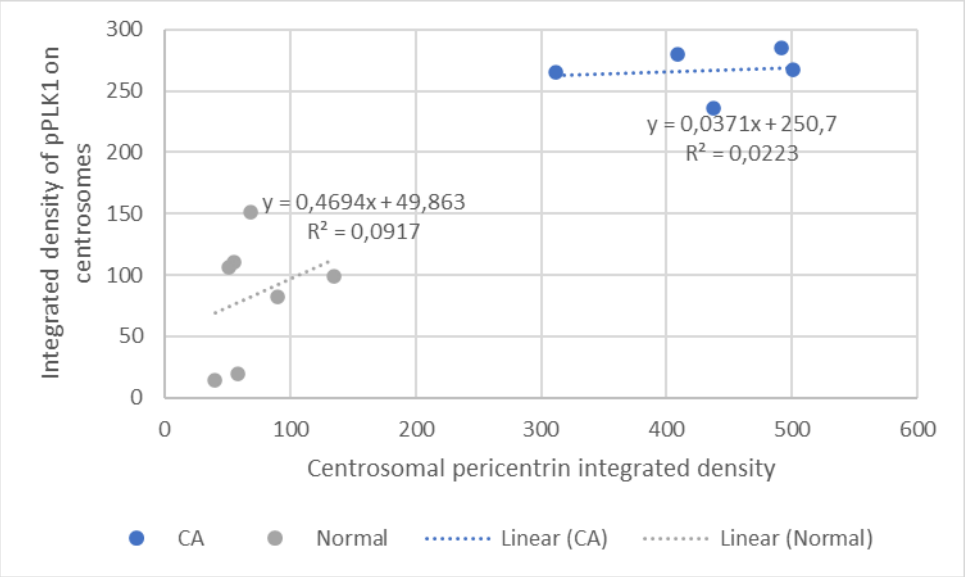

Figure 5.2.26: **The integrated density of centrosomal pPLK1 against the integrated density of centrosomal pericentrin**. Line of best fit equations: CA: y = 0,0371x + 250,7; R^2 = 0,0223. Normal: y = 0,4694x + 49,863; R^2 = 0,0917.

From figure 5.2.26, it can be seen that the tested parameters do not correlate with each other for either category.

The next figure portrays the relationship between the pPLK1 fluorescence area and the integrated density of centrosomal pericentrin.

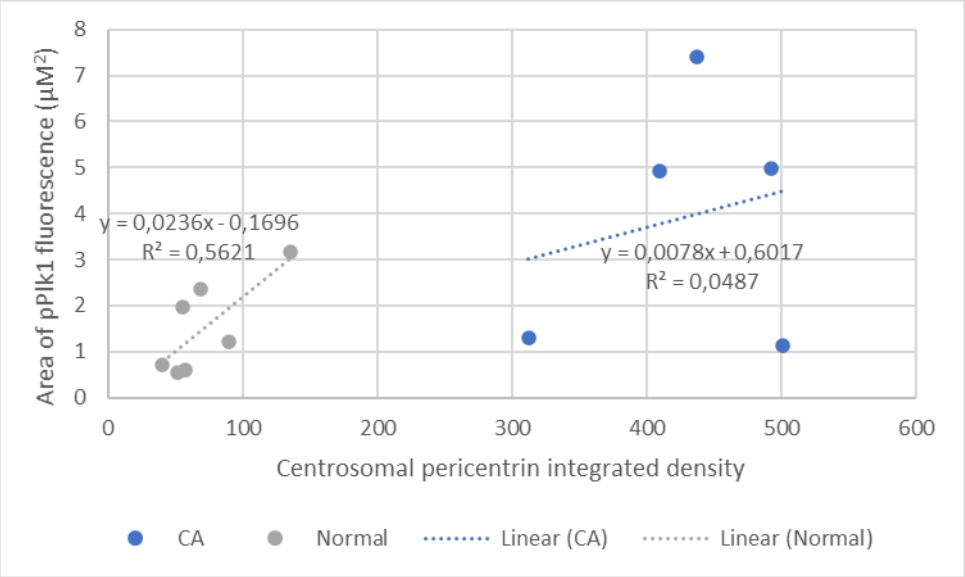

Figure 5.2.27: **The integrated density of centrosomal pAURKA against the integrated density of centrosomal pericentrin**. Line of best fit equations: CA: y = 0,0078x + 0,6017; R^2 = 0,0487. Normal: y = 0,0236x - 0,1696; R^2 = 0,5621.

Looking at the scatter plot in figure 5.2.27, it can be said only in normal cells integrated density of centrosomal pericentrin positively correlates with the area of pPLK1 fluorescence.

Chapter 5.3: Discussion and overview of the results.

The figures of Chapter 5.2 compare the centrosome area and the integrated density of centrosomal pericentrin with various parameters of the 3 cell cycle proteins. Comparing the parameters with centrosome area shows whether the increase in centrosome size affects the potential activity of the cell cycle proteins. The pericentrin integrated density is expected to represent centrosome maturity, thus this will allow us to draw a conclusion on whether the change in centrosome maturity does affect the cell cycle proteins.

Centrosome size and maturity may not represent the same thing, since here, maturity is based on integrated density which depends on the area and the mean grey value of pericentrin, and the mean grey value of pericentrin varies. However, centrosome size is only based on the area. In other words, the integrated density of centrosomal pericentrin may change without the centrosome size changing.

Some inaccuracies may be portrayed, since in cells with centrosome amplification the number can vary from 2 to about 6 centrosomes, thus centrosome size will include the cumulative area of multiple centrosomes: this can lead to a misrepresentation. For example, if 5 smaller centrosomes are present in a cell with a total area of X μM, 2 larger centrosomes can be present with the same area of X μM.

<u>Centrosomal AURKA and its correlations against centrosome size:</u>

Looking at Figure 5.2.10 which compares the integrated density of centrosomal AURKA against centrosome size, it can be seen that neither normal nor centrosome amplified cells show a correlation between the two parameters. As a result, it can be said that centrosome amplification does not change the relationship between the centrosome area and the total quantity of centrosomal AURKA.

The next figure, figure 5.2.11 shows that the mean gray value or the concentration of centrosomal AURKA decreases as the centrosome grows in size for normal cells. The latter is most likely due to the integrated density or the quantity not changing in response to centrosome size. However, for centrosome-amplified cells, the correlation is lost, indicating that centrosome amplification creates some loss of dependency between the two parameters.

Figure 5.2.12 shows that the area of AURKA fluorescence near-perfectly correlates with the area of centrosomes. The latter is due to AURKA being localised on centrosomes. As a result, it can be said that despite centrosomes being amplified, AURKA still covers the area of them evenly.

Overall, the only parameter that centrosome amplification has changed was the mean grey value/concentration of AURKA on centrosomes – loss of dependency between AURKA concentration and centrosome size when centrosomes are amplified.

Lastly, from part B of each figure, comparing normal cells with centrosome amplified cells, it can be said that neither the centrosome area nor the integrated density of AURKA is affected by amplified centrosomes, showing that amplified centrosomes exist in smaller sizes each (figure 5.2.10 B). This is supported by the figure showing that the area of AURKA fluorescence (which colocates with pericentrin fluorescence) is unaffected by centrosome amplification (figure 5.2.12 B). The concentration of AURKA (figure 5.2.11B) on centrosomes is unaffected by centrosome amplification, meaning that increased centrosome number maintains the concentration of AURKA in their area. Overall, it is apparent, that centrosomal AURKA parameters are not changed when centrosomes are amplified.

Centrosomal pAURKA and its correlations against centrosome size:

Figure 5.2.13A shows that neither normal nor centrosome amplified cells show a correlation of pAURKA concentration against centrosome size. It is seen that normal cells show two populations of pAURKA data distribution, which is speculated here to represent pAURKA before and after activation. Overall, centrosome amplification has no effect on the relationship between centrosome size and pAURKA centrosomal concentration.

Figure 5.2.14A portrays that neither centrosome amplified nor normal cells show a dependency between centrosome area and total pAURKA centrosomal quantity. This indicates that centrosome amplification has no effect on the relationship between the two parameters. However, it affects the absolute values of the two parameters and is explained later.

Lastly, figure 5.2.15A shows that the centrosome area correlates with the area of pAURKA fluorescence for centrosome-amplified cells, but not for normal cells. However, the R^2 value is very close to 0,5 for normal cell data. Assuming that the correlation is indeed not present in normal

cells, this figure shows that in centrosome amplified cells there is a gain of dependency between the two parameters.

Overall, it appears, that the only change observed from the latter 3 scatter plots described as a result of centrosome amplification was that centrosome amplified cells gain dependency of pAURKA fluorescence area and centrosome size, assuming R^2 value of 0,4734 indicates no correlation.

Comparing centrosome amplified against normal cells' parameters (bar charts), pAURKA protein concentration (MGV) (figure 5.2.13B) and covered area (figure 5.2.15B) are unaffected by centrosome amplification, but its total quantity (figure 5.2.14 B) is affected. The latter is an interesting finding since for total AURKA, the total quantity is unchanged by centrosome amplification, thus it appears that centrosome amplification increases the quantity of active pAURKA compared to total AURKA. In Figure 5.2.13B it is apparent that normal cells have two populations of data, which could be attributed to pAURKA before activation (low values) and then after activation (high values). CA+ sample data shows a much lower variation of data, which could be due to the fact that centrosome amplified cells spend longer in mitosis due to the requirement to cluster them, increasing the probability of finding a cell in mitosis (after activation of AURKA). Looking at Figure 5.2.14B, it is apparent that the two populations exist in the normal sample also: lower value and higher value ones, which is related to the pattern obtained in Figure 5.2.13B. Once again this can be due to pAURKA before and after its activation. Centrosome amplified sample has shown that the range of data is much lower which can once again be attributed to the fact that in centrosome amplified cells mitosis takes longer thus there is a higher probability of finding a cell in mitosis. Overall, looking at figures 5.2.13B and 5.2.14B, there is much more pAURKA in CA cells thus more active pAURKA. This may imply a faster advancement through G2/M transition or maybe the requirement for more pAURKA to cluster the centrosomes. However, the area of pAURKA fluorescence is the same for both normal and centrosome-amplified cells (figure 5.2.15B). The latter is consistent with the finding that normal and centrosome amplified cells have the same cumulative centrosome area.

Centrosome amplification results in higher quantities of pAURKA within cells, and relatively consistent levels of total AURKA (includes pAURKA and AURKA). It can be suggested that the latter occurs due to cells with centrosome amplification spending longer in mitosis resulting in a higher

probability of finding a cell with activated pAURKA rather than a mitotic cell without yet active pAURKA, in addition to the possibility that more pAURKA is required for cells with the abnormality.

Centrosomal pPLK1 and its correlations against centrosome size:

Figure 5.2.16A shows that neither normal nor centrosome amplified cells show a dependency between centrosome area and pPLK1 centrosomal mean gray value. As a result, it is apparent that centrosome amplification does not affect pPLK1 centrosomal concentration.

Figure 5.2.17A shows that centrosome area correlates with total pPLK1 quantity in both normal and centrosome amplified cells. However, for centrosome amplified cells, despite more overall pPLK1 present, the correlation is negative. As a result, it appears that centrosome amplification may alter the relationship between centrosome area and pPLK1 quantity: as area increases, pPLK1 levels seem to decrease. Even though it decreases, it still exists in higher quantities.

Lastly, the scatter in Figure 5.2.18A portrays that both normal cells and centrosome amplified cells show a correlation between centrosome area and pPLK1 area coverage. It is well known that pPLK1 resides on centrosomes (Gheghiani et al., 2017). Centrosome-amplified cells maintain the dependency.

Overall, comparing pPLK1 and centrosome area, it appears that centrosome amplification disregulates just one pathway: the one relating centrosome area and pPLK1 quantity reversing the correlation.

Comparing the differences in the average values of the parameters for normal and centrosome amplified cells, figure 5.2.16B shows that the concentration of pPLK1 on centrosomes remains the same irrespective of amplification, while Figure 5.2.17B shows that the total quantity of pPLK1 on centrosomes is much higher for centrosome amplified cells. It is unclear why the quantity changes without changing the protein concentration since figure 5.2.10B shows that the centrosome area remains the same for normal and centrosome amplified cells. The area of pPLK1 fluorescence is indifferent for normal and centrosome amplified cells (figure 5.2.18B) which is consistent with the observation that the centrosomal area is the same for both categories. Overall, for centrosomal parameters of pPLK1, it appears that amplification results in an increased quantity of pPLK1 molecules.

Centrosomal AURKA and its correlations against PCNT integrated density:

Figure 5.2.19A shows that AURKA concentration on centrosomes does not correlate with the centrosomal pericentrin levels for both normal and centrosome amplified cells. As a result, a conclusion can be made that centrosome amplification has no effect on the relationship between the two parameters.

Figure 5.2.20 shows that the integrated density of centrosomal AURKA correlates with that of pericentrin only for normal cells. Apparently, when centrosomes are amplified the relationship between the two parameters is lost. The centrosomal levels of pericentrin become no longer related to the centrosomal levels of AURKA.

Finally, 5.2.21 shows that AURKA area coverage does not correlate with the integrated density of centrosomal pericentrin for normal and centrosome amplified cells. As a result, it can be concluded that centrosomal pericentrin levels are not related to the AURKA area. However, the AURKA fluorescence area closely represents the centrosome area and would be expected to correlate with pericentrin levels. Furthermore, the R^2 value of the "Normal" category in this figure is very close to 0,5, but the trend is negative, however. This raises questions on whether AURKA is truly only located on centrosomes, assuming correlation does exist.

Overall, it appears that centrosome amplified cells have lost the relationship between centrosomal pericentrin levels and centrosomal AURKA integrated density, showing that the levels of these two proteins are not controlled together anymore under centrosome amplification.

Comparing the centrosomal integrated density of pericentrin for normal and centrosome amplified cells (figure 5.2.19B), it appears that it does not significantly differ for the two categories, hence centrosome amplification results in overall the same total centrosomal pericentrin quantity, which is consistent with the fact that centrosome cumulative area remains constant.

Centrosomal pAURKA against PCNT integrated density correlations:

Figure 5.2.22 shows that the quantity of centrosomal pericentrin correlates well with pAURKA centrosomal concentration. However, this relationship is lost for centrosome-amplified cells. It is most likely that concentration increases in response to pericentrin levels for normal cells, because the following figure shows that integrated density also increases. Centrosome-amplified cells show no relation between the two parameters indicating a loss of dependency/relationship.

Figure 5.2.23 shows that there is a loss of correlation once again: centrosomal pericentrin levels correlate well with centrosomal pAURKA levels in normal cells only. This indicates that once the centrosomes have been amplified, the increase in pericentrin levels does not occur in concordance with an increase in pAURKA levels on centrosomes.

Figure 5.2.24 shows that centrosomal pericentrin quantities do not correlate with pAURKA area coverage for both normal and centrosome amplified cells. It can be concluded that centrosome amplification does not create a gain of dependency/correlation between the two parameters.

Overall, it can be said that centrosome amplification causes loss of dependency/correlation between centrosomal pericentrin quantities and pAURKA concentration as well as pAURKA protein quantity.

Centrosomal pPLK1 against PCNT integrated density correlations:

Figure 5.2.25 shows that pPLK1 centrosomal concentration correlates with centrosomal pericentrin levels for centrosome amplified cells only. It appears that there is a gain of dependency or correlation between centrosomal pericentrin and pPLK1.

Figure 5.2.26 compares centrosomal pericentrin levels with pPLK1 levels of that. It is apparent that neither normal nor centrosome-amplified cells show a correlation between the two parameters. It can be concluded that centrosome amplification does not create a gain of correlation between pericentrin and pPLK1 quantity on centrosomes.

Figure 5.2.27 shows that the area of pPLK1 coverage correlates with centrosomal pericentrin levels only for normal cells. This implies that centrosome amplification results in the dysregulation of the pathway relating centrosomal pericentrin levels and pPLK1 covered area, which closely resembles the centrosome area.

It appears that centrosome amplification causes a gain of correlation between centrosomal pericentrin levels and pPLK1 centrosomal concentration. However, there is a loss of correlation between centrosomal pericentrin levels and pPLK1 area coverage upon centrosome amplification.

Overall, looking at phospho-PLK1 graphs, it is apparent that the data in the x-axis is always significantly shifted to the right with the shifted data points corresponding to centrosome amplification. In other words the centrosome area and pericentrin integrated density is significantly different for normal cells from centrosome amplified cells. The cells with anti-pPLK1 antibodies are only a fraction of the total cells that were used to extract data for centrosome size. However, the average centrosome area for all of the cells (set includes those with anti-pPLK1 antibody and all the other antibody combinations since they had pericentrin antibody) is indifferent for normal and centrosome amplified cells. This is most likely due to a chance, because staining cells with a different antibody cannot affect its centrosome size. Pericentrin integrated density has not been compared for normal and centrosome amplified cells.

Chapter 5.4: Discussion of the comparison of absolute values of centrosomal parameters between normal and centrosome amplified cells.

Firstly, looking at the bar charts, significantly different parameters between normal and centrosome amplified cells are these: Integrated density of pAURKA, integrated density of pPLK1 (figures 5.2.14B and 5.2.17B). As said before, pPLK1 scatters show that the x-axis variables are significantly different for normal and centrosome amplified cells, but these tested cells do not represent the average value from the total population of cells, just a fraction of them. The conclusion can be made that centrosome amplification affects only the total quantity of centrosomal proteins. Furthermore, those centrosomal proteins affected appear to be none other than the active form of cell cycle proteins – pPLK1 and pAURKA. The other two tested proteins for which integrated density has been compared between normal and centrosome amplified cells were total AURKA and total pericentrin, neither of which have shown to have significantly different integrated density for centrosome amplified cells. The idea that centrosome amplification requires more of these two proteins (pAURKA and pPLK1) has been postulated before. It is more often seen as a cause of centrosome amplification rather than a consequence.

Comparing the latter finding to what is already known, the best evidence of Aurora Kinase-A being the cause of centrosome amplification stems from the study performed by Meraldi et al., (2002) who revealed that in p53 double knockout cells AURKA overexpression allows centrosome amplification to occur. This may explain the increased quantities seen in the figure 5.2.14B. Even though the current literature contains limited evidence of elevated pAURKA specifically, directly resulting in centrosome amplification or that centrosome amplification results in elevated pAURKA levels, some studies, described later have shown the involvement of the protein in centrosomal dynamics, supportive of the finding of this study that centrosome amplification results into overall higher pAURKA quantities. In contrast, Marumoto et al., (2005) have stated that the kinase-inactive form of AURKA is sufficient to induce centrosome amplification. Loss of function mutations of AURKA have also led to centrosome amplification. Thus it appears that compromising AURKA functioning may also be a cause of centrosome amplification.

Hirota et al., (2003) explain that AURKA functions in the regulation of centrosome maturation, which could explain why more pAURKA is seen with amplified centrosomes as more of it is required to maintain a few extra centrosomes. Furthermore, they have shown that AURKA activatory phosphorylation T288, same as the one tested here, initially is seen on centrosomes,

and after some time, increased amounts are seen at the spindle poles, where centrosomes are located. Two things can be taken from the latter: firstly, this may explain the high and low populations of pAURKA in normal cells (figures 5.2.13B and 5.2.14B), and secondly, extra centrosomes may be the reason why more AURKA becomes phosphorylated as this phosphorylation (T288) happens on centrosomes. Marumoto et al., (2005) have speculated that Aurora Kinase A regulates centriole pair separation through phosphorylation events for example Eg5 phosphorylation. Knowing that the active form of AURKA is pT288 AURKA, it is possible that elevated pAURKA levels can be the cause of centrosome amplification as it potentially allows more frequent or faster centriole separation knowing that the protein also plays a role in centrosome maturation. Goepfert et al., (2002) have indeed found that centrosome amplification and Aurora Kinase-A expression alteration occur at similar time points within tumour development, usually early. This supports the argument that centrosome amplification requires higher AURKA quantities. In addition, Glover et al., (1995), state that AURKA loss of function mutations results in failure of centrosome separation, and subsequently amplification. Overall, it appears possible that centrosome amplification may require elevated pAURKA levels. More research should be done to examine the expression of AURKA or its phosphorylation patterns to prove that centrosome amplification is the consequence of the latter.

As for phospho-PLK1, the increased quantities (figure 5.2.17B) of it may be a direct result of increased pAURKA quantities as pAURKA directly phosphorylates PLK1 on T210, activating it (Colicino and Hehnly, 2018). Lenart et al., (2007) have found that PLK1 inhibition results in a weak staining of centrosomes, which can be interpreted as incomplete centrosome maturation or lack of growth. This may explain the requirement of higher pPLK1 amounts in centrosome amplified cells . Joukov et al., (2014) have shown the requirement of PLK1 in centrosome maturation directly. As a result, it can be suggested that centrosome amplification requires additional PLK1 molecules to deal with the potentially higher demands of centrosome growth and maturation as there are more of them. Meraldi et al., (2002) have shown that increased PLK1 expression levels result in centrosome amplification.

As a result, the observation of higher levels of pPLK1 and pAURKA in CA cells may be explained by the fact that these two proteins are required for centrosome overduplication and potentially are the cause of it. As said before, the latter has been suggestive by the findings of a number of

studies. However, the fact that only the phospho-forms of these two proteins are seen elevated in CA cells has not been directly presented before.

As for all the other bar charts which do not show significant differences, one is of special interest: figure 5.2.10B which shows that the total centrosome area is not significantly different for normal and centrosome amplified cells. This is consistent with the findings of Decker et al., (2011) who state that rapid cell divisions create a high demand for centrosomal proteins to keep up the centrosomal growth. As a result, lacking proteins reduce centrosome size, which indirectly explains why more centrosomes are smaller each. The authors also stated: “First, the combined volume of all centrosomes formed at any one time in the developing embryo is constant. Second, the total volume of centrosomes in any one cell is independent of centrosome number”. Goehring and Hyman (2012) have also suggested that increased organelle amounts will require additional protein components which is a limiting factor for growth in size. Overall, what can be taken from this is that centrosome amplification creates a higher demand for centrosomal proteins.

Chapter 5.5: Comparison of correlation pattern changes with other literature.

Looking at the scatter plots, the most striking observation for AURKA and pAURKA other than area coverage comparisons, is perhaps that every time a correlation has been observed for normal cell samples, it has not been observed for cell samples with amplified centrosomes. The latter is indicative of some form of deregulation of cell cycle kinetics when centrosomes are amplified which is a new finding. Overall, pAURKA and total AURKA parameters have shown a loss of correlation with pericentrin parameters 4 times (figures 5.2.11A; 5.2.20; 5.2.22; 5.2.23) and a gain of correlation once(figure 5.2.15A), (both when compared against PCNT integrated density and centrosome area).

<u>Pattern changes regarding AURKA/pAURKA:</u>

1. Loss of correlation between the mean grey value of centrosomal AURKA and the area of centrosomes (figure 5.2.11A).

2. Loss of correlation between the integrated density of centrosomal AURKA and centrosomal pericentrin integrated density (figure 5.2.20).

3. Loss of correlation between the Integrated density of centrosomal phospho-Aurora Kinase-A and the integrated density of centrosomal pericentrin (figure 5.2.23).

4. Loss of correlation between the mean grey value of phospho-Aurora Kinase-A on centrosomes and the integrated density of centrosomal pericentrin (figure 5.2.22).

5. Gain of correlation between pAURKA fluorescence area and centrosome area (figure 5.2.15A).

Here, pAURKA/AURKA will be referred to as one entity since the literature does not present clearly the functions of each form of the protein i.e. the phosphorylated form is often not distinct from the general form. There is no information in the literature specific enough that review the specific parameters tested here in the form of their relationship. However, it is available in a more general form relating AURKA/pAURKA and PCNT, thus the paragraph below represents a discussion of all of the loss/gain of correlation patterns observed with AURKA and pAURKA proteins against PCNT-derived parameters.

Discussion of pAURKA correlation losses:

As said before, AURKA/pAURKA is involved in centrosome maturation and growth (Hirota et al., 2003; Marumoto et al., 2005). As a result, it is natural to assume that more pAURKA will result in more centrosome maturation hence more pericentrin levels, as observed from the trend for normal cells (figure 5.2.23). However, it is unexpected that Figure 5.2.14A shows that pAURKA levels do not correlate with the size of the centrosomes. Despite that, a question arises: why does centrosome amplification result in a loss of the relationship between pAURKA/AURKA parameters and pericentrin parameters. Based on the findings of Jiang et al., (2021) and Barretta et al., (2016), AURKA is recruited to centrosomes in G2, while pericentrin is recruited at G2/M and early mitosis, leaving a hint that pericentrin recruitment is a follow-up of AURKA/pAURKA activities and not the other way around. To explain the loss of correlation, it can be speculated that a combination of genomic instability due to centrosome amplification (Sabat-Pospiech et al., 2019), and mutations in AURKA genes (Glover et al., 1995; Geopfert et al., 2002) leads to pAURKA errors leading dysfunctional signalling pathways relating pAURKA and pericentrin levels.

Discussion of the gain of correlation between pAURKA fluorescence area and centrosome area:

As for the gain of correlation between pAURKA fluorescence area and centrosome area (figure 5.2.15) after centrosome amplification, it is very likely that the correlation existed in normal cells also, since the R^2 value was very close to 0,5 for normal cell data. Assuming the correlation did not exist for normal cells, it can be suggested that the resulting smaller centrosomes consequently of centrosome overduplication show a better response of pAURKA area coverage to centrosome growth in size. Normally, when centrosomes get bigger, pAURKA potentially may not cover the whole area anymore. Barretta et al., (2016) say that AURKA is recruited to centrosome early in G2, meaning that centrosome growth after that phase may not result in AURKA recruitment to it anymore. Hence, no correlation between the two parameters in normal cells, because in normal cells centrosome grows bigger, thus perhaps longer, after AURKA is done being recruited to them.

Pattern changes regarding Phospho-PLK1:

1. The area of pPLK1 coverage has shown a loss of correlation with PCNT levels due to centrosome amplification (figure 5.2.27).

2. pPLK1 concentration has shown a gain of correlation with PCNT levels after centrosome amplification (figure 5.2.25).

3. pPLK1 centrosomal quantity has shown a change of correlation with centrosome area from positive to negative upon centrosome amplification (figure 5.2.17).

Discussion of loss of correlation between pPLK1 area coverage and PCNT levels:

It is justified to think that pericentrin quantities relate to centrosome maturity as seen in chapter 1.6. As a result, a correlation between pPLK1 area coverage (which accurately resembles centrosome size) and pericentrin integrated density is seen for normal cells is seen (figure 5.2.27). However, the loss of correlation after centrosome amplification suggests that centrosome area does not increase with the growth or the maturation of centrosome following centrosome amplification. It is likely that due to smaller centrosomes being present within the cell (Decker et al., 2011), pPLK1 distribution is affected, leading to the observation that pPLK1 area coverage does not correlate with pericentrin levels.

Discussion of gain of correlation between between pPLK1 concentration and PCNT levels:

pPLK1 concentration has gained a correlation with PCNT centrosomal quantities after centrosome amplification (figure 5.2.25). It is possible that centrosome amplification causes dysfunction of pPLK1, because as said before AURKA, an activator of PLK1 is likely dysregulated by CA. It is hard to explain what exactly may cause the gain of this relationship between pPLK1 concentrations and PCNT levels, perhaps altered signalling pathways regulating PCNT recruitment. pPLK1 normally only phosphorylates PCNT once it is already recruited to centrosomes (Lee and Rhee, 2011). Further studies could be done to test whether centrosome amplification affects the pPLK1-PCNT interaction.

Discussion of change of correlation between pPLK1 levels and centrosome area:

Lastly, to discuss the change of correlation described previously, it is hard to understand why pPLK1 decreases in protein quantity with increasing centrosome size once centrosomes are amplified (figure 5.2.17). Since pPLK1 controls the process of centrosome duplication through cell cycle control (Bruinsma et al., 2015), it is thus required for duplication. One possible explanation is to be proven: amplified centrosomes grow larger due to lower pPLK1 levels which prevents their duplication for another round. Hence the downward trend. Such suggestion is supported by the fact normal cells show overall lower pPLK1 levels, perhaps that's why they have normal centrosome numbers.

Chapter 5.6: Limitations.

Having area (fluorescence area or coverage), concentration (mean grey value) and quantity (integrated density), it is expected here that the 3 parameters are interdependent. For example, an increase in concentration would require the quantity/area ratio to be higher. In the case of the tested parameters, if an increase in integrated density of AURKA with respect to centrosome size is seen, it is expected that the other two parameters (mean grey value and area) would show a logical change. For example, if the area stays constant, but mean grey value increases, the integrated density is expected to increase likewise. For example, figures 5.2.16-5.2.18, which show the relationships of pPLK1 parameters with centrosome size show that for centrosome amplified cells as centrosome size increases, pPLK1 area coverage also increases, while the quantity (integrated density) decreases, suggesting that concentration should decrease drastically, but figure 5.2.16 shows that it is not affected by centrosome size (R^2 = 0,1326). The method for determining these 3 parameters has been consistent for every acquisition. However, the explanation here could be that the consistent thresholding method works differently for each image or that the presence of noise within the area of interest affects the data differently in every image.

To gain a better insight, next time the study could include the various parameter comparisons "per centrosome" rather than for all the centrosomes, since when centrosomes are amplified, each individual centrosome may display different parameters.

As seen from the pPLK1 scatter plots, normal cell data and centrosome amplified data are always apparent to be distributed discretely on the x-axis. For example, figures comparing pPLK1 parameters with centrosome area show that centrosome amplified cells must have larger centrosome area, even tough figure 5.2.10B portrays that the total centrosome area is unchanged for cells with amplified centrosomes. This is because pPLK1 data samples use only a fraction of the data that was used to portray the centrosome area differences between “CA” and “normal”. The figure below explains the latter.

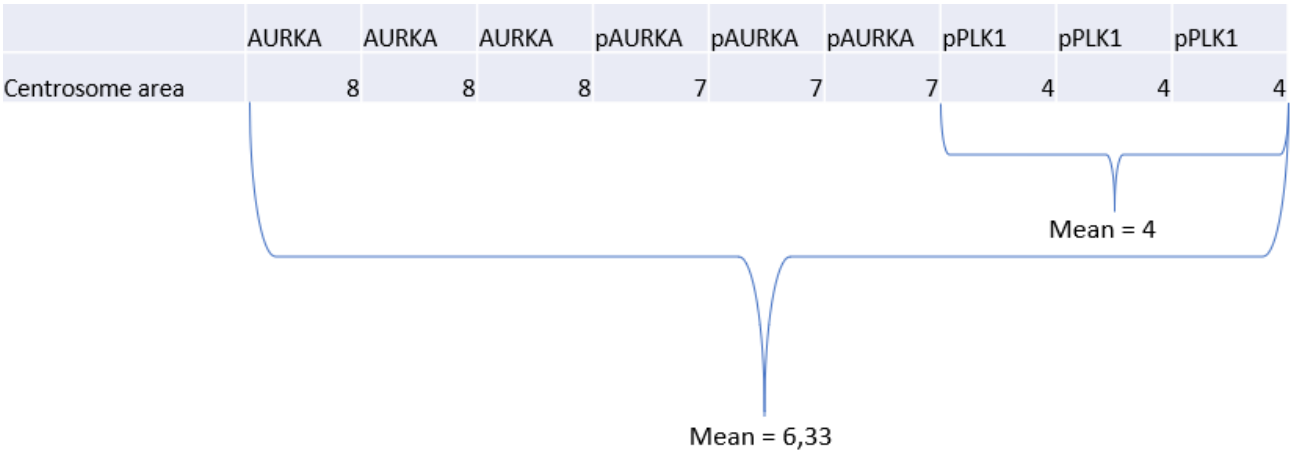

Figure 5.6.1: **The pPLK1 data samples use a smaller pool of values.** As a result of a smaller pool of data used for pPLK1, the data points may show a smaller range. As a result of that, pPLK1 data points may by coincidence be shifted to the right in the x-axis. In the figure table, AURKA stands for the data points with the rabbit anti-AURKA primary antibodies. pAURKA stands for the data points with the rabbit anti-pAURKA primary antibodies. pPLK1 stands for the data points with the rabbit anti-pPLK1 primary antibodies. This figure does not represent actual values or the actual number of values.

Chapter 6. Discussion.

The purpose of this study was to understand and explore the concept of centrosome amplification from a holistic point of view. That is, rather than "zooming in" into the phenomena to hopefully find a solution, here it was shown and examined by "zooming out" to see the wider system of the concept. As seen in the literature, there was minimal information suggestive of the role of KIFC1 in the cell cycle, mainly through flow cytometry experiments. Secondly, with the aid of bioinformatics tools, pAURKA and pPLK1 have been identified as proteins which link centrosomes with the cell cycle. These proteins were tested to confirm the role of centrosome amplification in the cell cycle.

As a result, it was discovered that a protein preceding the event of centrosome amplification, known as KIFC1, affects cell cycle rates to a degree. Likewise, a novel event succeeding centrosome amplification has been assigned to be the altered parameters of cell cycle machinery and altered responses of cell cycle machinery to changes in centrosomal parameters. The figure below summarises the findings of this study.

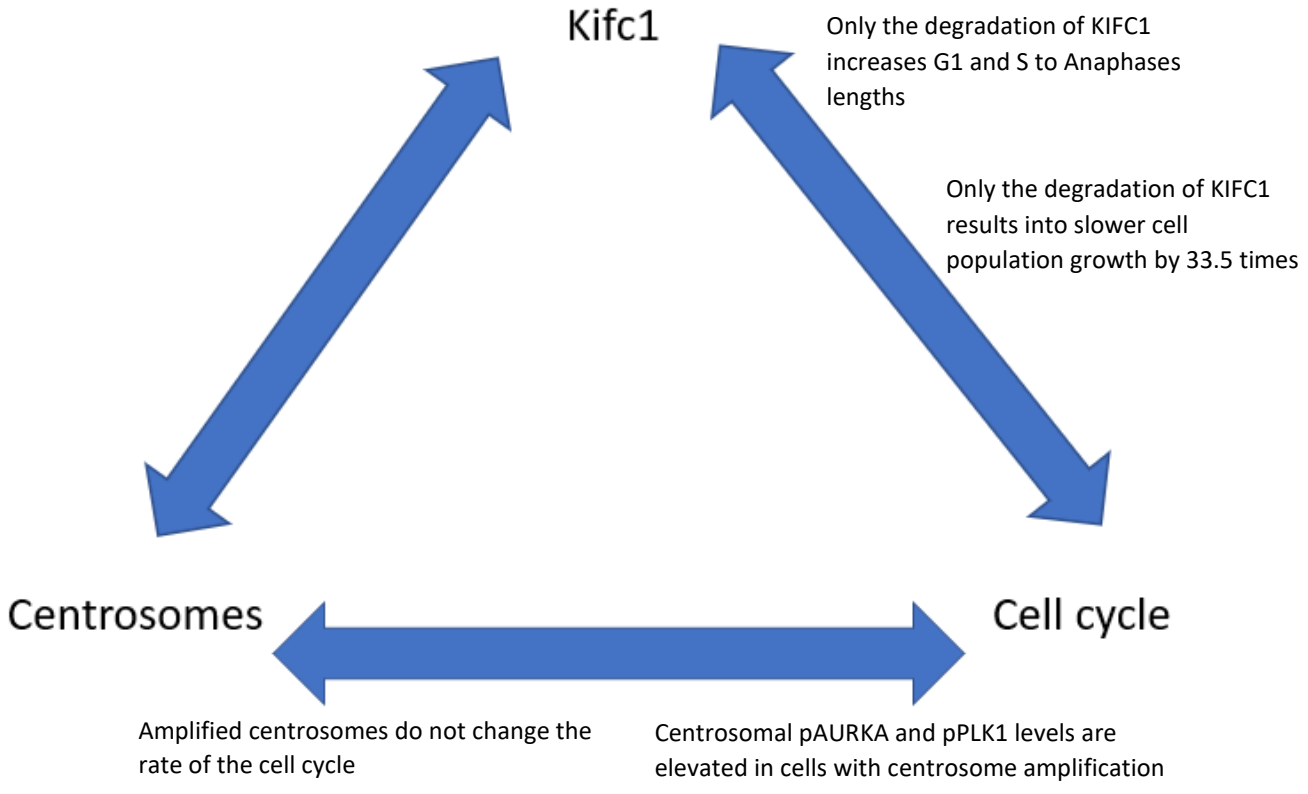

The findings of this study related to KIFC1 function, particularly the severe slowing of the cell-cycle and therefore cell growth, lend further support to the potential for KIFC1 as a therapeutic drug target. KIFC1 having additional effects on the cell cycle likely reduces the specificity of the effects of KIFC1-targeting drugs. However, the degradation of KIFC1 would also reduce the rate of the cell cycle which is therapeutically favourable in cancer cells.

In addition, to our knowledge, this is the first study to examine the link between centrosome amplification and the cell cycle. This study provides the first insights to this relationship, where it has been found that centrosome amplification does not significantly affect cell cycle length but does lead to higher levels of active forms of the key mitotic kinases Aurora-A and PLK1, suggestive of a requirement for higher levels of these proteins in cells with centrosome amplification and opening the door to further study. Lastly, it has been found that centrosome amplification affects the certain relationships between centrosomes and cell cycle proteins.

References:

Albertson, D. G., Collins, C., Mccormick, F. & Gray, J. W. (2003) Chromosome aberrations in solid tumors. *Nature Genetics,* 34(4), 369-376.

Ali, M., Rabbad, A. H. & Soliman, M. E. (2024) Monastrol disrupts KIFC1-ATP dynamics: Towards newer anticancer mechanism. *Chemical Physics Impact,* 8, 100480.

Anon (2017) Chapter 34 - Microtubules and Centrosomes. In: Pollard, T. D., Earnshaw, W. C., Lippincott-Schwartz, J. & Johnson, G. T. (eds.) *Cell Biology (Third Edition).* Elsevier.

Arnandis, T., Monteiro, P., Adams, S. D., Bridgeman, V. L., Rajeeve, V., Gadaleta, E., Marzec, J., Chelala, C., Malanchi, I., Cutillas, P. R. & Godinho, S. A. (2018) Oxidative Stress in Cells with Extra Centrosomes Drives Non-Cell-Autonomous Invasion. *Developmental Cell,* 47(4), 409-424.e9.

Asteriti, I., Mattia, F. & Guarguaglini, G. (2015) Cross-Talk between AURKA and Plk1 in Mitotic Entry and Spindle Assembly. *Frontiers in Oncology,* 5.

Astuti, P. & Gabrielli, B. (2011) Phosphorylation of Cdc25B3 Ser169 regulates 14-3-3 binding to Ser151 and Cdc25B activity. *Cell Cycle,* 10(12), 1960-7.

Bain, G., Maandag, E. C. R., Riele, H. P. J. t., Feeney, A. J., Sheehy, A., Schlissel, M., Murre, C. (1997) Both E12 and E47 Allow Commitment to the B Cell Lineage. *Immunity,* 6(2), 145-154.

Barbiero, M., Cirillo, L., Veerapathiran, S., Coates, C., Ruffilli, C., Pines, J. (2022) Cell cycle-dependent binding between Cyclin B1 and Cdk1 revealed by time-resolved fluorescence correlation spectroscopy. *Open Biology,* 12(6), 220057.

Barr, A., Kilmartin, J. & Gergely, F. (2010) CDK5RAP2 functions in centrosome to spindle pole attachment and DNA damage response. *The Journal of cell biology,* 189, 23-39.

Barretta, M. L., Spano, D., D'ambrosio, C., Cervigni, R. I., Scaloni, A., Corda, D. & Colanzi, A. (2016) Aurora-A recruitment and centrosomal maturation are regulated by a Golgi-activated pool of Src during G2. *Nature Communications,* 7(1), 11727.

Beck, K., Peak, M. M., Ota, T., Nemazee, D., Murre, C. (2009) Distinct roles for E12 and E47 in B cell specification and the sequential rearrangement of immunoglobulin light chain loci. *Journal of Experimental Medicine,* 206(10), 2271-2284.

Békés, M., Langley, D. R. & Crews, C. M. (2022) PROTAC targeted protein degraders: the past is prologue. *Nature Reviews Drug Discovery,* 21(3), 181-200.

Belinky, F., Nativ, N., Stelzer, G., Zimmerman, S., Iny Stein, T., Safran, M. & Lancet, D. (2015) PathCards: multi-source consolidation of human biological pathways. *Database,* 2015, bav006.

Bettencourt-Dias, M. & Glover, D. M. (2007) Centrosome biogenesis and function: centrosomics brings new understanding. *Nature Reviews Molecular Cell Biology,* 8(6), 451-463.

Bouché, J. P., Froment, C., Dozier, C., Esmenjaud-Mailhat, C., Lemaire, M., Monsarrat, B., Burlet-Schiltz, O. & Ducommun, B. (2008) NanoLC-MS/MS analysis provides new insights into the phosphorylation pattern of Cdc25B in vivo: full overlap with sites

of phosphorylation by Chk1 and Cdk1/cycB kinases in vitro. *J Proteome Res,* 7(3), 1264-73.

Boutros, R., Lobjois, V. & Ducommun, B. (2007) CDC25 phosphatases in cancer cells: key players? Good targets? *Nature Reviews Cancer,* 7(7), 495-507.

Brownlee, C. W., Klebba, J. E., Buster, D. W. & Rogers, G. C. (2011) The Protein Phosphatase 2A regulatory subunit Twins stabilizes Plk4 to induce centriole amplification. *J Cell Biol,* 195(2), 231-43.

Bruinsma, W., Aprelia, M., Kool, J., Macurek, L., Lindqvist, A. & Medema, R. H. (2015) Spatial Separation of Plk1 Phosphorylation and Activity. *Front Oncol,* 5, 132.

Bulavin, D. V., Higashimoto, Y., Demidenko, Z. N., Meek, S., Graves, P., Phillips, C., Zhao, H., Moody, S. A., Appella, E., Piwnica-Worms, H. & Fornace, A. J., Jr. (2003) Dual phosphorylation controls Cdc25 phosphatases and mitotic entry. *Nat Cell Biol,* 5(6), 545-51.

Cazales, M., Schmitt, E., Montembault, E., Dozier, C., Prigent, C. & Ducommun, B. (2005) CDC25B phosphorylation by Aurora-A occurs at the G2/M transition and is inhibited by DNA damage. *Cell Cycle,* 4(9), 1233-8.

Cha, H., Wang, X., Li, H. & Fornace, A. J., Jr. (2007) A Functional Role for p38 MAPK in Modulating Mitotic Transit in the Absence of Stress *. *Journal of Biological Chemistry,* 282(31), 22984-22992.

Childs, G. (2014) *Cillia And Flagella*. Available at: https://cytochemistry.net/cell-biology/cilia.htm.

Chu, C., John, C., Kohtz, D. S. (1997) MyoD Functions as a Transcriptional Repressor in Proliferating Myoblasts. *The Journal of Biological Chemistry,* 272(6), 3145-3148.

Chuang, J. Y., Wang, S. A., Yang, W. B., Yang, H. C., Hung, C. Y., Su, T. P., Hung, J. J. (2012) Sp1 phosphorylation by cyclin-dependent kinase 1/cyclin B1 represses its DNA-binding activity during mitosis in cancer cells. *Oncogene,* 31(47), 4946-4959.

Cogswell, J. P., Godlevski, M. M., Bonham, M., Bisi, J. & Babiss, L. (1995) Upstream stimulatory factor regulates expression of the cell cycle-dependent cyclin B1 gene promoter. *Mol Cell Biol,* 15(5), 2782-90.

Colicino, E. G. & Hehnly, H. (2018) Regulating a key mitotic regulator, polo-like kinase 1 (PLK1). *Cytoskeleton,* 75(11), 481-494.

Collins, K., Jacks, T. & Pavletich, N. P. (1997) The cell cycle and cancer. *Proceedings of the National Academy of Sciences,* 94(7), 2776-2778.

Cottee, M. A., Johnson, S., Raff, J. W. & Lea, S. M. (2017) A key centriole assembly interaction interface between human PLK4 and STIL appears to not be conserved in flies. *Biol Open,* 6(3), 381-389.

Coulonval, K., Kooken, H. & Roger, P. P. (2011a) Coupling of T161 and T14 phosphorylations protects cyclin B-CDK1 from premature activation. *Mol Biol Cell,* 22(21), 3971-85.

Cubillos-Ruiz, J. R., Bettigole, S. E. & Glimcher, L. H. (2017) Tumorigenic and Immunosuppressive Effects of Endoplasmic Reticulum Stress in Cancer. *Cell,* 168(4), 692-706.

De Gooijer, M. C., Van Den Top, A., Bockaj, I., Beijnen, J. H., Würdinger, T. & Van Tellingen, O. (2017) The G2 checkpoint-a node-based molecular switch. *FEBS Open Bio,* 7(4), 439-455.

Decker, M., Jaensch, S., Pozniakovsky, A., Zinke, A., O'connell, Kevin f., Zachariae, W., Myers, E. & Hyman, Anthony a. (2011) *Current Biology*, 21(15), 1259-1267.

Desai, D., Wessling, H. C., Fisher, R. P. & Morgan, D. O. (1995) Effects of phosphorylation by CAK on cyclin binding by CDC2 and CDK2. *Mol Cell Biol,* 15(1), 345-50.

Dobbelaere, J., Josué, F., Suijkerbuijk, S., Baum, B., Tapon, N. & Raff, J. (2008) A Genome-Wide RNAi Screen to Dissect Centriole Duplication and Centrosome Maturation in Drosophila. *PLOS Biology*, 6(9), e224.

Dodson, C. A. & Bayliss, R. (2012) Activation of Aurora-A kinase by protein partner binding and phosphorylation are independent and synergistic. *J Biol Chem*, 287(2), 1150-7.

Duijf, P. H. G., Schultz, N. & Benezra, R. (2013) Cancer cells preferentially lose small chromosomes. *International Journal of Cancer,* 132(10), 2316-2326.

Dzhindzhev, N., Yu, Q., Weiskopf, K., Tzolovsky, G., Cunha-Ferreira, I., Riparbelli, M., Rodrigues-Martins, A., Bettencourt-Dias, M., Callaini, G. & Glover, D. (2010) Asterless is a scaffold for the onset of centriole assembly. *Nature,* 467, 714-8.

Fabregat, A., Sidiropoulos, K., Viteri, G., Forner, O., Marin-Garcia, P., Arnau, V., D'eustachio, P., Stein, L. & Hermjakob, H. (2017) Reactome pathway analysis: a high-performance in-memory approach. *BMC Bioinformatics,* 18(1), 142.

Fang, N., Gu, T., Wang, Y., Wang, S., Wang, F., An, Y., Wei, W., Zhang, W., Guo, X., Nazarali, A. & Ji, S. (2017) Expression of PTEN-long mediated by CRISPR/Cas9 can repress U87 cell proliferation. *Journal of cellular and molecular medicine,* 21.

Farina, F., Pierobon, P., Delevoye, C., Monnet, J., Dingli, F., Loew, D., Quanz, M., Dutreix, M. & Cappello, G. (2013) Kinesin KIFC1 actively transports bare double-stranded DNA. *Nucleic Acids Research,* 41(9), 4926-4937.

Franckhauser, C., Mamaeva, D., Heron-Milhavet, L., Fernandez, A. & Lamb, N. J. (2010) Distinct pools of cdc25C are phosphorylated on specific TP sites and differentially localized in human mitotic cells. *PLoS One,* 5(7), e11798.

Fu, J., Hagan, I. M. & Glover, D. M. (2015) The centrosome and its duplication cycle. *Cold Spring Harb Perspect Biol,* 7(2), a015800.

Ganem, N. J., Godinho, S. A. & Pellman, D. (2009) A mechanism linking extra centrosomes to chromosomal instability. *Nature,* 460(7252), 278-282.

Gardino, A. K. & Yaffe, M. B. (2011a) 14-3-3 proteins as signaling integration points for

cell cycle control and apoptosis. *Semin Cell Dev Biol,* 22(7), 688-95.

Gavet, O. & Pines, J. (2010) Progressive activation of CyclinB1-Cdk1 coordinates entry to mitosis. *Dev Cell,* 18(4), 533-43.

Gheghiani, L., Loew, D., Lombard, B., Mansfeld, J. & Gavet, O. (2017) PLK1 Activation in Late G2 Sets Up Commitment to Mitosis. *Cell Rep,* 19(10), 2060-2073.

Gillespie, M., Jassal, B., Stephan, R., Milacic, M., Rothfels, K., Senff-Ribeiro, A., Griss, J., Sevilla, C., Matthews, L., Gong, C., Deng, C., Varusai, T., Ragueneau, E., Haider, Y., May, B., Shamovsky, V., Weiser, J., Brunson, T., Sanati, N., Beckman, L., Shao, X., Fabregat, A., Sidiropoulos, K., Murillo, J., Viteri, G., Cook, J., Shorser, S., Bader, G., Demir, E., Sander, C., Haw, R., Wu, G., Stein, L., Hermjakob, H. & D'eustachio, P. (2022) The reactome pathway knowledgebase 2022. *Nucleic Acids Research,* 50(D1), D687-D692.

Glover, D. M., Leibowitz, M. H., Mclean, D. A. & Parry, H. (1995) Mutations in aurora prevent centrosome separation leading to the formation of monopolar spindles. *Cell,* 81(1), 95-105.

Goehring, Nathan w. & Hyman, Anthony a. (2012) Organelle Growth Control through Limiting Pools of Cytoplasmic Components. *Current Biology,* 22(9), R330-R339.

Goepfert, T. M., Adigun, Y. E., Zhong, L., Gay, J., Medina, D. & Brinkley, W. R. (2002) Centrosome Amplification and Overexpression of Aurora A Are Early Events in Rat Mammary Carcinogenesis1. *Cancer Research,* 62(14), 4115-4122.

Gopalakrishnan, J., Mennella, V., Blachon, S., Zhai, B., Smith, A. H., Megraw, T. L., Nicastro, D., Gygi, S. P., Agard, D. A. & Avidor-Reiss, T. (2011) Sas-4 provides a scaffold for cytoplasmic complexes and tethers them in a centrosome. *Nature Communications,* 2(1), 359.

Goulet, B., Baruch, A., Moon, N.-S., Poirier, M., Sansregret, L. L., Erickson, A., Bogyo, M. & Nepveu, A. (2004) A Cathepsin L Isoform that Is Devoid of a Signal Peptide Localizes to the Nucleus in S Phase and Processes the CDP/Cux Transcription Factor. *Molecular Cell,* 14(2), 207-219.

Goulet, B., Sansregret, L., Leduy, L., Bogyo, M., Weber, E., Chauhan, S. S. & Nepveu, A. (2007) Increased Expression and Activity of Nuclear Cathepsin L in Cancer Cells Suggests a Novel Mechanism of Cell Transformation. *Molecular Cancer Research,* 5(9), 899-907.

Grallert, A., Chan, Kuan y., Alonso-Nuñez, M.-L., Madrid, M., Biswas, A., Alvarez-Tabarés, I., Connolly, Y., Tanaka, K., Robertson, A., Ortiz, J.-M., Smith, Duncan l. & Hagan, Iain m. (2013a) Removal of Centrosomal PP1 by NIMA Kinase Unlocks the MPF Feedback Loop to Promote Mitotic Commitment in S. pombe. *Current Biology,* 23(3), 213-222.

Granger, B. R., Chang, Y. C., Wang, Y., Delisi, C., Segrè, D. & Hu, Z. (2016) Visualization of Metabolic Interaction Networks in Microbial Communities Using VisANT 5.0. *PLoS Comput Biol,* 12(4), e1004875.

GraphPad prism 9.0.0. Boston, Massachusets, USA: GraphPad software.

Guichard, P., Hachet, V., Majubu, N., Neves, A., Demurtas, D., Olieric, N., Fluckiger, I., Yamada, A., Kihara, K., Nishida, Y., Moriya, S., Steinmetz, Michel o., Hongoh, Y. & Gönczy, P. (2013) Native Architecture of the Centriole Proximal Region Reveals Features Underlying Its 9-Fold Radial Symmetry. *Current Biology,* 23(17), 1620-1628.

Gönczy, P. (2015) Centrosomes and cancer: revisiting a long-standing relationship. *Nature Reviews Cancer,* 15(11), 639-652.

Hagan, Iain m. (2008) The spindle pole body plays a key role in controlling mitotic commitment in the fission yeast Schizosaccharomyces pombe. *Biochemical Society Transactions,* 36(5), 1097-1101.

Hall, V. J., Compton, D., Stojkovic, P., Nesbitt, M., Herbert, M., Murdoch, A. & Stojkovic, M. (2007) Developmental competence of human in vitro aged oocytes as host cells for nuclear transfer. *Human Reproduction,* 22(1), 52-62.

A, L. E., Bleiler, M. & Giardina, C. (2018) A look into centrosome abnormalities in colon cancer cells, how they arise and how they might be targeted therapeutically. *Biochemical Pharmacology,* 147, 1-8.

Hirota, T., Kunitoku, N., Sasayama, T., Marumoto, T., Zhang, D., Nitta, M., Hatakeyama, K. & Saya, H. (2003) Aurora-A and an Interacting Activator, the LIM Protein Ajuba, Are Required for Mitotic Commitment in Human Cells. *Cell,* 114(5), 585-598.

Hsu, L.-C. (2007) Identification and functional characterization of a PP1-binding site in

BRCA1. *Biochemical and Biophysical Research Communications,* 360(2), 507-512.

Hwang, A., Mckenna, W. G. & Muschel, R. J. (1998) Cell cycle-dependent usage of transcriptional start sites. A novel mechanism for regulation of cyclin B1. *J Biol Chem,* 273(47), 31505-9.

Ishibashi, J., Perry, R. L., Asakura, A., Rudnicki, M. A. (2005) MyoD induces myogenic differentiation through cooperation of its NH2- and COOH-terminal regions. *The Journal of Cell Biology,* 171(3), 471-482.

Ito, M. (2000) Factors controlling cyclin B expression. *Plant Molecular Biology,* 43(5), 677-690.

Jackman, M., Lindon, C., Nigg, E. A. & Pines, J. (2003) Active cyclin B1–Cdk1 first appears on centrosomes in prophase. *Nature Cell Biology,* 5(2), 143-148.

Jaiswal, M., Karn, A., Das, A., Kumari, A., Tiwari, S., Dalal, S. (2024) 14-3-3 epsilon inhibits premature centriole disengagement by inhibiting the activity of Plk1 and Separase. *[Preprint]*.

Jana, S. C. (2021) Centrosome structure and biogenesis: Variations on a theme? *Semin Cell Dev Biol,* 110, 123-138.

Jiang, X., Ho, D. B. T., Mahe, K., Mia, J., Sepulveda, G., Antkowiak, M., Jiang, L., Yamada, S. & Jao, L.-E. (2021) Condensation of pericentrin proteins in human cells illuminates phase separation in centrosome assembly. *Journal of Cell Science,* 134(14), jcs258897.

Joukov, V., Walter, Johannes c. & De nicolo, A. (2014) The Cep192-Organized Aurora A-Plk1 Cascade Is Essential for Centrosome Cycle and Bipolar Spindle Assembly. *Molecular Cell,* 55(4), 578-591.

Kaldis, P., Russo, A. A., Chou, H. S., Pavletich, N. P. & Solomon, M. J. (1998) Human and yeast cdk-activating kinases (CAKs) display distinct substrate specificities. *Mol Biol Cell,* 9(9), 2545-60.

Katula, K. S., Wright, K. L., Paul, H., Surman, D. R., Nuckolls, F. J., Smith, J. W., Ting, J. P., Yates, J. & Cogswell, J. P. (1997) Cyclin-dependent kinase activation and S-phase induction of the cyclin B1 gene are linked through the CCAAT elements. *Cell Growth Differ,* 8(7), 811-20.

Kleylein-Sohn, J., Pöllinger, B., Ohmer, M., Hofmann, F., Nigg, E. A., Hemmings, B. A. & Wartmann, M. (2012) Acentrosomal spindle organization renders cancer cells dependent on the kinesin HSET. *Journal of Cell Science,* 125(22), 5391-5402.

Kowalczyk, K. M., Hartmuth, S., Perera, D., Stansfield, P. & Petersen, J. (2013) Control of Sty1 MAPK activity through stabilisation of the Pyp2 MAPK phosphatase. *Journal of Cell Science,* 126(15), 3324-3332.

Krämer, A., Mailand, N., Lukas, C., Syljuåsen, R. G., Wilkinson, C. J., Nigg, E. A., Bartek, J. & Lukas, J. (2004) Centrosome-associated Chk1 prevents premature activation of cyclin-B–Cdk1 kinase. *Nature Cell Biology,* 6(9), 884-891.

Ku, N. O., Michie, S., Resurreccion, E. Z., Broome, R. L. & Omary, M. B. (2002) Keratin binding to 14-3-3 proteins modulates keratin filaments and hepatocyte mitotic progression. *Proc Natl Acad Sci U S A*, 99(7), 4373-8.

Lammer, C., Wagerer, S., Saffrich, R., Mertens, D., Ansorge, W. & Hoffmann, I. (1998) The cdc25B phosphatase is essential for the G2/M phase transition in human cells. *J Cell Sci*, 111 (Pt 16), 2445-53.

Landry, B. D., Mapa, C. E., Arsenault, H. E., Poti, K. E., Benanti, J. A. (2014) Regulation of a transcription factor network by Cdk1 coordinates late cell cycle gene expression. *The EMBO Journal*, 33(9), 1044-1060.

Laoukili, J., Kooistra, M. R. H., Brás, A., Kauw, J., Kerkhoven, R. M., Morrison, A., Clevers, H. & Medema, R. H. (2005) FoxM1 is required for execution of the mitotic programme and chromosome stability. *Nature Cell Biology*, 7(2), 126-136.

Lawrence, C. J., Dawe, R. K., Christie, K. R., Cleveland, D. W., Dawson, S. C., Endow, S. A., Goldstein, L. S. B., Goodson, H. V., Hirokawa, N., Howard, J., Malmberg, R. L., Mcintosh, J. R., Miki, H., Mitchison, T. J., Okada, Y., Reddy, A. S. N., Saxton, W. M., Schliwa, M., Scholey, J. M., Vale, R. D., Walczak, C. E. & Wordeman, L. (2004) A standardized kinesin nomenclature. *Journal of Cell Biology*, 167(1), 19-22.

Lee, K. & Rhee, K. (2011) PLK1 phosphorylation of pericentrin initiates centrosome maturation at the onset of mitosis. *Journal of Cell Biology*, 195(7), 1093-1101.

Li, J.-P., Yang, Y.-X., Liu, Q.-L., Pan, S.-T., He, Z.-X., Zhang, X., Yang, T., Chen, X.-W., Wang, D., Qiu, J.-X. & Zhou, S. (2015) The investigational Aurora kinase A inhibitor alisertib (MLN8237) induces cell cycle G2/M arrest, apoptosis, and autophagy via p38 MAPK and Akt/mTOR signaling pathways in human breast cancer cells. *Drug design, development and therapy,* 9, 1627-52.

Lin, M., Xie, S. S. & Chan, K. Y. (2022) An updated view on the centrosome as a cell cycle regulator. *Cell Div,* 17(1), 1.

Lindqvist, A., Källström, H., Lundgren, A., Barsoum, E. & Rosenthal, C. K. (2005) Cdc25B cooperates with Cdc25A to induce mitosis but has a unique role in activating cyclin B1-Cdk1 at the centrosome. *J Cell Biol,* 171(1), 35-45.

Lindqvist, A., Rodríguez-Bravo, V. & Medema, R. H. (2009) The decision to enter mitosis: feedback and redundancy in the mitotic entry network. *J Cell Biol,* 185(2), 193-202.

Lu, H., Gomaa, A., Wang-Bishop, L., Ballout, F., Hu, T., Mcdonald, O., Washington, M. K., Livingstone, A. S., Wang, T. C., Peng, D., El-Rifai, W. & Chen, Z. (2022) Unfolded Protein Response Is Activated by Aurora Kinase A in Esophageal Adenocarcinoma. *Cancers*, 14(6).

Lucanus, A. J. & Yip, G. W. (2018) Kinesin superfamily: roles in breast cancer, patient prognosis and therapeutics. *Oncogene,* 37(7), 833-838.

Lucie, V., Arun Prasath, D., Olivia, G., Stéphanie Le, B. & Claude, P. (2017) Regulation of Aurora Kinases and Their Activity. In: Claude, P. (ed.) *Protein Phosphorylation.* Rijeka: IntechOpen.

Lénárt, P., Petronczki, M., Steegmaier, M., Di Fiore, B., Lipp, J. J., Hoffmann, M., Rettig, W. J., Kraut, N. & Peters, J.-M. (2007) The Small-Molecule Inhibitor BI 2536 Reveals Novel Insights into Mitotic Roles of Polo-like Kinase 1. *Current Biology,* 17(4), 304-315.

Maciver, F. H., Tanaka, K., Robertson, A. M. & Hagan, I. M. (2003) Physical and functional interactions between polo kinase and the spindle pole component Cut12 regulate mitotic commitment in S. pombe. *Genes Dev,* 17(12), 1507-23.

Maguire, E., Menzies, G. E., Phillips, T., Sasner, M., Williams, H. M., Czubala, M. A., Evans, N., Cope, E. L., Sims, R., Howell, G. R., Lloyd-Evans, E., Williams, J., Allen, N. D. & Taylor, P. R. (2021) PIP2 depletion and altered endocytosis caused by expression of Alzheimer's disease-protective variant PLCγ2 R522. *The EMBO Journal*, 40(17), e105603.

Margolis, S. S., Walsh, S., Weiser, D. C., Yoshida, M., Shenolikar, S. & Kornbluth, S. (2003) PP1 control of M phase entry exerted through 14-3-3-regulated Cdc25 dephosphorylation. *Embo j,* 22(21), 5734-45.

Marumoto, T., Zhang, D. & Saya, H. (2005) Aurora-A — A guardian of poles. *Nature Reviews Cancer,* 5(1), 42-50.

Mazzocchi, F. (2012) Complexity and the reductionism–holism debate in systems biology. *WIREs Systems Biology and Medicine,* 4(5), 413-427.

Megraw, T. L., Sharkey, J. T. & Nowakowski, R. S. (2011) Cdk5rap2 exposes the centrosomal root of microcephaly syndromes. *Trends in Cell Biology,* 21(8), 470-480.

Melixetian, M., Klein, D. K., Sørensen, C. S. & Helin, K. (2009) NEK11 regulates CDC25A degradation and the IR-induced G2/M checkpoint. *Nat Cell Biol,* 11(10), 1247-53.

Meraldi, P., Honda, R. & A.Nigg, E. (2002) Aurora-A overexpression reveals tetraploidization as a major route to centrosome amplification in p53^{−/−} cells. *The EMBO Journal,* 21(4), 483-492-492.

Microsoft (2023) *Microsoft Whiteboard*. Available at: https://learn.microsoft.com/en-us/microsoft-365/whiteboard/?view=o365-worldwide.

Midgley, C. A. & Lane, D. P. (1997) p53 protein stability in tumour cells is not determined by mutation but is dependent on Mdm2 binding. *Oncogene,* 15(10), 1179-1189.

Mort, R., Ford, M., Sakaue-Sawano, A., Lindstrom, N., Casadio, A., Douglas, A., Keighren, M., Hohenstein, P., Miyawaki, A. & Jackson, I. (2014) Fucci2a: A bicistronic cell cycle reporter that allows Cre mediated tissue specific expression in mice. *Cell cycle (Georgetown, Tex.),* 13, 2681-2696.

Mouawad, R., Himadewi, P., Kadiyala, D., Arnosti, D. N. (2020) Selective repression of the *Drosophila* cyclin B promoter by retinoblastoma and E2F proteins. *Biochimica et Biophysica Acta (BBA) - Gene Regulatory Mechanisms,* 1863(7), 194549.

Nath, S., Bananis, E., Sarkar, S., Stockert, R. J., Sperry, A. O., Murray, J. W. & Wolkoff, A. W. (2007) Kif5B and Kifc1 Interact and Are Required for Motility and Fission of Early Endocytic Vesicles in Mouse Liver. *Molecular Biology of the Cell,* 18(5), 1839-1849.

O'connell, M. J., Raleigh, J. M., Verkade, H. M. & Nurse, P. (1997) Chk1 is a wee1 kinase in the G2 DNA damage checkpoint inhibiting cdc2 by Y15 phosphorylation. *The EMBO Journal,* 16(3), 545-554.

Pannu, V., Rida, P. C., Ogden, A., Turaga, R. C., Donthamsetty, S., Bowen, N. J., Rudd, K., Gupta, M. V., Reid, M. D., Cantuaria, G., Walczak, C. E. & Aneja, R. (2015) HSET overexpression fuels tumor progression via centrosome clustering-independent mechanisms in breast cancer patients. *Oncotarget,* 6(8), 6076-91.

Park, J.-E., Zhang, L., Bang, J. K., Andresson, T., Dimaio, F. & Lee, K. S. (2019a) Phase separation of Polo-like kinase 4 by autoactivation and clustering drives centriole biogenesis. *Nature Communications,* 10(1), 4959.

Park, S.-H., Yu, G.-R., Kim, W.-H., Moon, W.-S., Kim, J.-H., Kim, D.-G. (2007) NF-Y–Dependent Cyclin B2 Expression in Colorectal Adenocarcinoma. *Clinical Cancer Research,* 13(3), 858-867.

Patel, H., Abduljabbar, R., Lai, C.-F., Periyasamy, M., Harrod, A., Gemma, C., Steel, J. H., Patel, N., Busonero, C., Jerjees, D., Remenyi, J., Smith, S., Gomm, J. J., Magnani, L., Győrffy, B., Jones, L. J., Fuller-Pace, F., Shousha, S., Buluwela, L., Rakha, E. A., Ellis, I. O., Coombes, R. C. & Ali, S. (2016) Expression of CDK7, Cyclin H, and MAT1 Is Elevated in Breast Cancer and Is Prognostic in Estrogen Receptor–Positive Breast Cancer. *Clinical Cancer Research,* 22(23), 5929-5938.

Patel, N., Weekes, D., Drosopoulos, K., Gazinska, P., Noel, E., Rashid, M., Mirza, H., Quist, J., Brasó-Maristany, F., Mathew, S., Ferro, R., Pereira, A. M., Prince, C., Noor, F., Francesch-Domenech, E., Marlow, R., De Rinaldis, E., Grigoriadis, A., Linardopoulos, S., Marra, P. & Tutt, A. N. J. (2018) Integrated genomics and functional validation identifies malignant cell specific dependencies in triple negative breast cancer. *Nature Communications,* 9(1), 1044.

Petersen, J. & Hagan, I. M. (2005a) Polo kinase links the stress pathway to cell cycle control and tip growth in fission yeast. *Nature,* 435(7041), 507-512.

Potapova, T. A., Sivakumar, S., Flynn, J. N., Li, R. & Gorbsky, G. J. (2011) Mitotic progression becomes irreversible in prometaphase and collapses when Wee1 and Cdc25 are inhibited. *Mol Biol Cell,* 22(8), 1191-206.

Puklowski, A., Homsi, Y., Keller, D., May, M., Chauhan, S., Kossatz, U., Grünwald, V., Kubicka, S., Pich, A., Manns, M. P., Hoffmann, I., Gönczy, P. & Malek, N. P. (2011) The SCF-FBXW5 E3-ubiquitin ligase is regulated by PLK4 and targets HsSAS-6 to control centrosome duplication. *Nat Cell Biol,* 13(8), 1004-9.

Sabat-Pośpiech, D., Fabian-Kolpanowicz, K., Prior, I. A., Coulson, J. M. & Fielding, A. B. (2019) Targeting centrosome amplification, an Achilles' heel of cancer. *Biochemical Society Transactions,* 47(5), 1209-1222.

Saini, P., Li, Y. & Dobbelstein, M. (2015) Wee1 is required to sustain ATR/Chk1 signaling upon replicative stress. *Oncotarget,* 6(15), 13072-87.

Sansregret, L. & Nepveu, A. (2008) The multiple roles of CUX1: insights from mouse models and cell-based assays. *Gene,* 412(1-2), 84-94.

Sansregret, L., Vadnais, C., Livingstone, J., Kwiatkowski, N., Awan, A., Cadieux, C., Leduy, L., Hallett, M. T. & Nepveu, A. (2011) Cut homeobox 1 causes chromosomal instability by promoting bipolar division after cytokinesis failure. *Proc Natl Acad Sci U S A,* 108(5), 1949-54.

Sava, G. P., Fan, H., Coombes, R. C., Buluwela, L. & Ali, S. (2020) CDK7 inhibitors as anticancer drugs. *Cancer Metastasis Rev,* 39(3), 805-823.

Schindelin, J., Arganda-Carreras, I., Frise, E., Kaynig, V., Longair, M., Pietzsch, T., Preibisch, S., Rueden, C., Saalfeld, S., Schmid, B., Tinevez, J.-Y., White, D. J., Hartenstein, V., Eliceiri, K., Tomancak, P. & Cardona, A. (2012) Fiji: an open-source platform for biological-image analysis. *Nature Methods,* 9(7), 676-682.

Schmucker, S. & Sumara, I. (2014) Molecular dynamics of PLK1 during mitosis. *Mol Cell Oncol,* 1(2), e954507.

Sciortino, S., Gurtner, A., Manni, I., Fontemaggi, G., Dey, A., Sacchi, A., Ozato, K. & Piaggio, G. (2001) The cyclin B1 gene is actively transcribed during mitosis in HeLa cells. *EMBO Rep,* 2(11), 1018-23.

Sekino, Y., Oue, N., Koike, Y., Shigematsu, Y., Sakamoto, N., Sentani, K., Teishima, J., Shiota, M., Matsubara, A. & Yasui, W. (2019) KIFC1 Inhibitor CW069 Induces Apoptosis and Reverses Resistance to Docetaxel in Prostate Cancer. *Journal of Clinical Medicine,* 8, 225.

She, Z.-Y. & Yang, W.-X. (2017) Molecular mechanisms of kinesin-14 motors in spindle assembly and chromosome segregation. *Journal of Cell Science,* 130(13), 2097-2110.

Slevin, L. K., Nye, J., Pinkerton, D. C., Buster, D. W., Rogers, G. C. & Slep, K. C. (2012) The structure of the plk4 cryptic polo box reveals two tandem polo boxes required for centriole duplication. *Structure,* 20(11), 1905-17.

Stelzer, G., Rosen, N., Plaschkes, I., Zimmerman, S., Twik, M., Fishilevich, S., Stein, T. I., Nudel, R., Lieder, I., Mazor, Y., Kaplan, S., Dahary, D., Warshawsky, D., Guan-Golan, Y., Kohn, A., Rappaport, N., Safran, M. & Lancet, D. (2016) The GeneCards Suite: From Gene Data Mining to Disease Genome Sequence Analyses. *Current Protocols in Bioinformatics,* 54(1), 1.30.1-1.30.33.

Sumiyoshi, E., Fukata, Y., Namai, S. & Sugimoto, A. (2015) Caenorhabditis elegans Aurora A kinase is required for the formation of spindle microtubules in female meiosis. *Molecular Biology of the Cell,* 26(23), 4187-4196.

Szklarczyk, D., Gable, A. L., Nastou, K. C., Lyon, D., Kirsch, R., Pyysalo, S., Doncheva, N. T., Legeay, M., Fang, T., Bork, P., Jensen, L. J. & Von Mering, C. (2021) The STRING database in 2021: customizable protein-protein networks, and functional characterization of user-uploaded gene/measurement sets. *Nucleic Acids Res,* 49(D1), D605-d612.

Tibelius, A., Marhold, J., Zentgraf, H., Heilig, C., Neitzel, H., Ducommun, B., Rauch, A., Ho, A., Bartek, J. & Krämer, A. (2009) Microcephalin and pericentrin regulate mitotic entry via centrosome-associated Chk1. *The Journal of cell biology,* 185, 1149-57.

Tinel, A. & Tschopp, J. (2004) The PIDDosome, a Protein Complex Implicated in Activation of Caspase-2 in Response to Genotoxic Stress. *Science,* 304(5672), 843-846.

Van Vugt, M. A. T. M., Brás, A. & Medema, R. H. (2004) Polo-like Kinase-1 Controls Recovery from a G2 DNA Damage-Induced Arrest in Mammalian Cells. *Molecular Cell,* 15(5), 799-811.

Vertii, A., Hehnly, H. & Doxsey, S. (2016) The Centrosome, a Multitalented Renaissance Organelle. *Cold Spring Harbor Perspectives in Biology,* 8, a025049.

Vigneron, S., Sundermann, L., Labbé, J. C., Pintard, L., Radulescu, O., Castro, A. & Lorca, T. (2018) Cyclin A-cdk1-Dependent Phosphorylation of Bora Is the Triggering Factor Promoting Mitotic Entry. *Dev Cell,* 45(5), 637-650.e7.

Vázquez-Novelle, M. D., Mailand, N., Ovejero, S., Bueno, A. & Sacristán, M. P. (2010) Human Cdc14A phosphatase modulates the G2/M transition through Cdc25A and Cdc25B. *J Biol Chem,* 285(52), 40544-53.

Watanabe, N., Arai, H., Iwasaki, J., Shiina, M., Ogata, K., Hunter, T. & Osada, H. (2005) Cyclin-dependent kinase (CDK) phosphorylation destabilizes somatic Wee1 via multiple pathways. *Proc Natl Acad Sci U S A,* 102(33), 11663-8.

Wei, Y.-L. & Yang, W.-X. (2019) Kinesin-14 motor protein KIFC1 participates in DNA synthesis and chromatin maintenance. *Cell Death & Disease,* 10(6), 402.

Woodruff, J., Wueseke, O. & Hyman, A. (2014) Pericentriolar material structure and dynamics. *Philosophical transactions of the Royal Society of London. Series B, Biological sciences,* 369.

Wu, J., Mikule, K., Wang, W., Su, N., Petteruti, P., Gharahdaghi, F., Code, E., Zhu, X., Jacques, K., Lai, Z., Yang, B., Lamb, M. L., Chuaqui, C., Keen, N. & Chen, H. (2013) Discovery and Mechanistic Study of a Small Molecule Inhibitor for Motor Protein KIFC1. *ACS Chemical Biology,* 8(10), 2201-2208.

Xiao, Y.-X. & Yang, W.-X. (2016) KIFC1: a promising chemotherapy target for cancer treatment? *Oncotarget; Vol 7, No 30*.

Yang, W.-X. & Sperry, A. O. (2003) C-Terminal Kinesin Motor KIFC1 Participates in Acrosome Biogenesis and Vesicle Transport1. *Biology of Reproduction,* 69(5), 1719-1729.

Zhao, H., Watkins, J. L. & Piwnica-Worms, H. (2002) Disruption of the checkpoint kinase 1/cell division cycle 25A pathway abrogates ionizing radiation-induced S and G2 checkpoints. *Proc Natl Acad Sci U S A,* 99(23), 14795-800.